VOLUME 29 JULY, 1951 NUMBER 4

Canadian Journal of Physics

Editor: G. M. VOLKOFF

Published by THE NATIONAL RESEARCH COUNCIL
OTTAWA CANADA

CANADIAN JOURNAL OF PHYSICS

This was formerly *Section A, Canadian Journal of Research.* The change to the new name took place January 1, 1951. The CANADIAN JOURNAL OF PHYSICS is published six times annually.

The CANADIAN JOURNAL OF PHYSICS is published by the National Research Council of Canada under the authority of the Chairman of the Committee of the Privy Council on Scientific and Industrial Research. Matters of general policy are the responsibility of a joint Editorial Board consisting of members of the National Research Council of Canada and the Royal Society of Canada.

The National Research Council of Canada publishes also the following Journals: *Canadian Journal of Botany, Canadian Journal of Chemistry, Canadian Journal of Medical Sciences, Canadian Journal of Technology, Canadian Journal of Zoology.*

EDITORIAL BOARD

Representing
NATIONAL RESEARCH COUNCIL

DR. J. H. L. JOHNSTONE (*Chairman*),
Professor of Physics,
Dalhousie University,
Halifax, N.S.

DR. OTTO MAASS,
Macdonald Professor of
Physical Chemistry,
McGill University,
Montreal, P.Q.

DR. CHARLES W. ARGUE,
Dean of Science,
University of New Brunswick,
Fredericton, N.B.

DR. A. G. MCCALLA,
Department of Plant Science,
University of Alberta,
Edmonton, Alta.

Ex officio

DR. LÉO MARION, Editor-in-Chief,
Division of Chemistry,
National Research Laboratories,
Ottawa.

DR. H. H. SAUNDERSON,
Director, Division of Information Services,
National Research Council,
Ottawa.

Representing
ROYAL SOCIETY OF CANADA

DR. G. M. VOLKOFF,
Professor of Physics,
University of British Columbia,
Vancouver, B.C.

DR. J. W. T. SPINKS,
Dean, College of Graduate
Studies,
University of Saskatchewan,
Saskatoon, Sask.

} Section III

DR. H. S. JACKSON,
Head, Department of Botany,
University of Toronto,
Toronto, Ont.

DR. E. HORNE CRAIGIE,
Department of Zoology,
University of Toronto,
Toronto, Ont.

} Section V

Representing
THE CHEMICAL INSTITUTE OF CANADA

DR. H. G. THODE,
Department of Chemistry,
McMaster University,
Hamilton, Ont.

Subscription rate: $2.00 a year. All enquiries concerning subscriptions should be addressed to the CANADIAN JOURNAL OF PHYSICS, National Research Council, Ottawa, Canada. Special rates can be obtained for subscriptions to more than one of the Journals published by the National Research Council.

Canadian Journal of Physics

Issued by THE NATIONAL RESEARCH COUNCIL OF CANADA

VOLUME 29 JULY, 1951 NUMBER 4

THE EMISSION OF RADIOACTIVE NUCLEI IN COSMIC RAY STARS[1]

BY E. PICKUP AND L. VOYVODIC

Abstract

It has been found that a certain proportion of the fragments emitted in cosmic ray stars formed at about 85,000 ft. consists of radioactive nuclei, i.e., in electron sensitive photographic emulsions, tracks of electrons with energies of several mega electron volts can be seen originating at the end of the track of the fragment. Details of such events are given, together with energy measurements for the disintegration electrons made by the multiple Coulomb scattering method. The significance of the results, and possible identification of the fragments, are discussed.

Introduction

Occasionally, heavy fragments (i.e., nuclei heavier than the helium nucleus) are emitted in stars in photographic emulsions. If these fragments are sufficiently energetic they will produce an appreciable number of delta rays, and show a characteristic thinning down in track width before ending their ranges. By means of these criteria, identification can be made within fairly close limits, as has been done for those nuclei which constitute the heavy component of the primary cosmic rays (3).

Nuclei which are energetic enough to be identified in this way occur infrequently in stars, however (13). In general, the fragments are either of very short range (i.e., one or two microns long, and called recoil nuclei), or of a range less than or of the order of the thinning down length. It is such fragments with which we are concerned here. In this case identification is practically impossible unless the nuclei show some special characteristics at the ends of their ranges, e.g., Li_3^8 which undergoes β-disintegration into Be_4^8, the Be_4^8 nucleus then splitting up into two oppositely directed α-particles to form a "hammer" track. An account of such Li_3^8 nuclei, first observed by Occhialini and Powell, has been given by Hodgson (6) and by the present authors* (11) recently.

Some of the other heavy fragments are also radioactive and, whilst they have no characteristic feature such as a "hammer" track, disintegration electrons can

[1] *Manuscript received November 13, 1950, and, as revised, March 14, 1951.*
Contribution from the Division of Physics, National Research Laboratories, Ottawa, Canada. Issued as N.R.C. No. 2431.

* *Alvarez (1) has reported the production of B_5^8, undergoing positron decay to Be_4^8 with formation of a "hammer" track. The lifetime and β-ray energy end point are very similar to those for Li_3^8. Thus, as pointed out by Alvarez, it is quite possible that some "hammer" track events previously ascribed to Li_3^8 are due to B_5^8 although, because of its smaller charge, we might expect a greater number of Li_3^8 fragments. In the present work we continue to use the number of "hammer" tracks events as a basis for comparison with the other radioactive nuclei observed.*

be seen originating at the ends of the fragments if electron sensitive emulsions are used. We have observed many such examples, and the energies of the disintegration electrons have been measured in suitable cases by the multiple Coulomb scattering method. In this way it has been possible to draw certain conclusions about the identity of some of these nuclei. A preliminary account of this work was reported recently (12). Perkins (10) has noted one example of a fairly long range heavy fragment ($Z \sim 8$), which emits a β-particle after coming to rest.

2. Frequency of Occurrence of Radioactive Nuclei

(*a*) *Number of Events*

The events were recorded in Ilford G5 (electron sensitive) emulsions, 250 microns thick, exposed to cosmic radiation in a balloon flight for five hours at about 85,000 ft. From a total of 4000 stars with 6 or more prongs* 33 events were observed in each of which an electron, of energy ~ 1 Mev., was emitted from the end of a fairly short, heavy fragment from a star. Twenty-seven events were observed also, in which electrons with energies $\sim$1-2 Mev. appeared to originate at the centers of stars. In some of the cases very short recoil tracks (one or two microns long) could be detected at the centers, and the disintegration electrons could have come from the ends of these or from other residual nuclei insufficiently energetic to cause visible tracks. Two of the stars had two electrons originating at the centers and there was one case of a 9-pronged star with 3 electrons, the energies of two of which were considerably less than 1 Mev.

In the same batch of emulsions 34 fragments, showing "hammer" tracks, were emitted. It will thus be seen that the number of other radioactive fragments emitted is comparable with the number of such fragments. Since all the other radioactive fragments almost certainly consist of different types of nuclei (mostly heavier than Li_3^8 or B_5^8) it would appear that the ejection of the lighter fragments is more probable.

(*b*) *Certainty of Identification*

Unless the electron grain count in the emulsion is at least 30 grains per 100 microns, the disintegration electrons are not easy to recognize, and to associate definitely with fragments. In the present work the minimum grain count for electrons was ~ 32 grains per 100 microns. Cases, which we considered too doubtful, have been excluded from the tables of events.

An indication of the reliability of the results is given by the fact that in 31 out of the 34 cases of Li_3^8 or B_5^8 fragments observed, a disintegration electron was detected with certainty. Of the remaining three cases one hammer track was very near the glass backing of the emulsion, and in two examples identifi-

* *Stars with fewer prongs are not included here, since a proportion of these would have been missed with the low microscope magnification* ($\sim 95\times$) *used in the routine searching of the emulsion. In the same batch of emulsions, we recorded* $\sim$*900 stars with 5 or fewer prongs, and this included one star with a* Li^8 *nucleus, two with other radioactive fragments, and 6 stars with electrons originating at the center. The total volume of emulsion for the 4000 stars was 26 cc.*

cation of an electron track was doubtful, partly because of the presence of background electron tracks near the hammer track.

3. Occurrence of Two Radioactive Nuclei in One Star

One definite case has been observed where two radioactive fragments were ejected in the same nuclear disintegration in the 4000 stars recorded. The

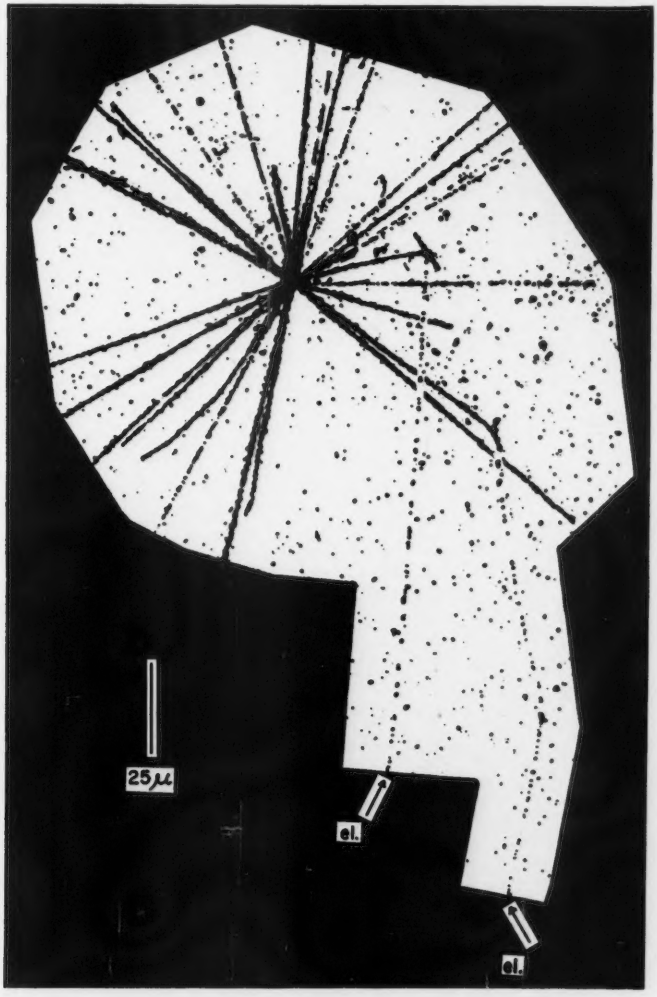

FIG. 1. *34-pronged star in which two nuclei with "hammer" tracks were emitted (see event 11 in Table III).*

fragments showed "hammer" tracks and thus were either Li_3^8 or B_5^8. A mosaic of photomicrographs of this event, a 34-pronged star, is shown in Fig. 1. The energies of the nuclei, if Li_3^8, were 24 Mev. and 15.5 Mev. The tracks of the disintegration electrons can be clearly seen in Fig. 1. Some of the stars discussed in the present work also have at least one heavy, stable fragment in addition to the radioactive fragment. However, it is difficult to distinguish these from α-particle and proton tracks in electron sensitive emulsions, unless they are of sufficiently long range to show the characteristic thinning down in track width.

4. Measurement of the Energies of the Disintegration Electrons

(*a*) *Method*

The energies of the disintegration electrons were measured, in the case of suitably long tracks, by the method of multiple Coulomb scattering, using a technique similar to that described by Fowler (5). The actual scattering

TABLE I

RADIOACTIVE NUCLEI EMITTED IN STARS

Event	No. of prongs	Range, microns	Electron energy, Mev.
1	14	35	4.6 ± 0.8
2	6	2.0	0.7 ± 0.3
3	21	3.0	2.0 ± 0.7
4	16	14	8.8 ± 0.9
5	21	5.5	1.2 ± 0.3
6	21	7.0	4.4 ± 0.6
7	10	5.0	2.4 ± 0.5
8	19	14	4.5 ± 1.0
9	24	6.5	0.5 ± 0.2
10	16	10	1.7 ± 1
11	12	3.5	5.0 ± 1.0
12	9	10	1.2 ± 0.2
13	12	3.5	3.2 ± 1
14	25	14.0	5.7 ± 1.5
15	16	3	
16	12	8	
17	24	10.5	
18	10	15.5	
19	35	41	
20	14	2.5	
21	27	12	
22	11	4	
23	23	36	
24	18	34	
25	16	13	
26	26	27	
27	11	6.5	
28	15	43	
29	12	18	
30	13	5	
31	11	12.5	
32	17	9	
33	11	6.5	

TABLE II

STARS WITH ELECTRONS FROM CENTER

No. of prongs	Electron energy, Mev.
6	1.2 ± 0.2
10	2.4 ± 0.4
7	1.2 ± 0.3
12	0.5 ± 0.1
5	1.1 ± 0.3

Other electrons with energies 1 Mev. were observed in stars whose size, by number of prongs, was 16, 10, 11, 17, 15, 11, 9, 12, 8, 12, 8, 8, 6, 7, 6, 16, 7, 7, 9, 11, 7, 8, 6.

measurements were analyzed according to the detailed statistical theory of Williams (16) in order to deduce the electron energies. A calibration experiment by Voyvodic and Pickup (15) on electron pairs formed in emulsions by

TABLE III

Li_3^8 NUCLEI EMITTED IN STARS

Event	No. of prongs	Range Li^8, microns	Electron energy, Mev.
1	26	71	4.5 ± 1.0
2	21	44	3
3	30	43	0.6 ± 0.2
4	40	18	5.0 ± 1.0
5	12	45	4.5 ± 1.0
6	9	76	4
7	17	60	6.8 ± 1.0
8	13	41	4.2 ± 1.0
9	20	54	
10	14	57	
11	34	70, 36	
12	25	42	
13	20	29	
14	18	20	
15	23	22	
16	22	63	
17	21	44	
18	20	22	
19	22	50	
20	60	400	
21	47	100	
22	12	45	
23	26	71	
24	22	20	
25	18	38	
26	18	125	
27	34	26	
28	13	76	
29	18	25	
30	23	54	
31	23	25	
32	16	17	

the gamma radiation from the $Li^7(p, \gamma)Be^8$ reaction, which indicates the validity of this procedure, will be described fully in a subsequent publication.

(b) Results

Details of the various stars with fragments showing disintegration electrons are given in tabular form, together with electron energies for some of the events. Table I gives the results for stars with fragments showing electrons at

FIG. 2. *Part of a 35-pronged star in which a radioactive fragment was emitted (see event 19 in Table I).*

the ends of their ranges. Mosaics of photomicrographs of several of these events have been constructed, and these are illustrated in Figs. 2, 3A, 3B, 4A, and 4B. Table II gives details of the stars for which tracks of electrons with energies $\sim$ a few mega electron volts could be seen originating at the centers. One 5-pronged star (C19) from Ilford G5 emulsions exposed in an airplane flight at about 12,000 ft. is included in this table, since the electron energy had been previously measured. Table III lists the stars having Li_3^8 or B_5^8 fragments (i.e., "hammer" tracks).

The energy values in Table III for the few electrons measured indicate a most probable energy $\sim$ 4.5 Mev., which is in reasonably good agreement with

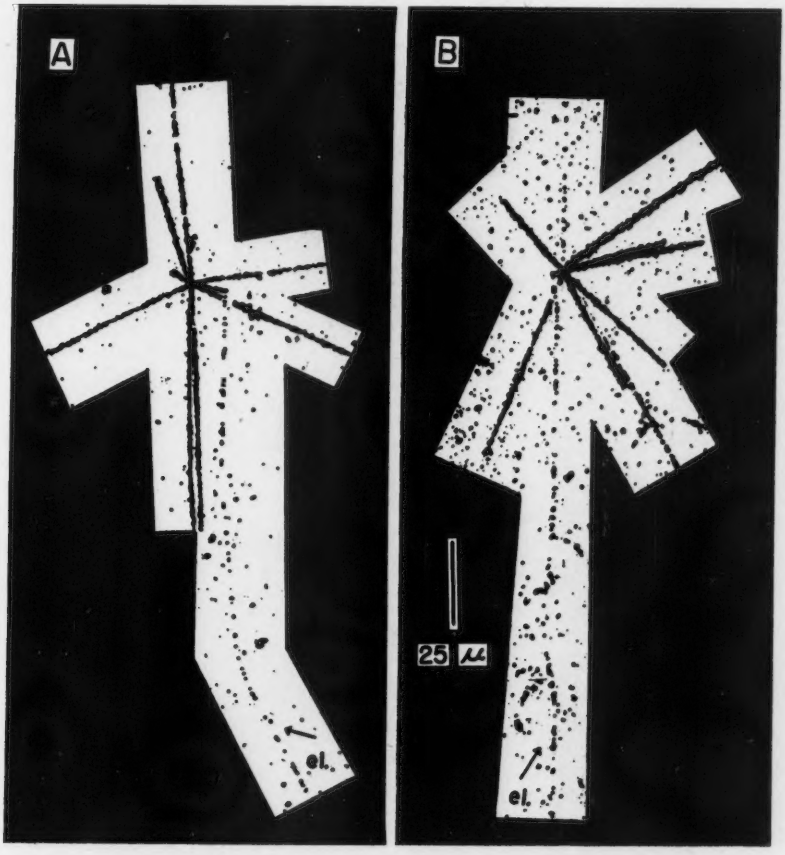

FIG. 3. *(A) 9-pronged star, (B) 12-pronged star, both with radioactive nuclei (see events 12 and 11 respectively in Table I).*

the value 5.0 Mev. for the most probable energy obtained from the Li_3^8 β-ray energy distribution spectrum given by Hornyak and Lauritsen (7).

For the other radioactive nuclei, the energy values for the disintegration

FIG. 4. *Parts of (A) 18-pronged star, (B) 12-pronged star, both with radioactive nuclei (see events 24 and 29 respectively in Table I).*

electrons range from about 1 to 9 Mev., as shown in Table I. The nature of the spread in energy values does not seem characteristic of a single radioactive nucleus, and it is almost certain that there is an admixture of different kinds of nuclei. This is to be expected since the parent stars have 6 or more prongs and most of them must be due to disintegrations in the Ag and Br nuclei in the emulsion rather than in the light nuclei. The star prongs are due mostly to protons, deuterons, tritons, and α-particles (2). However, in many of the stars, even after taking account of these prongs, there is still an appreciable mass and charge excess which could give a variety of possibilities for the nature of additional nuclear fragments.

The energy values for electrons originating at the centers of stars seem to be lower, on the whole, than for electrons which originate at the end of a fragment. Most of the former stars have relatively few prongs, but are probably due to disintegrations in the Ag and Br nuclei in the emulsion, and fairly heavy residual nuclei could have been left. Because of the heavy mass and high charge, these may have a short range in the emulsion, and give no recognizable track. Also, if they were radioactive, we would expect them to have a fairly low β-ray energy end point.

5. Range Distribution of the Radioactive Nuclei

The distribution in range of the "hammer" track nuclei and the other radioactive fragments is shown graphically in Fig. 5. The most probable range

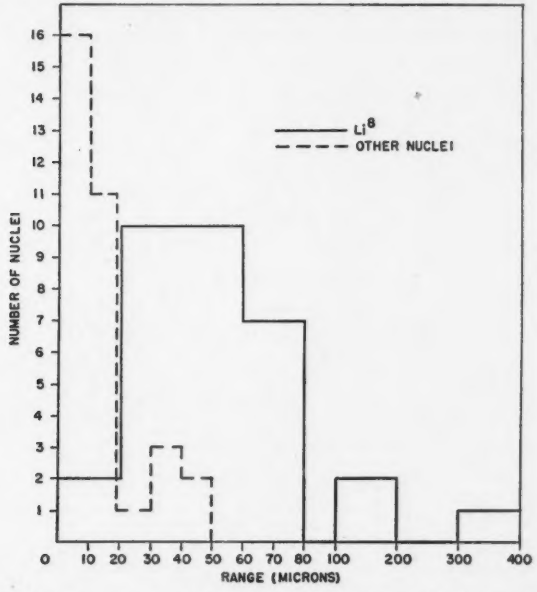

FIG. 5. *Frequency versus range distribution for "hammer" track nuclei, and for other radioactive fragments.*

for the former is 50 microns which, for Li_3^8, would correspond to an energy of 20 Mev. As will be indicated in the next section it appears likely that some of the other radioactive fragments are also fairly light nuclei, e.g., boron or nitrogen. The average range of nuclei listed in Table I, and for which the energy of the disintegration electron has been measured and is at least 4.4 Mev., is 14.6 microns.* If we use an extrapolation of the range–energy curve given by Millar and Cameron (9) for boron nuclei in photographic emulsions, this average range corresponds to an energy of 10 Mev. which is somewhat less than that for Li_3^8 nuclei.

6. Discussion

(*a*) *Identification of the Radioactive Nuclei*

As mentioned earlier, identification of the short range heavy fragments is practically impossible by any of the usual methods. However, reference to Table I shows that, for the cases measured, an appreciable fraction had decay electrons whose energies were $\gtrsim$ 4.5 Mev. For a radioactive nucleus, the β-ray energy end point is approximately three times the most probable value of the electron energy. Therefore, some of the nuclei, whose decay electron energies were measured, would seem to have β-ray energy end points $\sim$ 13.5 Mev. There are very few such nuclei, and reference to a chart of nuclear species (14) indicates that they are probably due to either B^{12} (end point, 13.4 Mev.), N^{12} (end point, 16.6 Mev.), or N^{15} (end point, 10 Mev.). Since the nature of the spread in electron energies does not seem to be indicative of a unique β-ray emitter and there is a variety of possible nuclei with lower β-ray energy end points, it may be impossible to identify fragments with electrons in the lower energy range.

(*b*) *Comparison of Results with Theory*

Table IV shows the fraction of stars with "hammer" tracks and with other radioactive nuclei for stars of different sizes. The results for hammer tracks compare reasonably well with those of Hodgson (6) in the region of star size, 12–25 prongs. Also, for an average star size of 14 prongs, the fraction of hammer tracks agrees fairly well with unpublished calculations of LeCouteur,

TABLE IV

FRACTION OF STARS WITH RADIOACTIVE NUCLEI

Star size No. of prongs	No. of stars	No. of Li^8	Fraction Li^8 per star	No. of other radioactive nuclei
14 (12-16)	1040	6	0.006	12
19 (17-21)	539	10	0.02	6
24 (22-26)	265	9	0.035	5
32 (27-36)	178	4	0.02	2
36-60	46	3	0.07	0

* *The correction due to fragments being missed because they leave the emulsion will be negligible.*

as given graphically by Hodgson, and made for Li_3^8 of zero spin on the basis of the evaporation theory, i.e., 0.01 for 14 prongs. For the larger stars, although statistics are poor, the fraction of events seems somewhat greater than an extension of the theoretical curve would indicate. Since some of the Li^8 fragments here are the most energetic ones, they may be formed as knock-on fragments in secondary collisions in the nuclear disintegrations, as discussed in an earlier paper (11).

Not much can be said of the other radioactive nuclei owing to the uncertainty of their nature. However, since the number to be identified as boron or nitrogen nuclei is certainly less than the number of "hammer" track nuclei, this may be taken as an indication that most of the latter are due to Li_3^8 rather than B_5^8.

(*c*) *Neutron Excess in Stars*

It has been pointed out (8) that, if equal numbers of neutrons and protons were emitted generally in stars, then the residual nuclei would have a large neutron excess, and could reach stability by β-transitions. Thus electrons with energies ~ 1 Mev. might be expected to occur frequently, especially in the smaller stars. As we have seen, only a small proportion of stars seem to have electrons originating at the centers, or to have short radioactive fragments. In the absence of any other means of accounting for the neutron excess at present, it must be assumed that it is emitted as neutrons in the disintegrations.

Acknowledgments

The photographic emulsions used in this experiment were exposed at high altitude through a collaborative program of cosmic ray investigations by the Bartol Research Foundation and the National Research Council of Canada, with the co-operation of the Office of Naval Research Project, "Skyhook".

The routine searching of emulsions was done by Miss B. Mear, Miss S. W. Young, and Miss B. Woodruff. Mr. D. Rushton was responsible for constructing the mosaics of photomicrographs which illustrate this paper. We are also indebted to Mr. I. B. McDiarmid, of Queen's University, who made most of the scattering measurements on the decay electrons.

References

1. Alvarez, L. W. Phys. Rev. 80: 519. 1950.
2. Bradt, H. L. and Kaplon, M. F. Phys. Rev. 78: 680. 1950.
3. Bradt, H. L. and Peters, B. Phys. Rev. 74: 511. 1948.
4. Camerini, U., Fowler, P. H., Lock, W. O., and Muirhead, H. Phil. Mag. 41: 413. 1950.
5. Fowler, P. H. Phil. Mag. 41: 169. 1950.
6. Hodgson, P. E. Phil. Mag. 42: 207. 1951.
7. Hornyak, W. F. and Lauritsen, T. Phys. Rev. 77: 160. 1950.
8. LeCouteur, K. J. Proc. Phys. Soc. (London) 63: 259. 1950.
9. Millar, C. H. and Cameron, A. G. W. Phys. Rev. 78: 78. 1950.
10. Perkins, D. H. Proc. Roy. Soc. A (London) 203: 339. 1950.
11. Pickup, E. and Voyvodic, L. Can. J. Research, A, 28: 616. 1950.
12. Pickup, E. and Voyvodic, L. Phys. Rev. 80: 1100. 1950.
13. Sorensen, S. O. C. Phil. Mag. 40: 947. 1949; 42: 188. 1951.
14. Sullivan, W. H. Trilinear Chart of Nuclear Species.
15. Voyvodic, L. and Pickup, E. Phys. Rev. 81: 471. 1951.
16. Williams, E. J. Proc. Roy. Soc. 169: 531. 1939.

ON THE THEORY OF THE HALL EFFECT[1]

By H. Koppe and J. M. Bryan

Abstract

A phenomenological theory of the Hall effect is applied to: (1) the effect of an inhomogenous magnetic field on the Hall effect in thin layers (par. 4, par. 5); (2) the magnetic increase of resistivity under the same conditions (par. 6); (3) the Hall effect in a homogenous magnetic field in inhomogenous layers (par. 7–9). The first paragraphs give a simple kinetic theory.

1. This paper is mainly concerned with the phenomenological theory of the Hall effect; especially with the influence of inhomogeneities of the magnetic field or the specimen. As a matter of orientation, the next paragraph gives a simple kinetic theory of the influence of the magnetic field on conduction in metals, which is a modification of a method suggested by Becker (1).

2. We make the simplifying assumption that after a collision an electron starts with a given velocity $\mathbf{v}$ and an isotropic distribution of directions, and proceed to calculate the path $\mathbf{r}(t)$ between two collisions. The equations of motion are

$$m\dot{\mathbf{r}} = e\left\{\mathbf{E} + \frac{1}{c}[\dot{\mathbf{r}} \times \mathbf{H}]\right\}. \tag{2.1}$$

Without loss of generality, we can assume that $\mathbf{H}$ has a z-component H_z only. Putting

$$\zeta = v_x + iv_y\,; \quad \eta = E_x + iE_y$$

(1) is equivalent to

$$m\dot{\zeta} = e\left\{\eta - \frac{i}{c}\,\zeta H_z\right\} \tag{2.2}$$

$$m\dot{v}_z = eE_z.$$

Assuming that the last collision took place at $\mathbf{r} = 0$ and $t = 0$, we can integrate (2) and obtain:

$$\zeta(t) = \frac{c\eta}{iH_z} + \left(\zeta(0) - \frac{c\eta}{iH_z}\right)e^{-i\frac{eH_z}{cm}t} \qquad v_z(t) = v_z(0) + \frac{eE_z}{m}t. \tag{2.3}$$

Integrating again with respect to t, we obtain for the equation of the path

$$\xi(t) = \frac{cy}{iH_z}\,t + \left(\zeta(0) - \frac{cy}{iH_z}\right)\left\{e^{-i\frac{eH_z}{cm}t} - 1\right\}\frac{icm}{eH_z} \tag{2.4}$$

$$z(t) = v_z(0)t + \frac{eE_z}{2m}t^2,$$

where

$$\xi = x + iy.$$

If we average this over the initial direction of $\mathbf{v}$, we obtain, owing to isotropy

[1] *Manuscript received December 27, 1950.*
Communicated by the Department of Physics, University of British Columbia, Vancouver, B.C.

of the directions of $\mathbf{v}$, expressions for $\bar{\xi}(t)$ and $\bar{z}(t)$ which arise from (4) if one puts $\zeta(0) = v_z(0) = 0$. We have now to calculate the average displacements $\overline{\Delta\xi} = \overline{\Delta x} + i\overline{\Delta y}$ and $\overline{\Delta z}$. If $w(t)dt$ is the probability that the second collision takes place between t and $t + dt$, and τ the average time between two collisions, then

$$\overline{\Delta\xi} = \int_0^\infty w(t)\,\xi(t)\,dt. \tag{2.5}$$

$$\tau = \int_0^\infty t\,.\,w(t)dt. \tag{2.6}$$

Becker (1), assumes that $w(t) = \delta(t - \tau)$, i.e., that the time interval between two collisions is always exactly equal to τ. This is a rather artificial assumption, which finally leads to a wrong value of the Hall coefficient. Since it can be assumed that the probability that a collision takes place within a time element dt, is independent of t, and equal to dt/t we can put

$$w(t) = \frac{1}{\tau}\,e^{-t/\tau}. \tag{2.7}$$

It turns out that this even simplifies the calculations and we obtain

$$\overline{\Delta\xi} = \frac{e\tau^2}{m}\eta\frac{1 - \dfrac{ie\tau}{mc}H_z}{1 + \left(\dfrac{e\tau}{mc}\right)^2 H_z{}^2}$$

$$\overline{\Delta z} = \frac{e\tau^2}{m}E_z. \tag{2.8}$$

From these expressions the average current $\mathbf{j} = en\overline{\Delta\mathbf{r}}/\tau$ (n = density of electrons) can be calculated, and by separating the real from the imaginary, we obtain with $\sigma = e^2\tau n/m$ and $\beta = e\tau/mc$

$$j_x = \sigma\frac{E_x + \beta E_y H_z}{1 + \beta^2 H_z{}^2}$$

$$j_y = \sigma\frac{E_y - \beta E_x H_z}{1 + \beta^2 H_z{}^2}$$

$$j_z = \sigma E_z. \tag{2.9}$$

It must be possible to express the connection between $\mathbf{j}$, $\mathbf{E}$, and $\mathbf{H}$ in invariant form by means of vectors. Since the last equation (2.9) can be written in the form

$$j_z = \sigma\frac{E_z + \beta^2 E_z H_z{}^2}{1 + \beta^2 H_z}$$

it can be seen that

$$\mathbf{j} = \sigma\frac{\mathbf{E} + \beta[\mathbf{E} \times \mathbf{H}] + \beta^2(\mathbf{EH})\mathbf{H}}{1 + \beta^2 H^2}, \tag{2.10}$$

which is identical with (2.9) as soon as the basic vectors are orientated such that $H_x = H_y = 0$. An alternative expression for (2.10) is

$$\mathbf{j} = \sigma \mathbf{E} + \sigma \frac{\beta[\mathbf{E} \times \mathbf{H}] + \beta^2[[\mathbf{E} \times \mathbf{H}] \times \mathbf{H}]}{1 + \beta^2 H^2}, \tag{2.11}$$

which shows that, at least for the simple model considered here, there is no influence of a magnetic field parallel to the electric field.*

3. That the current, according to (2.11), is given by a formula which involves two constants only is of course due to the very simplified model considered here. A general expression up to second order terms in H is

$$\mathbf{j} = \sigma \mathbf{E} + \sigma\beta[\mathbf{E} \times \mathbf{H}] - \sigma' \beta^2 \mathbf{E} \cdot H^2 + \sigma'' \beta^2 \mathbf{H}(\mathbf{E}\mathbf{H}), \tag{3.1}$$

which involves four arbitrary constants. That these constants are partly written as products is a matter of convenience with regard to dimensions: each σ has the dimensions of a conductivity and β has the dimensions of a reciprocal magnetic field strength. $\sigma' = \sigma''$ means that there is no influence of a longitudinal field. A difference between σ and σ' arises if one takes into account the fact that the conduction in metals can be due to holes, which behave like positrons, as well as to electrons.

Experimentally, galvanomagnetic effects are usually investigated by giving $\mathbf{j}$ and $\mathbf{H}$ and measuring the components of $\mathbf{E}$. If we resolve (3.1) for $\mathbf{E}$, we obtain (up to second order terms in H):

$$\mathbf{E} = \frac{1}{\sigma}\mathbf{j} - \frac{\beta}{\sigma}[\mathbf{j} \times \mathbf{H}] + (\sigma' - \sigma)\frac{\beta^2}{\sigma^2}\mathbf{j} \cdot H^2 - (\sigma'' - \sigma)\frac{\beta^2}{\sigma^2}\mathbf{H}(\mathbf{j}\,\mathbf{H}) \tag{3.2}$$

If $\mathbf{H}$ is perpendicular to $\mathbf{j}$, then $\mathbf{E}$ has a component $E_\perp$ perpendicular to $\mathbf{j}$ and $\mathbf{H}$, and a component $E_{||}$ parallel to $\mathbf{j}$. If the Hall coefficient R and the apparent conductivity σ_{eff} are defined by

$$E_\perp = -R\,|j|\,|H|$$
$$\sigma_{eff} E_{||} = |j|.$$

We have

$$R = \frac{\beta}{\sigma} \tag{3.3}$$

$$\sigma_{eff} = \sigma\left\{1 - \frac{\sigma' - \sigma}{\sigma}\beta^2 H^2\right\} = \sigma\{1 - \sigma(\sigma' - \sigma)R^2 H^2\}. \tag{3.4}$$

All these formulae hold only up to terms of order H^2. If $\mathbf{H}$ and $\mathbf{j}$ are not at right angles, somewhat more complicated formulae hold, which can easily be obtained from (3.2).

An interesting fact is that the influence of the magnetic field on the conductivity would vanish if $\sigma' = \sigma$. We shall see later that even in this case an inhomogeneous magnetic field can lead to an increase in resistivity.†

* *R. Peierls (3) has shown that this holds, as long as the surfaces of constant electron energy in* $\mathbf{p}$*—space are concentrical spheres.*

† *It should be pointed out that the formulae for the magnetic increase of resistivity which are generally found in text books and which go back to a paper of Gans (2) are wrong, for they calculate a second order effect by means of a first order approximation, which inconsistently contains some higher order terms in H.*

4. Galvanomagnetic effects are generally measured using an arrangement similar to that shown in Fig. 1, in which we have a thin layer of metal of width $2l$. We assume that the magnetic field $\mathbf{H}$ has a z-component only and that H_z

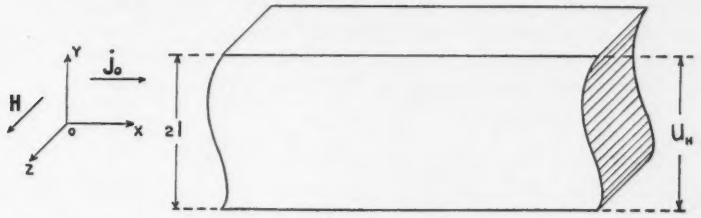

FIG. 1

is a given function $H(x)$. Further we assume that $\mathbf{E}$ and $\mathbf{j}$ have x- and y-components only and that these do not depend on z. For a stationary field, we must have

$$\text{curl } \mathbf{E} = 0 \tag{4.1}$$

and this implies

$$\mathbf{E} = -\text{ grad } V. \tag{4.2}$$

An equation for V is obtained by taking the divergence of (3.1), which must be zero. This gives:

$$\Delta V = -\beta \frac{dH}{dx}\frac{\partial V}{\partial y} + \frac{\sigma'}{\sigma}\beta^2 \left\{ H^2 \Delta V + 2H \frac{dH}{dx}\frac{\partial V}{\partial x} \right\}. \tag{4.3}$$

Since the normal component of $\mathbf{j}$ must vanish at the boundary of the metal we obtain the following boundary conditions for V:

$$\frac{\partial V}{\partial y} = \beta H(x)\frac{\partial V}{\partial x} + \frac{\sigma'}{\sigma}\beta^2 H^2 \frac{\partial V}{\partial y} \quad \text{for } y = \pm l. \tag{4.4}$$

In order to solve this set of equations we set:

$$V = -\frac{1}{\sigma} j_0 x + \beta V^{(1)} + \beta^2 V^{(2)} + \ldots, \tag{4.5}$$

where j_0 is the current density which would correspond to an even distribution of the total current.

Inserting (4.5) into (4.3) and (4.4) and equating like powers of β we obtain:

$$\Delta V^{(1)} = 0$$

$$\frac{\partial V^{(1)}}{\partial y} = -\frac{j_0}{\sigma} H(x) \quad \text{for } y = \pm l \tag{4.6}$$

$$\Delta V^{(2)} = -\frac{dH}{dx}\frac{\partial V^{(1)}}{\partial y} - 2\frac{\sigma^1}{\sigma^2} j_0 H \frac{dH}{dx}$$

$$\frac{\partial V^{(2)}}{\partial y} = H \frac{\partial V^{(1)}}{\partial x} \quad \text{for } y = \pm l. \tag{4.7}$$

The equations (4.6) give the (linear) Hall effect while the equations (4.7) will be used later to determine the change in resistivity. This is due to the fact that only those terms of V which are odd in β can contribute to the Hall potential while only even terms can contribute to the change in resistivity. In the above calculations we neglected the magnetic field generated by the currents compared to the external field and assumed $\mathbf{H}$ had only a z-component $H(x)$. Such assumptions concerning $\mathbf{H}$ can be in contradiction to:

$$\text{curl } \mathbf{H} = \frac{4\pi}{e}\mathbf{j}. \tag{4.8}$$

In order to fulfill this equation it would become necessary to introduce x- and y-components of $\mathbf{H}$ which would depend on z. Thus the problem could no longer be treated as two dimensional. On the other hand, in a sufficiently thin layer these x- and y-components will be everywhere very small, so that it seems to be permissible to neglect them. In this case Equation (4.8) must not be used in the course of the calculations since its use would lead to wrong results.

5. We proceed to determine the first order approximation. It is assumed that $H(x)$ will vanish for sufficiently large $|x|$. Then $V^{(1)}$ goes to zero for $|x| \to \infty$. Since it is an odd function of y it is always zero for $y = 0$. The e.m.f. U_H actually measured is given by

$$U_H = 2\beta V^{(1)}(x, l). \tag{5.1}$$

A partial solution of Equation (4.6) is $\sinh kye^{ikx}$, so that we can put

$$V^{(1)}(x, y) = \int_{-\infty}^{+\infty} A(k) \sinh kye^{ikx}dk. \tag{5.2}$$

The boundary condition gives

$$-\frac{j_0}{\sigma}H(x) = \int_{-\infty}^{+\infty} A(k) \cosh kl\, e^{ikx}\, kdk$$

or

$$A(k) = -\frac{j_0}{2\pi\sigma k \cosh kl}\int_{-\infty}^{+\infty} H(x)e^{-ikx}dx$$

and inserting this into (5.2) we obtain

$$\begin{aligned} U_H &= -\frac{j_0\beta}{\pi\sigma}\int_{-\infty}^{+\infty} dk\, \frac{\tanh kl}{k} e^{ikx}\int_{-\infty}^{+\infty} dx'\, H(x')e^{-ikx'} \\ &= \frac{2j_0\beta}{\pi\sigma}\int_{-\infty}^{+\infty} H(x') \log \tanh \frac{\pi}{4l}|x - x'|\, dx'. \end{aligned} \tag{5.3}$$

(The first integral is sometimes more convenient for actual evaluation.) As an example, we calculate U_H for a magnetic field

$$H(x) = \frac{H_0}{1 + a^2x^2},$$

which corresponds to the field between two long, sharp-edged pole pieces. We obtain:

$$U_H(x) = -\frac{2\beta j_0 H_0}{\sigma a}\left\{\frac{1}{2}\log\left|\frac{1}{4al} + \frac{ix}{4l}\right|^2 + \log\left|\frac{\Gamma\left(\frac{1}{4al} + \frac{ix}{4l}\right)}{\Gamma\left(\frac{1}{4al} + \frac{ix}{4l} + \frac{1}{2}\right)}\right|^2\right\}. \quad (5.4)$$

In Fig. 2 this formula has been evaluated for $x = 0$ (the line of symmetry of the magnetic field). The diagram shows the ratio r of the Hall tension to the value corresponding to a homogeneous field H_0 as a function of the dimensionless parameter al.

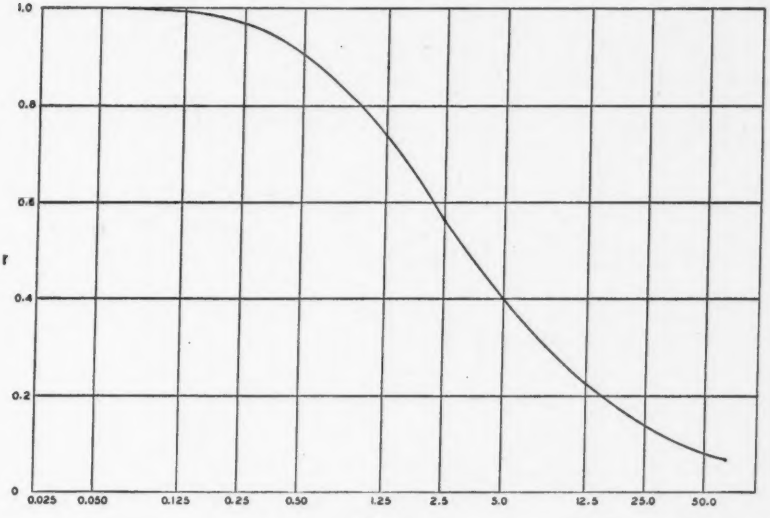

FIG. 2

If $H(x)$ varies slowly over distances comparable with l, then a Taylor expansion of $H(x)$ gives the formula:

$$U_H(x) = -\frac{4j_0\beta}{\sigma}\sum_{n=0}^{\infty}\frac{2^{2n+2} - 1}{(2n+2)!}(2l)^{2n+1}B_{n+1}\frac{d^{2n}H}{dx^{2n}} \quad (5.5)$$

$$= -\frac{j_0\beta}{\sigma}\left\{2lH + \frac{(2l)^3}{12}\frac{d^2H}{dx^2} + \frac{(2l)^5}{120}\frac{d^4H}{dx^4} + \cdots\right\}.$$

(The B_n are the Bernouillian numbers; the series might be asymptotic.)

6. The second order perturbation determines the changes in resistivity, but does not affect the Hall potential since $V^{(2)}$ is an even function of y. If we assume that the magnetic field acts only within a finite region, then $V^{(2)}$ will be constant at large distances from this region. However, in contrast to $V^{(1)}$ it need not be zero. We have to calculate

$$\delta U = \beta^2 \{ V^{(2)}(+\infty, y) - V^{(2)}(-\infty, y) \}.$$

This quantity will not actually depend on y. If we therefore introduce the average

$$\overline{V^{(2)}}(x) = \frac{1}{2l} \int_{-l}^{+l} V^{(2)}(x, y) dy \tag{6.1}$$

then δU will be given by

$$\delta U = \beta^2 \{ \overline{V^{(2)}}(\infty) - \overline{V^{(2)}}(-\infty) \}. \tag{6.2}$$

If we integrate the first equation (4.7) with respect to y, and divide by $2l$, we obtain:

$$\frac{d^2 \overline{V^{(2)}}}{dx^2} + \frac{1}{2l} \left[\frac{\partial V^{(2)}}{\partial y} \right]_{-l}^{+l} = - \frac{\sigma'}{\sigma^2} \frac{dH^2}{dx} j_0 - \frac{1}{2l} \frac{dH}{dx} \Big| V^1(x, y) \Big|_{-l}^{+l}$$

or, using the boundary conditions for $V^{(2)}$ and remembering that $V^{(1)}$ is an odd function of y:

$$\frac{d^2 \overline{V^{(2)}}}{dx^2} = - \frac{\sigma'}{\sigma^2} j_0 \frac{dH^2}{dx} - \frac{1}{l} \frac{d}{dx} \{ H(x) \; V^{(1)}(x, l) \}. \tag{6.3}$$

This is an ordinary differential equation for $\overline{V^{(2)}}$, which has to be solved under the initial conditions $V^{(2)}(-\infty) = 0$ and $\dfrac{d V^{(2)}(-\infty)}{dx} = 0$. We shall give the solution for the case that $H(x)$ is a slowly varying function of x so that we can use (5.5),

$$V^{(1)}(x, l) \approx - \frac{j_0 l}{\sigma} \left\{ H + \frac{l^2}{3} \frac{d^2 H}{dx^2} \right\}.$$

If we insert this into (6.3) and observe the identity

$$H \frac{d^2 H}{dx^2} = \frac{1}{2} \frac{d^2 H^2}{dx^2} - \left(\frac{dH}{dx} \right)^2$$

we obtain

$$\delta U \approx - \beta^2 \frac{j_0}{\sigma} \left(\frac{\sigma'}{\sigma} - 1 \right) \int_{-\infty}^{+\infty} H^2 dx - \beta^2 \frac{j_0}{\sigma} \frac{l^2}{3} \int_{-\infty}^{+\infty} \left(\frac{dH}{dx} \right)^2 dx. \tag{6.4}$$

In this expression the first term is exactly what we should expect on account of (3.4). But there is a second term which depends on inhomogeneities of the magnetic field. It is obviously due to the fact that in an inhomogeneous field the Hall tension is partly short-circuited through the conductor, and that these short-circuit currents lead to an increase of the Joule heat.

7. For the determination of the Hall coefficient, evaporated layers are frequently used. For these the assumption of the preceding paragraphs, namely that the layer is bounded in the z-direction by two parallel planes, is no longer quite true. Evaporated layers consist of many small crystals and this makes it necessary to investigate the influence of surface roughness and of small holes in the layer.

Even if **H** was constant, the treatment of these geometrical inhomogeneities would be rather difficult. On the other hand, detailed data of the geometry of an evaporated layer will generally not be available. We shall therefore limit the discussion to two simplified cases, which might give an idea of what is to be expected in general.

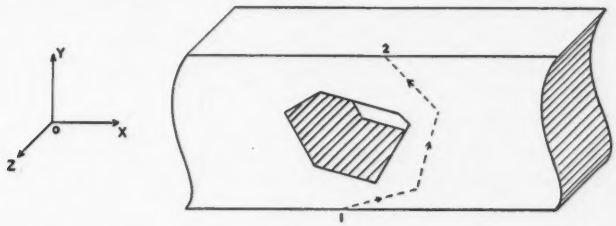

FIG. 3

In par. 9 we prove the rather curious theorem that holes of any shape, in a layer of uniform thickness (Fig. 3) exposed to a uniform magnetic field, have no influence on the Hall voltage, whereas they can have of course a considerable influence on the resistivity.

As the opposite possibility, we treat in par. 8 a layer with a slightly rough surface, Fig. 4. It is easy to see that a roughness consisting of ripples parallel to the direction of the current would have no influence on the Hall effect if the current density is calculated from the total current and the average thick-

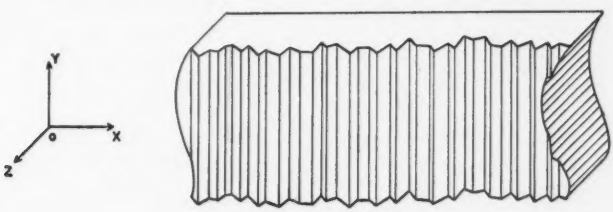

FIG. 4

ness. For this reason, it seems permissible to assume that the roughness consists of ripples perpendicular to the current. The surface is therefore given by $z = t(x)$. Here we aim at a statistical theory, hence we assume that $t(x)$ admits averages of the type

$$\langle f(t)\rangle = \lim_{L\to\infty}\frac{1}{2L}\int_{-L}^{+L} f(t(x+\tau))d\tau,$$

which are independent of x. The Hall tension itself would of course be a complicated function of x. It seems sensible to calculate instead of this the average Hall tension

$$\langle U_H\rangle = \lim_{L\to\infty}\frac{1}{2L}\int_{-L}^{+L} U_H(x)dx.$$

It will turn out, at least in the approximation considered here, that the relation between $\langle U_H\rangle$ and the average resistivity is the same as that for a homogeneous layer.

These results seem to be in good agreement with the experimental facts in so far as the annealing of evaporated layers produces a considerable decrease of resistance (mostly due to filling out of small holes between crystallites) and a small change in the Hall tension. It seems reasonable, therefore, to calculate the Hall constant for annealed layers by means of (5.3), using the average thickness and the observed value of the (average) resistivity.

8. In a layer as given by Fig. 4, in the absence of a magnetic field the current density will have only an x and a z-component. We neglect the small z-component and set the current density equal to its average value with respect to z. We thus obtain:

$$j_0 = \frac{j_{00}\langle t\rangle}{t(x)} = j_{00}f(x), \tag{7.1}$$

where j_{00} is a constant, $f(x) = \langle t\rangle/t(x)$, and where the average thickness of the metal is defined to be

$$\langle t\rangle = \lim\frac{1}{2L}\int_{-L}^{+L} t(x)dx.$$

Comparison of Equations (4.6), (7.1), and (5.3) leads at once to:

$$U_H(x) = \frac{2\beta j_{00}}{\sigma\pi}\int_{-\infty}^{+\infty} H(x')f(x')\log\tanh\frac{\pi}{4l}|x-x'|\,dx' \tag{7.2}$$

as the equation for the Hall potential. This relation shows that surface irregularities are equivalent to inhomogeneous magnetic fields. The average value of the Hall potential is:

$$\langle U_H\rangle = \frac{2\beta j_{00}}{\sigma\pi}\lim_{L\to\infty}\frac{1}{2L}\int_{-L}^{+L}dx\int_{-\infty}^{+\infty}dx'H(x')f(x')\log\tanh\frac{\pi}{4l}|x-x'|. \tag{7.3}$$

If H is constant for a sufficiently large range of values of x we can transform Equation (7.3) into:

$$\langle U_H \rangle = \frac{2\beta j_{00}}{\pi\sigma} \int_{-\infty}^{+\infty} H \log \tanh \frac{\pi}{4e} | y | \, dy \lim_{L\to\infty} \frac{1}{2L} \int_{-L}^{+L} f(x)dx.$$

Letting U_0 be the Hall potential in the case of a smooth surface we obtain:

$$\frac{\langle U_H \rangle}{U_0} = \lim_{L\to\infty} \frac{1}{2L} \int_{-L}^{+L} f(x)dx. \tag{7.4}$$

Letting $\langle \zeta \rangle$ be the average resistivity for a metal with an irregular surface we have, in the zero order approximation with respect to β:

$$\langle \zeta \rangle = \zeta \lim_{L\to\infty} \frac{1}{2L} \int_{-L}^{+L} f(x)dx. \tag{7.5}$$

Hence we have:

$$\frac{\langle U_H \rangle}{\langle \zeta \rangle} = \frac{U_0}{\zeta}, \tag{7.6}$$

which implies that the ratio U_0/δ is not affected by ripples on the surface of the metal.

9. We now consider a conductor which has a number of holes in its interior and which has the same profile in any plane parallel to the x–y plane. (Fig. 3.) We apply a uniform magnetic field $\mathbf{H}$ in the z-direction and obtain a current $\mathbf{j}(x,y)$ given by the equations:

$$\begin{aligned} \mathbf{j}^{(0)} &= \sigma \mathbf{E}^{(0)} \\ \mathbf{j}^{(1)} &= \sigma \mathbf{E}^{(1)} + [\mathbf{j}_0 \times \mathbf{H}] \end{aligned} \tag{7.8}$$

valid to first order terms in β, where

$$\mathbf{j} = \mathbf{j}^{(0)} + \beta \mathbf{j}^{(1)}; \quad \mathbf{E} = \mathbf{E}^{(0)} + \beta \mathbf{E}^{(1)}.$$

Calculating the curl of $\mathbf{j}^{(1)}$ from (7.8) and (4.1) we obtain: curl $\mathbf{j}^{(1)} = 0$ which together with div $\mathbf{j}^{(1)} = 0$ and the fact that the normal component of $\mathbf{j}^{(1)}$ vanishes at all surfaces of the metal including those at infinity indicates that $\mathbf{j}^{(1)} = 0$. Therefore the second of Equations (7.8) becomes:

$$\sigma \mathbf{E}^{(1)} = -[\mathbf{j}^{(0)} \times \mathbf{H}].$$

We select two points, 1 and 2, such that for zero magnetic field the potential difference between them is zero. Then the Hall potential between these points is:

$$\begin{aligned} U_H &= -\beta \int_1^2 \mathbf{E}^{(1)} d\mathbf{s} \\ &= -\frac{\beta H}{\sigma} \int_1^2 j_n^{(0)} \, ds, \end{aligned}$$

where $j_n^{(0)}$ is the component of $\mathbf{j}^{(0)}$ normal to the path of integration between 1 and 2. The integral:

$$\int_1^2 j_n^{(0)}\, ds$$

equals the total current flowing in a slab of the conductor which has unit height in the z-direction. Therefore, since we fix the total current flowing in the conductor, the Hall potential is unchanged by the presence of holes in the metal.

Acknowledgment

We wish to thank the National Research Council for the support of this work.

References

1. BECKER, R. Theorie der Elektrizitaet., Vol. 2. Leipzig. 1933. p. 208.
2. GANS, R. Ann. Phys. 20: 293. 1906.
3. PEIERLS, R. Ann. Phys. 10: 97. 1931.

SCALE MODEL EXPERIMENTS IN ELECTROMAGNETIC METHODS OF GEOPHYSICAL EXPLORATION[1]

By A. R. Clark and A. G. Mungal

Abstract

A method of accurately measuring the phase as well as the amplitude of alternating magnetic fields of small amplitude has been devised and applied to the investigation of the response of conducting bodies placed in an electromagnetic field.

The results have indicated how the position, dimensions, and dip of buried conductors may be evaluated.

Introduction

The principle upon which one of the electromagnetic inductive methods of geophysical investigation is based is that transfer of power from a horizontal exciting loop to a conductor beneath the surface results in a deformation of the phase and amplitude of the magnetic field at points within the loop. This field has two components, one a small, nearly horizontal secondary field whose phase and amplitude are functions of the distance from the conductor and the other a primary field which is vertical except in the regions close to the edge of the loop. The two combine to form a rotating variable amplitude field vector, describing an ellipse of polarization (1). A study of the characteristics of the ellipse of polarization leads to information concerning the size and shape of the conducting body.

When a square or circular horizontal exciting loop is used the calculation of the amplitude and phase distortion encounters severe mathematical difficulties since the boundary conditions of current flow in conductors placed in a cylindrical electromagnetic field are extremely difficult to apply. The use of scale model conductors affords a method of investigating phase and amplitude variations in those cases in which the mathematics is too involved.

In an electromagnetic model which is to be a true geometric reduction of the original, it is desirable that the electromagnetic vectors at corresponding points be identical, so that the model will constitute a direct reading replica of the field problem. Consideration of Maxwell's equations shows that if the intensities and phase of the electric and magnetic fields are to be preserved in the model, a change in linear scale must be compensated by changes in the frequency of the exciting field and the conductivity (4).

Slichter has shown a close agreement between the theoretical and experimental response of conducting spheres in the vicinity of a vertical exciting loop (3). Thus model experiments using a horizontal exciting loop would be expected to produce some of the large amount of detailed knowledge concerning electromagnetic response which is necessary for the successful interpretation of field data.

[1] *Manuscript received in original form October 6, 1950, and, as revised February 21, 1951. Contribution from the Department of Physics, The University of British Columbia, Vancouver, B.C.*

Experimental Arrangement

In these model experiments the source field was produced by a plane circular horizontal loop 10 ft. in diameter below which the conducting bodies were supported on nonconducting stands, either inside or outside the loop. An exciting frequency of 50,000 cycles was utilized, corresponding to a scale factor of 100 to 1 on the basis of 500 cycle field work. Power for the field was supplied by a signal generator with voltage and power amplification stages.

Phase and amplitude measurements were made by detecting the e.m.f. induced in a 1 cm. radius vertical coil which could be placed at any point on a diameter of the loop. The amplitude of the e.m.f. induced in the search coil was given by a vacuum tube voltmeter calibrated to read the ratio between the horizontal field at any point and the undistorted vertical field at the center of the loop. The phase changes relative to the phase of the exciting field were measured by comparing the phase of this same e.m.f. with the output of a Drysdale variable phase constant amplitude transformer (2). The use of metal where it might influence the measured field was carefully avoided. All leads and equipment were shielded, and the measuring apparatus was removed some distance from the exciting loop.

The response of the following brass conductors at the center of the loop or at a distance 2.0 ft. from the center was noted for varying distances below the loop plane.

1. Cylinder 2½ ft. long, 1 ft. diameter,
2. Cylinder 3 in. long, 1 ft. diameter,
3. Disc. $^3/_{16}$ in. thick, 1 ft. diameter,
4. Rings $^3/_{16}$ in. thick, 1 ft. outside diameter 1½, 1, ¾, ½ in. wide respectively,
5. Plate 24 by 12 by ⅛ in.
6. Box of ⅛ in. brass, 24 by 12 by 3 in., fitted with angled end pieces to give a horizontal top surface for various angles of dip.,
7. Solid bar 1½ in. square, 11 in. long,
8. Box of ⅛ in. brass of same dimensions as conductor #7.

The response of conductor #6 placed 2 ft. outside the loop was investigated both when the conductor dipped toward and away from the loop. All readings of relative amplitude and phase were taken along a diameter of the loop directly above the center line of each conductor at intervals appropriate for accurate plotting.

Correction Applied to Measurements

It was found that when the search coil was rotated 180° about a vertical axis the magnitude of the voltages induced in the coil in the two positions were not the same and their phase did not differ by 180°. The discrepancy was attributed to extraneous potentials induced in all parts of the search coil circuit.

If the extraneous voltage is assumed to be the same for both orientations of the search coil and is represented by a vector V and if a vector V_1 represents the voltage which would be induced in the search coil by the secondary horizontal field component alone and V_2 represents the voltage induced by the same field component when the coil is rotated 180°, while vectors V_1, V_2 denote the phase and amplitude of the total induced voltage for the same two orientations of the coil, then the following diagram provides a means of evaluating V_1.

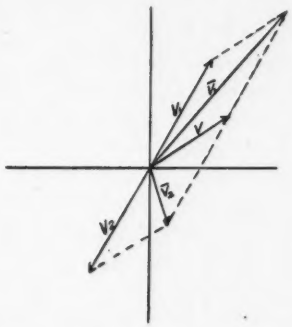

Since V_1 is proportional to the horizontal field component, determinations of the relative phase and amplitude of this component at different points may be made.

It was found necessary to subtract from these values a small field which was present even when all conductors were removed from the loop. This field varied over the loop but at any point was constant from day to day. The final resultant represented the response from the conductor alone.

Model Results

The following items of interest were noted:

(*a*) *Cylindrical Conductors Within the Loop*

1. A 180° phase discontinuity existed over the center of all conductors (Fig. 1).
2. Phase curves were symmetric about the center line of the conductors.
3. The position of phase maxima corresponded approximately to those of relative amplitude maxima.
4. The shape of the phase curves was independent of the depth or depth extent of the conductor and its position within the loop.
5. The amplitude values approached zero over the center of the conductor.
6. Maxima occurred near the boundaries of the conductors, and their value decreased rapidly as the depth to the conductor increased (Fig. 4).

7. The two maxima were equal for all conductors placed at the center of the loop.
8. When the conductors were off-center the two maxima were equal for conductors of short depth extent and unequal for long conductors (Figs. 2 and 3), thus providing a means of differentiating between the two types.

(*b*) *Rectangular Conductors Within the Loop*

1. The response of solid and hollow conductors of the same outside dimensions was found to be identical.
2. For 90° dip the phase and amplitude curves were similar to those from cylindrical conductors (Fig. 7).
3. The position of the 180° phase discontinuity and the relative amplitude minimum varied with dip (Figs. 7 and 8).
4. Relative amplitude maxima occurred slightly outside the edges of the vertical conductors and were approximately equal over the sides and ends provided the ratio of length to width was not greater than 5.
5. For dipping conductors, maxima occurred over the sloping surface and over the acute angled edge. The position of the maximum over the sloping surface depended on the dip and depth of the conductor while the magnitude of the other maximum depended on the dip and depth, but its position remained essentially constant, being directly above or slightly inside the edge of the conductor (Figs. 7 and 8).
6. The ratio between the two maxima was a double valued function of the dip (Fig. 9).

(*c*) *Rectangular Conductors Outside the Loop*

1. The phase discontinuity over a conductor was not of the same shape or magnitude as inside the loop (Figs. 10 and 11).
2. For a 0° dip the two amplitude maxima were unequal but occurred directly over the edge of the conductor.
3. The greater amplitude maxima still occurred over the acute angled edge, and the ratio of the two maxima was much greater for conductors dipping away from the loop than for those dipping toward the loop.

Inferences from Relative Amplitude Curves

The induced eddy currents were apparently concentrated near the edge of the top surface, as was determined by noting variations of the maximum as concentric rings were removed from the center of a disc. Negligible change was noted until the width of the ring reached 1 in. A histogram was plotted, the area of each section of which was a measure of the fraction of the amplitude maximum contributed by each of the annular rings. On the assumption that the total surface current varied directly as the amplitude maximum, a smooth normalized curve was constructed from this histogram (Fig. 5). Thus the

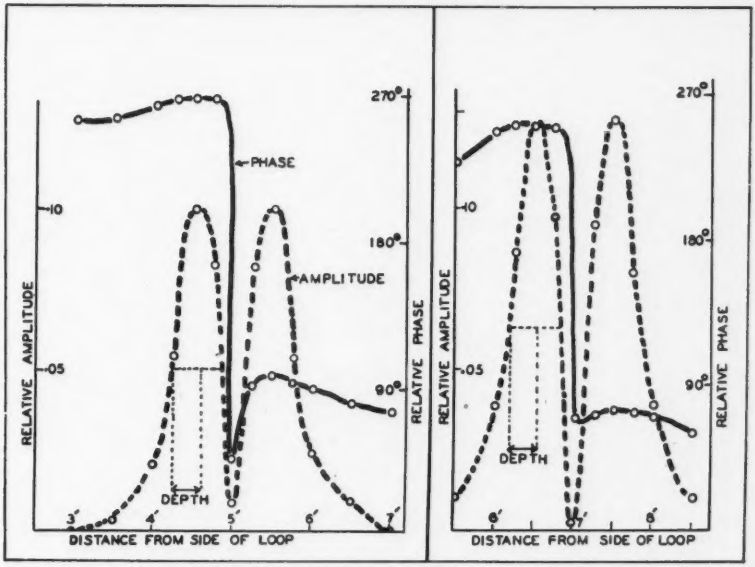

FIG. 1. *Conductor #3 at loop center, 4 in. deep.*
FIG. 2. *Conductor #1 at loop center, 4 in. deep.*

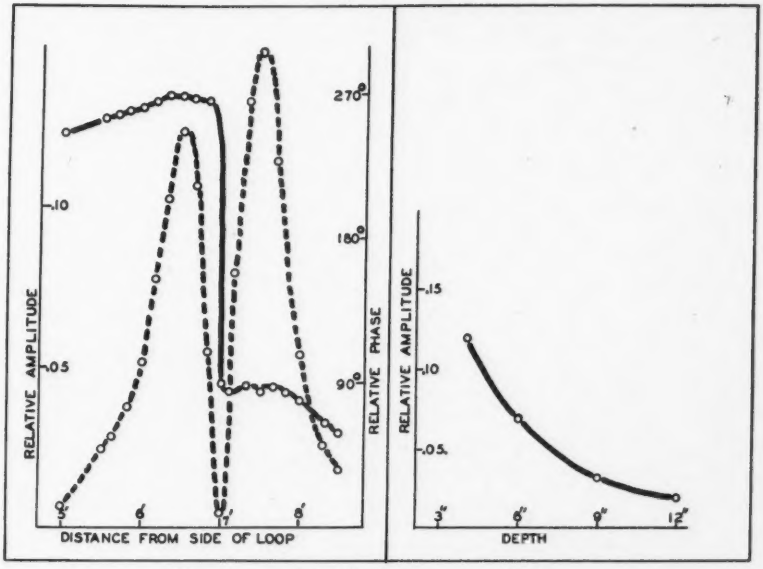

FIG. 3. *Conductor #1 off loop center, 4 in. deep.*
FIG. 4. *Variation of amplitude with depth, Conductor #1.*

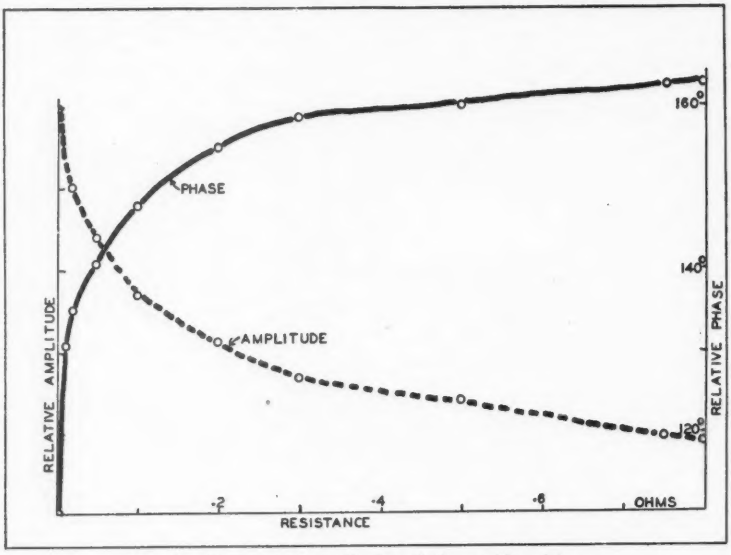

FIG. 6. *Variation of amplitude and phase with resistance.*

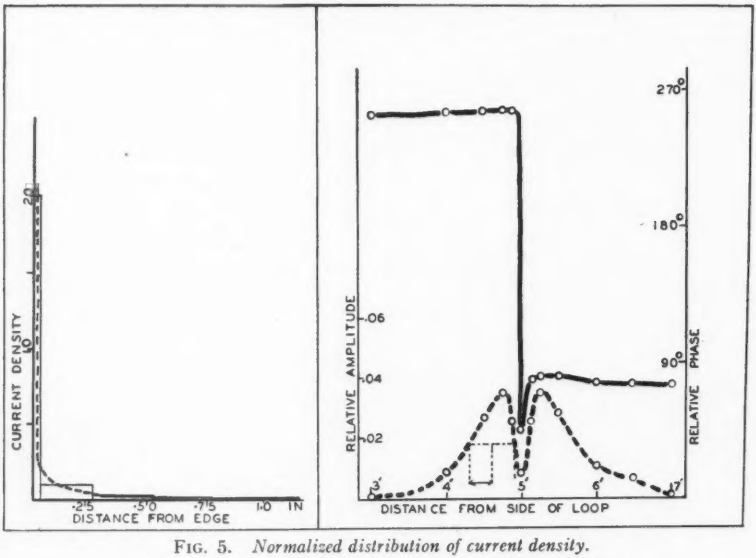

FIG. 5. *Normalized distribution of current density.*
FIG. 7. *Conductor #6 at loop center, depth 4 in. dip 90°.*

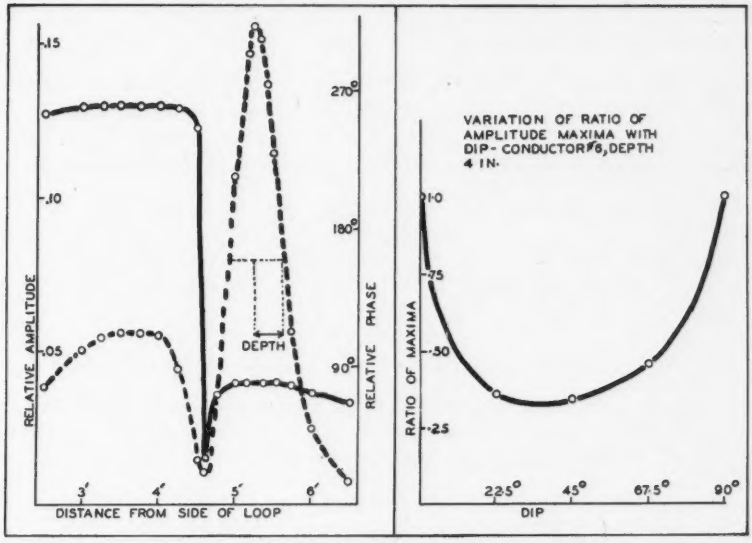

FIG. 8. *Conductor #6 at loop center, depth 4 in. dip 22.5°.*
FIG. 9. *Variation of ratio of amplitude maxima with depth. Conductor #6, depth 4 in.*

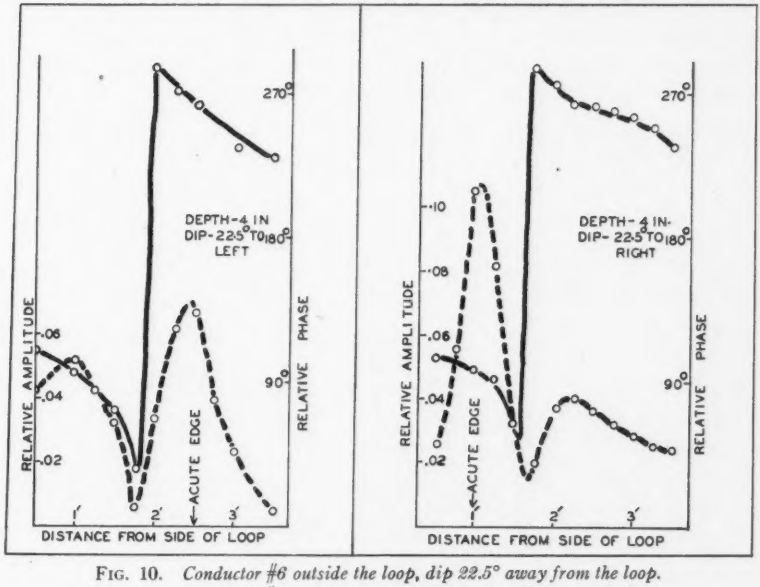

FIG. 10. *Conductor #6 outside the loop, dip 22.5° away from the loop.*
FIG. 11. *Conductor #6 outside the loop, dipping 22.5° toward the loop.*

concentration of eddy currents flow was approximately that which would be expected from a consideration of the skin effect.

Proof that the current flowed around the ring was demonstrated by cutting the ring and observing that the response dropped to a negligible value.

Effect of Change of Resistance on Phase and Relative Amplitude Curves

The variation of phase and relative amplitude with resistance was determined by inserting a 1.0 ohm variable resistance in a very narrow gap in the half inch wide brass ring. Phase and amplitude measurements for various values of resistance were taken at the position of the relative amplitude maxima. The results are shown in Fig. 6.

Application of Model Response to Field Interpretation

In field practice one wishes to use the measured response from conductors to determine their size, dip, vertical extent, and conductivity. A study of the response of models indicates how these parameters may be obtained.

Once the position of the conductor is known from a reconnaissance survey its detailed response at the center and some distance off center of the exciting loop may easily be obtained by shifting the loop.

If the conductor has a steep dip its boundaries may be obtained since they occur very nearly below the points of maximum amplitude response. Since the ratio of the maxima on either side of a conductor of short depth extent is not altered by its position relative to the loop, short conductors may be differentiated from those with considerable depth extent.

When the horizontal length of the conductor is large compared to its width the current near the long edges may be considered as an infinite line current. For such a current the half width of the amplitude response curve at half the maximum value is equal to the depth to the line current. This agrees well with the measured values (Fig. 7). It also appears to hold approximately for conductors whose horizontal length and breadth are the same (Figs. 1 and 2). It thus provides a means of estimating the depth to the surface of the conductor.

If the conductor dips, the position of the acute angled edge may be found accurately, since it lies below the larger maximum. The horizontal width cannot be deduced from the experimental curves, but the depth from the surface to the acute angled edge is given by the half width of the response curve at the half maximum value (Fig. 8).

For conductors of large depth extent an estimate of the dip may be made from the ratio of the two maxima (Fig. 9). Thus for dipping conductors their depth may be obtained quite accurately and their dip estimated.

Although Fig. 6 shows that both phase and amplitude depend on the total resistance of the conductor, insufficient evidence is available to deduce a

method of estimating the conductivity of the conductor from the experimental curves.

Acknowledgment

The authors wish to express their thanks to the National Research Council of Canada for the grant in aid of research under which these investigations were conducted.

References

1. HEILAND, C. A. Geophysical exploration. Prentice-Hall Inc., New York. 1946. p. 773.
2. LAWS, F. A. Electrical measurements. McGraw-Hill Book Company Inc., New York. 1938. p. 298.
3. SLICHTER, L. B. Geophysical prospecting. American Institute of Mining and Metallurgical Engineers. 1932. p. 443.
4. STRATTON, J. A. Electromagnetic theory. McGraw-Hill Book Company Inc., New York. 1931. p. 448.

PREDISSOCIATION AND DISSOCIATION OF THE N_2 MOLECULE[1]

BY A. E. DOUGLAS AND G. HERZBERG

Abstract

The predissociation in the upper state of the Lyman–Birge–Hopfield bands of nitrogen has been investigated under high resolution. A clear breaking-off of the fine structure has been found above $v' = 6$, $J' = 13$ both in the P and the Q branches. The predissociation limit is at 78,843 ± 50 cm.$^{-1}$ which is smaller than the well known dissociation limit 97,944 cm.$^{-1}$ by very nearly the excitation energy of the ^2D state of the N atom. This observation eliminates the intermediate value, 8.565 ev., for the dissociation energy of the N_2 molecule. A definite decision between the two remaining values, 9.756 and 7.373 ev., cannot yet be made. Acceptance of the former would involve the assumptions that the predissociation in the $a^1\Pi_g$ state is caused by the $^5\Sigma_g^+$ state resulting from normal atoms and that this $^5\Sigma_g^+$ state is not purely repulsive. The elimination of the value 8.565 ev. for $D(N_2)$ removes the value 7.5$_0$ ev. for D(CN) which has been fairly widely accepted.

A. Introduction

The dissociation energy of the nitrogen molecule has been the subject of much discussion in recent years. The present state of this problem has been summarized recently by one of us (6) and need not be reconsidered here in detail.

There is general agreement about the dissociation limit at 97,944 cm.$^{-1}$ (12.139 ev.)[2] which has been obtained from a predissociation limit in the upper $C^3\Pi_u$ state of the second positive group (see Fig. 1). The question is whether at this limit the molecule dissociates [1] into two atoms in the (metastable) ^2D state or [2] into one atom in the ^2D state and the other in the ^4S ground state or [3] into one atom in the (metastable) ^2P state and the other in the ^4S ground state. On the basis of a discussion of a predissociation in the upper $B^3\Pi_g$ state of the first positive group [investigated by van der Ziel (15)] Herzberg and Sponer (10) concluded that alternative [1] applied. But Gaydon (4) objected to the implicit use in Herzberg and Sponer's discussion of the selection rule $\Delta K = 0$ for the predissociation of a state ($^3\Pi_g$) that belonged by no means to pure case (b).

If the rule $\Delta K = 0$ is not used, a decision between the three alternatives [1], [2], and [3] is not possible on the basis of known spectroscopic data. Various indirect arguments have been used to make a decision, but not with concordant results. The present investigation was undertaken in the hope of obtaining a decision by a closer investigation of the predissociation in the $a^1\Pi_g$ state of N_2 which was first found by Herman (5) and later confirmed and discussed by G. and L. Herzberg (8). While this hope has not been fulfilled it has been pos-

[1] *Manuscript received March 13, 1951.*
Contribution from the Division of Physics, National Research Laboratories, Ottawa, Canada. Issued as N.R.C. No. 2437.

[2] *Throughout this paper the conversion factors used are those adopted in (6).*

sible to eliminate alternative [3], to obtain some evidence in favor of alternative [1], and to obtain independent support of the value of the dissociation limit at 12.139 ev.

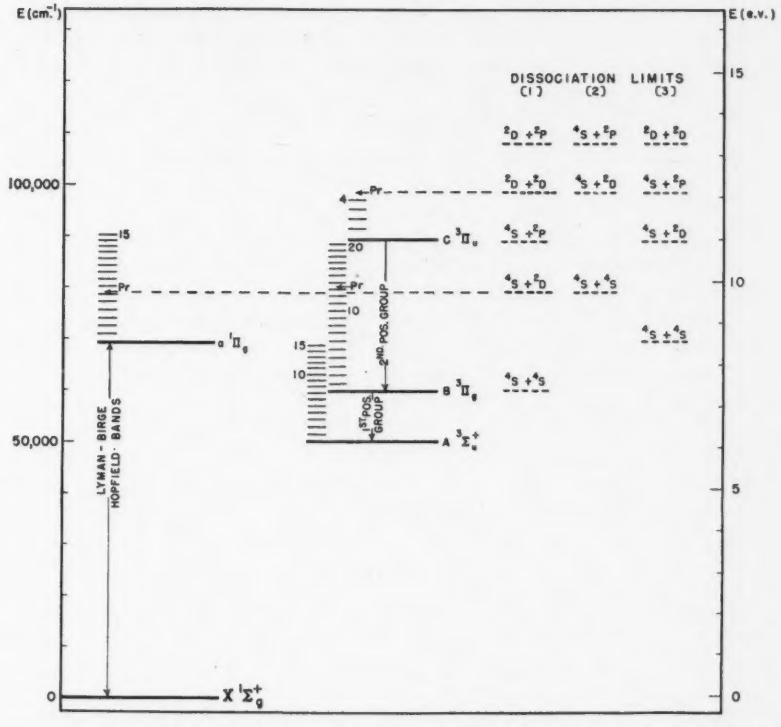

FIG. 1. *Part of the energy level diagram of the N_2 molecule. The three observed predissociation limits are indicated by short arrows marked Pr. The three columns at the right correspond to the three alternatives discussed in the text.*

B. Breaking-off in the Lyman–Birge–Hopfield Bands ($a^1\Pi_g - X^1\Sigma_g^+$)

The Lyman–Birge–Hopfield bands (in future referred to as a–X bands) of N_2 appear in any discharge through pure nitrogen even though not with very great intensity. They also occur in absorption below 1400Å with moderate intensity. As was shown by Herzberg (7) the a–X bands represent a forbidden transition, $^1\Pi_g - ^1\Sigma_g^+$. If these bands are excited at low pressure (less than 10 mm.) only bands with $v' \leq 6$ are produced while at higher pressures bands with v' up to 15 occur [see (5)]. We have investigated the breaking-off at low pressure under high dispersion (0.8Å per mm.) in order to ascertain whether there is also a breaking-off of the rotational fine structure. Using an electrodeless high frequency discharge at a pressure of the order of 0.001 mm. spectrograms

were obtained which showed a very clear breaking-off of the fine structure. Fig. 2 shows a spectrogram of the 6-14 band and for comparison one of the 5-13 band. The breaking-off is clearly visible both in the P and the Q branches of the 6-14 band. The R branch forms the head and is not sufficiently resolved to show the breaking-off clearly. In the P branch the breaking-off occurs at $J = 14$, in the Q branch at $J = 13$, that is, for the same value of the rotational quantum number of the upper state, $J' = 13$. The lines with $J' = 14$ and all higher lines are absent including all lines with higher vibrational quantum numbers. There can thus be no question that this is a genuine predissociation.

The energy of the breaking-off point, that is, the predissociation limit, is readily obtained. The head of the 6-14 band is at 48,549.4 cm.$^{-1}$ From the vibrational formula given by Herman (5) one finds that the $v'' = 14$, $J'' = 0$ level is 30,000 cm.$^{-1}$ above the ground state. The rotational constant B_6' was found from the combination differences $Q(J) - P(J)$ to be 1.500 cm.$^{-1}$ confirming the B_v formula given in (6). Using this B_6 value, the $J' = 13$ and $J' = 14$ levels are found to be 273 and 315 cm.$^{-1}$ respectively above the $J' = 0$ level. Taking the breaking-off point half-way between the levels $J' = 13$ and $J' = 14$ one obtains therefore for its energy above the $v = 0$, $J = 0$ level of the $X^1\Sigma_g^+$ ground state the value 78843 ± 50 cm.$^{-1}$ Here the uncertainty (± 50 cm.$^{-1}$) takes account of the fact that it is impossible to locate the limit closer than somewhere between the levels $J' = 13$ and $J' = 14$, and also includes the inaccuracy introduced by the fact that the vibrational constants have been evaluated from band heads not from band origins.

C. Discussion

Van der Ziel's predissociation has its limit at 79384 cm.$^{-1}$ and differs by 18560 cm.$^{-1}$ from the predissociation limit in the $C^3\Pi_u$ state (97944 cm.$^{-1}$) which has been shown to be equal to a dissociation limit. The proximity of this difference to the excitation energy of the ^2D state of the N atom, 19227 cm.$^{-1}$, has usually been considered as evidence that the two corresponding dissociation limits differ by the excitation energy of the ^2D state although some doubts have recently been raised [see (1)]. The energy of the new predissociation limit in the $a^1\Pi_g$ state, derived above, differs from the higher limit by 19101 cm.$^{-1}$ This difference is much closer to the ^2D excitation energy and makes it practically certain that there is a dissociation limit of the N_2 molecule at 78717 cm.$^{-1}$ Conversely this close agreement gives very strong support to the dissociation limit at 97944 cm.$^{-1}$

The very small remaining difference of 126 (± 50) cm.$^{-1}$ between the breaking-off point (predissociation limit) in the $a^1\Pi_g$ state and the dissociation limit is undoubtedly due to a slight potential hill separating the undissociated from the dissociated state. Such a hill will arise when the potential curves of the two states intersect at a point above the asymptote of the state causing the predissociation [case I(c)] or, if the point of intersection is below the asymptote, it may arise on account of the rotation of the system [case I(b)]. If case I(c)

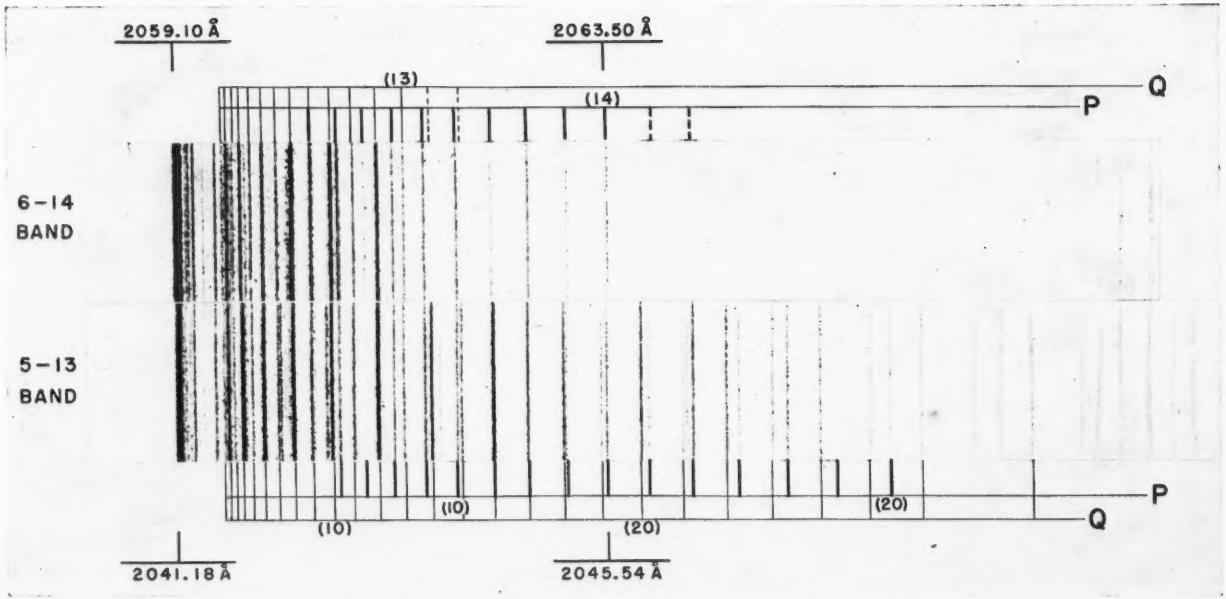

FIG. 2. *Spectrograms of the 6-14 and 5-13 bands of the a-X system of N_2.*

The lines of the P and Q branches are indicated by the short and long leading lines. The faint lines on the longward side of the breaking-off point in the 6-14 band can all be accounted for as due to an overlapping NO band. The intensity alternation in each branch should be noted. The last normal line of the P branch is a "strong" line, that of the Q branch a "weak" line in conformity with the Λ-type doubling in the upper state.

applies for the predissociation of the $a^1\Pi_g$ state of N_2 the potential maximum would be at an internuclear distance corresponding to the right limb of the potential energy curve of the $^1\Pi_g$ state, that is, assuming a Morse curve, at approximately 1.46Å. Substituting this r value into $B = h/8\pi^2 c\mu r^2$ yields $B \approx 1.13$ cm.$^{-1}$ The breaking-off point in case I(c) corresponds to the intersection of the *effective* potential curves and lies above the $K = 0$ curves by the amount $BK(K + 1)$ which in the present case ($B \approx 1.13$, $K = 13.5$) is 223 cm.$^{-1}$ Therefore the point of intersection of the $K = 0$ curves would be 97 ($\pm$ 50) cm.$^{-1}$ *below* the asymptote, contrary to the original assumption. Consequently the state causing the predissociation cannot be a purely repulsive state and the difference between breaking-off point and dissociation limit may well be due to a rotational potential hill at large r so that the point of intersection may be even lower than the value just given.

A similar consideration, applied to van der Ziel's predissociation in the $B^3\Pi_g$ state, shows that the point of intersection would lie 350 cm.$^{-1}$ below the asymptote of the state causing the predissociation which therefore also cannot be a purely repulsive state.

The conclusion that the difference of the dissociation limits responsible for the predissociation in the $C^3\Pi_u$ and $a^1\Pi_g$ states is equal to the excitation energy of the ^2D state of the N atom implies that at least one of the two N atoms at the higher limit (97944 cm.$^{-1}$) must be in the ^2D state and therefore at the lower limit (78717 cm.$^{-1}$) in the ^4S ground state. On this basis the intermediate value of 8.565 ev. for $D(N_2)$ [which has recently been revived, see (1)] is immediately and definitely excluded since it would involve the assumption that the dissociation products at the higher limit are in the states ^2P and ^4S.

The state of excitation of the second N atom at either predissociation limit is not as readily determined. It is the crucial question in the determination of the dissociation energy of the N_2 molecule. Only two possibilities need be considered: that the second N atom is in the ^4S ground state or that it is in the ^2D state. They correspond to the values $D(N_2) = 9.756$ and 7.373 ev. respectively. Any higher excitation of the second N atom would make $D(N_2)$ smaller and that appears impossible since the vibrational levels of the ground state have been observed up to 6.6 ev.

We have therefore to consider the two alternatives that at the 9.770 ev. (78819 cm.$^{-1}$) predissociation limit the products are $^4S + {}^4S$ or $^4S + {}^2D$. The molecular states arising from these combinations are $^1\Sigma_g^+$, $^3\Sigma_u^+$, $^5\Sigma_g^+$, $^7\Sigma_u^+$, and $^3\Sigma_g^+$, $^3\Sigma_u^+$, $^3\Pi_g$, $^3\Pi_u$, $^3\Delta_g$, $^3\Delta_u$, $^5\Sigma_g^+$, $^5\Sigma_u^+$, $^5\Pi_g$, $^5\Pi_u$, $^5\Delta_g$, $^5\Delta_u$ respectively. The rigorous selection rule that only states of the same parity can predissociate into one another eliminates immediately the states $^3\Sigma_u^+$, $^7\Sigma_u^+$, $^3\Sigma_u^+$, $^3\Pi_u$, $^3\Delta_u$, $^5\Sigma_u^+$, $^5\Pi_u$, $^5\Delta_u$ as possible states causing the predissociation of the $a^1\Pi_g$ state.

The $^1\Sigma_g^+$ state can be eliminated on the basis of the nature of the predissociation discussed in Section B. As is well known, in $^1\Pi - {}^1\Sigma$ transitions the upper states of the P and R branches are not identical with those of the Q branches

but belong to opposite Λ-doublet components. Therefore the observation that the breaking-off in the $a^1\Pi_g - X^1\Sigma_g^+$ bands of N_2 occurs at the same J' value in both the P and the Q branches shows conclusively that both Λ-doublet components of the $a^1\Pi_g$ state are affected by the predissociation. If the $^1\Sigma_g^+$ state were causing the predissociation only one Λ-doublet component for each J' could be predissociated since the other would not have the right $+-$ symmetry [see (6)].

We are thus left with the following possibilities for the state causing the predissociation of the $a^1\Pi_g$ state: $^5\Sigma_g^+$ from $^4S + {}^4S$ and $^3\Sigma_g^+$, $^3\Pi_g$, $^3\Delta_g$, $^5\Sigma_g^+$, $^5\Pi_g$, $^5\Delta_g$ from $^4S + {}^2D$. All of these would be forbidden predissociations violating the (nonrigorous) selection rule $\Delta S = 0$. The observation that the predissociation occurs only at low pressure does indeed indicate that the radiationless transition probability is low [see (9)]. This conclusion is strengthened by the fact that the $a - X$ transition itself is a forbidden transition and therefore the lifetime of the $a^1\Pi_g$ state is large so that it is more susceptible to radiationless transitions of low probability. Even considering this it does seem rather unlikely that the $^5\Sigma_g^+$ state causes the predissociation of the $a^1\Pi_g$ state since it would involve $\Delta S = 2$. In other words it appears rather unlikely that the predissociation can lead to two normal N atoms in the ^4S state. On this basis the low value $D(N_2) = 7.373$ ev. is somewhat favored.

Another argument tending to eliminate the $^5\Sigma_g^+$ state as the cause of the predissociation in the $a^1\Pi_g$ and $B^3\Pi_g$ states may be derived from elementary valence theory. Both the Heitler–London and the Hund–Mulliken methods lead one to expect the $^5\Sigma_g^+$ state arising from two normal N atoms in the ^4S state to be unstable [see (6)]. Since, as we have seen, the states causing the predissociations in the $a^1\Pi_g$ and $B^3\Pi_g$ states have at least slight potential minima, it appears unlikely that either one is identical with the $^5\Sigma_g^+$ state and therefore that two ^4S atoms are the dissociation products. However, it must be admitted that this argument is not conclusive since it is difficult to exclude the possibility that in higher approximations the theory would yield a slight stability of the $^5\Sigma_g^+$ state.

A further point that at first was thought to support the low $D(N_2)$ value but on closer study proved to be indecisive is the following: if both states involved in a predissociation belong to Hund's case (b) the selection rule $\Delta K = 0$ applies. It is readily seen that this leads again to only a partial predissociation of a multiplet Π state by a multiplet Σ state since, for a given level of the Π state, only one Λ-doublet component has the same $+-$ symmetry as the level of equal J and K in the Σ state [see (6)]. An excellent example is the predissociation of the $C^2\Pi$ state of MgH [see Pearse (12)]. Conversely when complete predissociation is observed one may conclude that the state causing the predissociation cannot be a Σ state. If one were to apply this rule to the predissociation of the $a^1\Pi_g$ state of N_2 one would conclude that the $^5\Sigma_g^+$ and $^3\Sigma_g^+$ states are eliminated and this would settle the question of the dissociation energy. However, the selection rule $\Delta K = 0$ holds only for transitions with

$\Delta S = 0$ (nonintercombinations) as in the case of MgH. For intercombinations ($\Delta S \neq 0$) this rule does not even approximately hold because they are due to spin-orbit interaction which is assumed to be negligibly small in the derivation of the rule $\Delta K = 0$. Indeed the detailed calculations of Budó and Kovács (2) show that in perturbations between singlet and triplet states the interactions of levels with different K are of the same order as those of levels with the same K if all other selection rules are fulfilled.[3] Thus the ΔK rule cannot be used in order to eliminate the states $^5\Sigma_g^+$, $^3\Sigma_g^+$ as causing the predissociation under consideration.

D. Conclusion

Of the three alternatives for $D(N_2)$ mentioned in the introduction the third has been definitely eliminated. Whether the first or the second alternative is correct could be decided on the basis of the data here presented if it were possible to say unambiguously whether or not a quintet state can cause an observable predissociation in a singlet state and whether or not the $^5\Sigma_g^+$ state arising from normal nitrogen atoms is purely repulsive. Since this has not been done the two values 7.373 ev. and 9.756 ev. still remain possible alternatives for $D(N_2)$. However, it must be realized that the adoption of the higher of these values would imply that the predissociation here considered is a singlet-quintet transition and that the $^5\Sigma_g^+$ resulting from normal N atoms is not purely repulsive.

The elimination of the intermediate value 8.565 ev. for $D(N_2)$ leads to the elimination of the value 7.50 ev. for the dissociation energy of the CN molecule, a value that has been fairly widely accepted in the literature (1, 3, 14). This $D(CN)$ value is based on a convergence limit obtained by Schmid, Gerö, and Zemplén (13) from an extrapolation of the vibrational levels of the $A^2\Pi$ state of CN with the help of data from perturbations in the $B^2\Sigma$ state. The values of $D(CN)$, $D(N_2)$, and $D(CO)$ are related to one another by the equation

$$D(CN) = \tfrac{1}{2}D(N_2) + D(CO) - 7.7_5 \text{ ev.},$$

which is based on various thermochemical data, particularly the now fairly well established heat of formation of CN [see (1, 11)]. No combination of the two possible values for $D(N_2)$ and the three possible values for $D(CO)$ gives 7.50 ev. for $D(CN)$ while the now excluded $D(N_2) = 8.565$ ev. would have given this $D(CN)$ value with $D(CO) = 11.108$ ev. The true value of $D(CN)$ may be any one of the six values obtained by combining the two $D(N_2)$ and three $D(CO)$ values. But the $D(CN)$ value 7.5_0 ev. must be considered as eliminated.

Acknowledgments

We are grateful to Dr. T. Y. Wu (Ottawa) for discussions and to Prof. I. Kovács (Budapest) for correspondence with regard to the selection rules for perturbations.

[3] *We are indebted to Prof. I. Kovács and Dr. T. Y. Wu for pointing this out to us.*

References

1. BREWER, L. and TEMPLETON, L. K. Unpublished report.
2. BUDÓ, A. and KOVÁCS, I. Z. Physik, 109: 396. 1938.
3. GAYDON, A. G. Dissociation energies and spectra of diatomic molecules. Chapman and Hall Limited, London. 1947.
4. GAYDON, A. G. Nature, 153: 407. 1944.
5. HERMAN, R. Compt. rend. 217: 141. 1943; Ann. phys. 11: 20. 241. 1945.
6. HERZBERG, G. Molecular spectra and molecular structure I. Spectra of diatomic molecules. 2nd Edition. D. Van Nostrand, New York. 1950.
7. HERZBERG, G. Phys. Rev. 69: 362. 1946.
8. HERZBERG, G. and HERZBERG, L. Nature, 161: 283. 1948.
9. HERZBERG, G. and MUNDIE, L. G. J. Chem. Phys. 8: 263. 1940.
10. HERZBERG, G. and SPONER, H. Z. physik. Chem. B, 26: 1. 1934.
11. LONG, L. H. Proc. Roy. Soc. 198: 62. 1949.
12. PEARSE, R. W. B. Proc. Roy. Soc. 122: 442. 1929.
13. SCHMID, R., GERÖ, L., and ZEMPLÉN, J. Proc. Phys. Soc. (London) 50: 283. 1938.
14. SPRINGALL, H. D. Trans. Far. Soc. 43: 177. 1947.
15. ZIEL, A. VAN DER. Physica, 1: 353. 1934.

ABSORPTION CORRECTIONS FOR RADIUM STANDARDIZATION[1]

By G. M. Keyser[2]

Abstract

The absorption corrections necessary for radium standardization have been redetermined. The measuring equipment and technique have been investigated to find the conditions necessary for minimum error. A lead filtered, aluminum walled chamber was found to have the best characteristics. The electronic absorption coefficients measured with this chamber fit an empirical formula depending only on the atomic number. This formula gives a value for the absorption coefficient of radium salts which was compared with a direct experimental value.

Introduction

The figure given for radium content of medical or industrial preparations is the result of an intercomparison of gamma-ray intensities with a standard of known content. The intensities are compared using an ionization chamber and an electroscope or other current detecting device. A description of the equipment and technique in use at various national laboratories has been given by: Oddie (6) for Australia, Curtiss (1) for the United States, Perry (9) for England, and Laurence (4) for Canada.

A figure for radium content can be obtained by multiplying the ratio of ionization currents by the content of the standard. This figure is sometimes called the "Equivalent Content." Although it can be determined with considerable accuracy it is seldom used since it is preferable to work with a figure giving the actual weight of radium. It is customary to measure the "Equivalent Content" and then apply a correction to get the actual weight of radium or "Actual Content." The necessity for the correction is caused by the absorption of the gamma rays in the radium container and the radium salt itself. In a typical case, the standard is in a thin glass tube which reduces the ionization by about 0.8% and the sample to be measured is in a platinum tube with 0.5 mm. walls which absorb about 5%. The difference in these figures, 4.2%, must be added to the equivalent content to correct for wall absorption. A similar correction must be applied where the gamma rays from the standard and the sample to be measured pass through different amounts of the radium salt. In a typical case where a 250 mgm. sample was measured the salt correction amounted to 3.4%. The corrections can be calculated if the dimensions and material of the sample and standard are known and can be combined with experimental absorption measurements. This paper is a report of such measurements and the results are arranged so that the correction necessary to convert "Equivalent Content" to "Actual Content" can be calculated.

[1] *Manuscript received December 29, 1950, and as revised April 9, 1951.*
Contribution from the Division of Physics, National Research Council, Ottawa. Issued as N.R.C. No. 2457.
[2] *Physicist, Radiology Laboratory, Division of Physics.*

Description of Equipment

The ionization chamber used for most of this work is shown in Fig. 1. The aim of the design was to provide an instrument similar to those used in the National Research Council yet flexible enough to attempt duplication of the measurements of other laboratories and to investigate the effects of ionization chamber design on the absorption corrections. The chamber itself consisted of a hollow aluminum cylinder with walls 5 mm. thick. This was covered with a close fitting lead shield 10 mm. thick. The front of the shield was left open so that filters of various thickness could be used. The collecting electrode was a disc of aluminum with rounded edges. The current detector was a d-c. amplifier using an FP–54 electrometer tube in a DuBridge and Brown circuit (2).

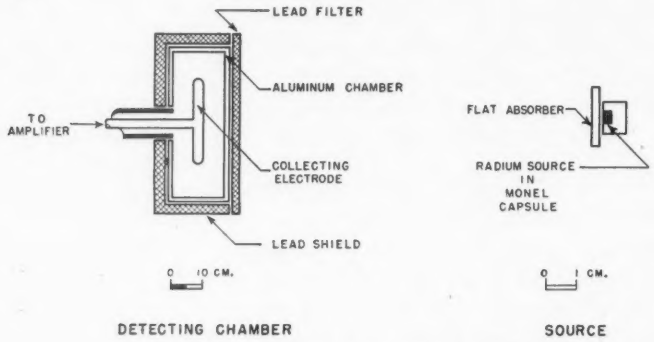

FIG. 1. *Special ionization chamber and radium source.*

Two special radium sources were obtained from Eldorado Mining and Refining (1944) Ltd. of Ottawa, Ontario. One source consisted of a compacted pellet of radium bromide 3 mm. diameter and 3 mm. high sealed in a monel capsule with one face 1.0 mm. thick. This source contained about 40 mgm. of radium. The second source contained about 20 mgm. of radium sulphate in a monel tube with walls 0.2 mm. thick and outer diameter 1.24 mm.

Two sets of platinum alloy absorbers were used. The alloy, 10% iridium and 90% platinum, is the one normally used for radium containers. The first set was a series of flat sheets 2 cm. square and with thicknesses: 3.98 mm., 2.025 mm., 0.985 mm., 0.565 mm., 0.296 mm., and 0.148 mm. The second set was a series of tubes with wall thicknesses: 3.96 mm., 2.05 mm., 0.962 mm., and 0.488 mm. This set had a fixed internal diameter of 1.50 mm. to hold the special tube source. The determination of the exact wall thickness of these tubes was done by the Metrology Section of the National Research Council. This was done by using a rod that fitted snugly in the hole of the tubes. The rod rested on V blocks at each end. A sensitive test indicator could then measure the distance between the rod and the outside of the tube.

This method was accurate to + 0.005 mm. The results indicated that the holes were both eccentric and varied in size throughout the length. This made it impossible to ascertain a mean wall thickness with an accuracy greater than 3%.

The absorption measurements were made by placing the absorbers in front of, or around, the radium sources and the two intensities of ionization noted. Since the absorption follows an exponential law with thickness it can be expressed as:

$$\frac{I_0}{I} = e^x$$

where I_0 is the ionization current without the absorber, I is the current with the absorber, x can be written as μt where μ is the linear absorption coefficient, and t the thickness of the absorber in cm., or as $\mu_e n$ where μ_e is the electronic absorption coefficient or cross section in cm.^{2} and n is the number of electrons per cm.^{2} in the absorber. There is a relationship between the two absorption coefficients:

$$\mu_e = \frac{A}{NZd}\mu$$

where A is the atomic weight and Z the atomic number of the absorber, N is Avogadro's number, 6.03×10^{23}, and d is the density of the absorber in grams per cc.

Effect of Chamber Walls

Ionization is produced in the chamber by electrons knocked out of the wall by the gamma radiation. Only the innermost part of the wall (0.5 cm. of aluminum) contributes any electrons. The remainder of the wall acts only as a filter for the gamma rays. In the filtering and electron production, the wall controls the efficiency of ionization for the various energy components of the gammas. Experience has shown that the greatest errors in radium measurement lie in the absorption correction. These can be reduced by using an ion chamber that is only sensitive to gamma rays with an energy that has a minimum absorption coefficient.

Chambers using a wall with lead on the outside as a filter and aluminum on the inside as a source of electrons have been used in standardization. These have the advantage over solid lead chambers with no aluminum lining that the electrons are produced only through the Compton effect which has very little energy dependence. The solid lead chambers produce electrons through the photoelectric process as well, but these electrons come from low energy gamma rays and hence increase the absorption correction.

The absorption coefficients found with various types of wall give an indication of the suitability of that wall. Measurements were made using the set of flat platinum absorbers, the first source and the special chamber arranged to have five types of wall.

(*a*) The aluminum chamber was lined completely with 1.5 mm. of lead and the outside face was covered with 5 mm. of lead.

(*b*) The aluminum chamber had all lead removed.

(*c*) The aluminum chamber had a 1.5 mm. lead filter on the outside face.

(*d*) The aluminum chamber had a 5 mm. lead filter on the outside face.

(*e*) The aluminum chamber had a 10 mm. lead filter on the outside face.

The results of these measurements are shown in Table I and on the graphs in Fig. 2.

TABLE I

LINEAR ABSORPTION COEFFICIENT OF PLATINUM IN CM.$^{-1}$

Chamber type	Platinum absorber thickness in mm.					
	.148	.296	.565	.985	2.025	3.98
a		1.26 cm.$^{-1}$ ±.10		1.22 cm.$^{-1}$ ±.05		1.19 cm.$^{-1}$ ±.03
b	2.170 ±.100		1.820 ±.080		1.440 ±.080	1.230 ±.080
c	1.200 ±.160		1.230 ±.050		1.180 ±.050	
d	0.960 ±.050	0.964 ±.030	0.990 ±.015	0.980 ±.020	0.990 ±.015	0.985 ±.012
e				1.000 ±.050	0.960 ±.050	0.960 ±.060

Much higher absorption coefficients for the platinum absorbers were found by using the solid lead chambers than with the aluminum lined chambers, as foreseen in the previous discussion. With large thicknesses of absorber the coefficient decreased but it was distinctly larger than the values found with the aluminum lined chamber even when the absorber reduced the intensity sufficiently to make the readings inaccurate. For this reason the lead lined chamber was not used for remainder of these measurements. It is of interest to note that Perry (10) finds absorption coefficients of 1.14 cm.$^{-1}$ using the National Physical Laboratories solid lead chamber.

The chamber (*b*) gave coefficients similar to those noted by many other experimenters. With a lead filter the coefficients decreased and approached a limiting value of about 1.00 cm.$^{-1}$ With a 5 mm. lead filter the values were near this minimum and showed no variation with different thicknesses of absorber. A thicker lead filter showed no improvement and decreased the ionization.

The chambers used for routine radium standardization by the National Research Council are similar to the ones described by Laurence (4). These

have ¼ in. aluminum walls and ¼ in. lead filters. Absorption coefficients were determined with one of these chambers using the technique described earlier. The results agreed at all points within one per cent of the results using the special chamber (*d*). This is as expected since the only difference is that the ¼ in. lead filter is slightly thicker and increased thickness has already been shown to cause no change in the absorption coefficient.

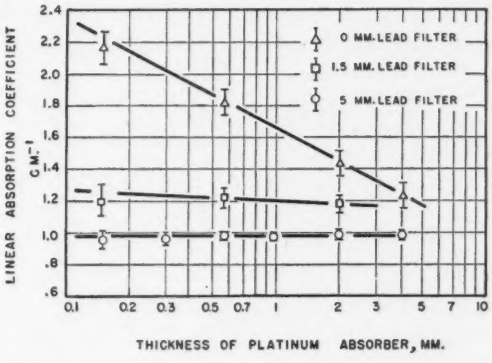

FIG. 2. *Variation in linear absorption coefficient for three thicknesses of lead filter.*

Variation with Distance

The distance between the radium and the ionization chamber during the measurement is not fixed for all measurements. It is necessary to measure the absorption coefficient with varying distances between the source and the chamber. At distances between one and four meters the absorption coefficient showed no changes greater than 3% which was the limiting accuracy of the measurement. At smaller distances the accuracy was too low to give any conclusive results, but there was no indication of any large change in the absorption coefficient.

These measurements can also be used to show the variation in the ionization current with distance. All readings within the range one-half to four meters were within 5% of the value expected from the assumption that the response is inversely proportional to the square of the distance from the center of the chamber.

Correlation with Cylinders

All the above work was done with the flat absorbers and the first source of radium. (The flat absorbers were used to simplify finding the thickness.) Normally the radium container walls are in the shape of a cylindrical tube. The curvature of the wall must be taken into account in calculating the absorption corrections from the coefficients as obtained above.

Theory of absorption in the wall of a cylindrical tube has been studied by Owen and Naylor (7), Evans and Evans (3), and others. Using the method of Evans and Evans, a value for the effective wall thickness was calculated and a curve representing the results is shown in Fig. 3. In this graph the ratio of the effective wall thickness and the actual wall thickness of the absorber tube is plotted against the ratio of the internal radius of the tube and the actual wall thickness. Thus with the dimensions of radium tube a value for the effective wall thickness can be found and this used with the linear absorption coefficient to get the absorption correction.

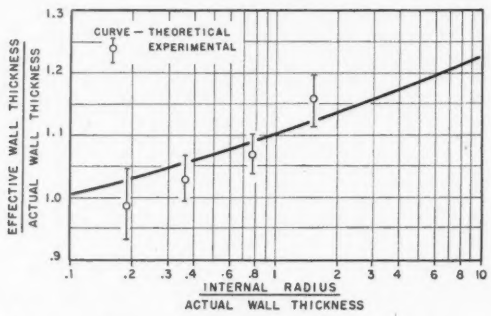

FIG. 3. *Effective wall thickness of cylindrical absorbers.*

The curve was checked experimentally with the special set of platinum tubes mentioned earlier. Using .985 cm.$^{-1}$ for the linear absorption coefficient of the tube and a measurement of the absorption, the effective wall thickness was found. The ratio of this and the actual wall thickness was then plotted on Fig. 3. The large error indicated is principally due to the variation in the wall thickness of the tubes.

Scattering Corrections

If the standard and the radium to be measured are not of comparable shape scattered radiation might be of considerable importance. Measurement of the scattered radiation was attempted through the introduction of additional scattering agents. The position of these is shown in Fig. 4. Under ordinary conditions the nearest material that could cause any scattering is 1.5 meters below the equipment. A table placed directly under the equipment simulated the effect of operation near a floor or wall. With this in place the reading increased 3.8%. Covering the table with lead produced no change in the reading. A lead block directly behind the source changed the reading by less than ½%. Another lead block, 2 in. thick and with a ¾ in. hole through it, placed in front of the source with the hole arranged to pass all the direct radiation increased the reading less than 0.3%.

With scattering representing such a small fraction of the radiation there will be no occasion where the shape of the source will introduce any change in the ionization through scattering.

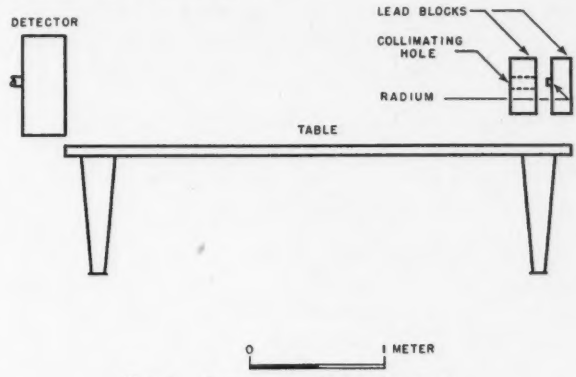

FIG. 4. *Arrangement of scattering agent.*

Magnitude of the Absorption Coefficient

Absorption corrections must be known occasionally for unusual wall materials and radium mixtures. Perry (10) made use of a graph of the absorption against atomic number to interpolate for the absorption of radium element.

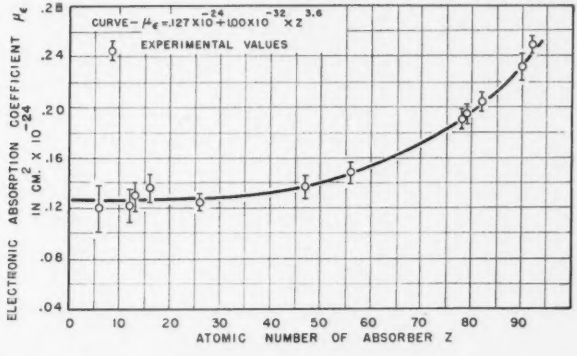

FIG. 5. *Magnitude of the electronic absorption coefficient of all elements.*

Perry assumed that the photoelectric component of the absorption would depend on Z^3. Mayneord and Cipriani (6) calculated that at 1.2 Mev. the dependence should be $Z^{3.56}$.

The electronic absorption coefficients of a series of elements were measured and are plotted against the atomic number in Fig. 5. The elements measured were uranium, thorium, lead, gold, platinum, barium, silver, iron, sulphur,

aluminum, magnesium, and graphite. Curves were fitted to the points to establish an empirical formula for the absorption coefficient.

A curve depending on Z^3 can not be drawn to pass within the experimental error of every point, whereas a curve depending on $Z^{3.6}$ will do this. The formula for the curve that gives the best fit to these points is:

$$\mu_e = 0.127 \times 10^{-24} + 1.00 \times 10^{-32} Z^{3.6}.$$

The fit of the points on this curve indicates that the formula will give the absorption coefficient for any element within 2%.

Salt Corrections

The usefulness of this formula is in particular evidence in making corrections in the radium salt itself. When the value of the electronic absorption coefficient is known it is possible to calculate the salt correction. According to Paterson *et al.* (8) the salt absorption for a cylindrical source can be calculated as:

$$\frac{I}{I_0} = 1 - \frac{8}{6\pi} x + \frac{1}{8} x^2 - \frac{4}{45\pi} x^3$$

where I is the reading with absorption, I_0 is the reading had there been no absorption, and x is the absorption of a beam of gamma rays crossing the axis of the absorbing cylinder.

Dr. G. C. Laurence, in this laboratory in 1938, used a special glass radium tube made with ends of different size. The radium was loose in the tube and could be shaken into one end or the other. When the radium was in the large end the absorption was greater than when in the small end. This gave a difference in the reading that could be measured. This difference could also be calculated using the absorption coefficient for the salt and the above formula for the absorption of a cylindrical source. The calculated result for this particular measurement gave an expected ratio of the ionizations as 1.010. The actual measurement was made in the chamber described in (4) in 1938 and the results on two separate occasions were 1.008 and 1.0104.

Acknowledgments

The author wishes to express his appreciation to Dr. G. C. Laurence for permission to refer to his unpublished measurements, and to Dr. A. Morrison for his helpful advice and consultations.

This work was part of the research program of the Division of Physics of the National Research Council.

References

1. Curtiss, L. F. J. Optical Soc. Am. and Rev. Sci. Instruments, 63: 363. 1928.
2. DuBridge, L. A. and Brown, H. Rev. Sci. Instruments, 4: 532. 1933.
3. Evans, R. D. and Evans, R. O. Revs. Modern Phys. 20: 305. 1948.

4. LAURENCE, G. C. Can. J. Research, 7: 103. 1932.
5 MAYNEORD, W. V. and CIPRIANI, A. J. Can. J. Research, A, 25: 303. 1947.
6. ODDIE, T. H. Proc. Phys. Soc. (London), 51: 905. 1939.
7. OWEN, E. A. and NAYLOR, B. Proc. Phys. Soc. (London), 34: 92. 1922.
8. PATERSON, C. C., WALSH, J. W. T., and HIGGINS, W. F. Proc. Phys. Soc. (London), 29: 215. 1917.
9. PERRY, W. E. Brit. J. Radiology, 9: 648. 1936.
10. PERRY, W. E. Proc. Phys. Soc. (London), 57: 78. 1945.

SOME RESULTS ON THE ELECTRICAL BREAKDOWN OF LIQUIDS USING PULSE TECHNIQUES[1]

By W. D. Edwards[2]

Abstract

Polar and nonpolar organic liquids of relatively simple structure have been used as test liquids. To obtain reproducible results and to avoid the considerable errors due to minute solid particles an apparatus has been constructed in which the liquid may be distilled and the breakdown measurements made within a completely enclosed system and at pressures less than atmospheric when desired. Single, rectangular pulses of voltage were applied to a pair of highly polished, metal spheres immersed in the test liquids. Time delays in breakdown of the order of one microsecond, the exact value depending on the gap width, have been found for the liquids used. In the liquid state hexane and ethyl alcohol were found to have negative temperature coefficients of breakdown strength. The breakdown strength of benzene was found to depend on the cathode metal but was independent of the anode metal. A reduction in gap width gave rise to an increase in breakdown strength for benzene and *n*-hexane.

Introduction

In the construction of radar equipment it is necessary to provide insulation for electrical pulses of very short duration and high voltage. This is achieved by the use of low loss dielectrics of high electric strength. In applications of this type, it has been found that the electrical "breakdown" strength for pulsed voltages is greater than that for direct or low frequency alternating voltages. As far as is known, the effect has not been systematically investigated. The initial object of the research described here was to carry out such an investigation by ascertaining the breakdown strength for pulses of different length. However, as the program developed, it became evident that the effect was connected with the fundamental properties of the material and that a more complete study of the intrinsic breakdown process was desirable.

The electric strength of a dielectric is considered here as an intrinsic property of the substance determined by its constituent ions, atoms, or molecules and their state of aggregation. Distinct from this are the values of breakdown strength obtained under experimental conditions which more or less mask the true, intrinsic breakdown strength of the material. Examples of such experimental conditions are a-c. voltages, nonuniform fields, prolonged voltage applications leading to breakdown due to thermal effects, and breakdown in the presence of corona. Such breakdown is here referred to as "technical" breakdown as distinct from "intrinsic" breakdown which is an inherent property of the substance. It is this intrinsic breakdown that is considered and the experimental conditions chosen, in the work to be described, were such that secondary factors of the type mentioned above would be eliminated.

[1] *Manuscript received February 12, 1951.*
Contribution from the University of Birmingham, England. (This work forms part of a Ph.D. thesis entitled "The Electrical Breakdown of Liquids" submitted to the University of Birmingham in 1949.)
[2] *Holder of a Postdoctorate Fellowship under the National Research Council of Canada.*

Liquids were chosen as test dielectrics because of an expected simplification of the experimental equipment and procedure compared with that required to test solids. The electrode system may be completely immersed in the test liquid thus eliminating the necessity for an auxiliary surrounding medium and facilitating the production of a uniform electrical field. Flaws and surface irregularities produced in the preparation of solid test pieces do not arise. Liquids can be obtained in a high degree of purity and may be further purified by distillation. As a further precaution against complicating factors the liquids chosen, both polar and nonpolar, were of simple molecular structure, the majority of them being organic liquids.

The durations of the voltage pulses used were so short that the possibility of thermal breakdown did not arise. It is also believed that effects due to the long distance motion of ions are negligible since acceleration of ions to velocities at which they would be important in the breakdown process would require fields of the order of 10^8 v. per cm. (2), whereas experiment yields values of the order of 10^6 v. per cm. for liquids. The breakdown considered here is believed to be electronic in nature (3, 4).

The Experimental Equipment and Procedure

To obtain single, reproducible results it was found necessary to use fresh, highly polished electrode surfaces and a fresh liquid sample after each breakdown. The presence of impurities, especially in the form of minute solid particles, was particularly troublesome (1). Uniform field conditions were obtained by the use of a suitably proportioned sphere gap (8).

A miniature spark gap, designed to operate within a completely enclosed glass system was finally developed. A schematic diagram of the spark gap and its containing vessel is shown in Fig. 1*A*. A photograph of the spark gap, operating rods, and containing vessel as set up for a test is shown in Fig. 1*B*. The spheres *S*,*S*, which were $\frac{3}{8}$ in. in diameter, were located immediately behind the plane glass window *G* which formed part of the wall of the containing vessel *P*, Fig. 1*A*. The gap was viewed and measured *in situ* through the glass window by means of a travelling microscope having a magnification of 260. The gap control rod, *A*, operated a small threaded rod which screwed through the sphere support E_1 and which keyed into the glass insulator *J*. This action adjusted the distance apart of the cantilever sphere supports, E_1 and E_2, and hence controlled the gap width. After each breakdown the spheres were rotated through a small angle by means of the control rods, *B*,*B* thereby presenting fresh, polished surfaces to the gap. The angle of rotation between breakdowns was such that 16 breakdowns could be obtained before the spheres were removed for repolishing. Products of breakdown in the form of minute particles which clung to the spheres were removed by the cotton wool wipers *C*,*C*. The 20 cc. of liquid which were required per breakdown filled the spark vessel to the level *F* marked on Fig. 1*A*. To permit operation at reduced pressures the control rods were passed into the spark vessel via the ground joints *D*,*D*,*D*, Fig. 1*B*.

The spark vessel was sealed to a distillation system which is represented schematically in Fig. 2. The purest grades of liquids commercially available were dried and distilled as required from the boiling flask S to the reservoir flask R. At atmospheric pressure liquid samples were transferred from flask R to the spark vessel V by gentle warming of flask R and appropriate

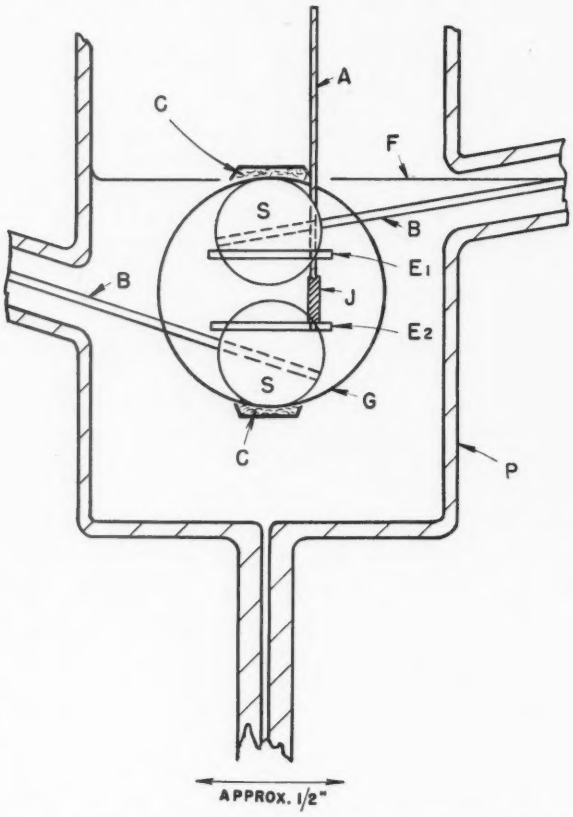

FIG. 1A. *A schematic drawing of the spark gap, operating rods, and containing vessel.*

manipulation of the control stopcocks T_1, T_2, and T_3. A similar procedure was followed in order to transfer the liquid sample after a breakdown from the spark vessel to the flask W. At pressures of the order of one centimeter of mercury, flask W was cooled with liquid air and again appropriate control of the stopcocks effected a liquid transfer because of vapor pressure differences. The latter method of liquid transfer was rather critical; the most effective tube diameters and design were experimentally determined. For operation at reduced pressures the system was evacuated while the liquid samples were

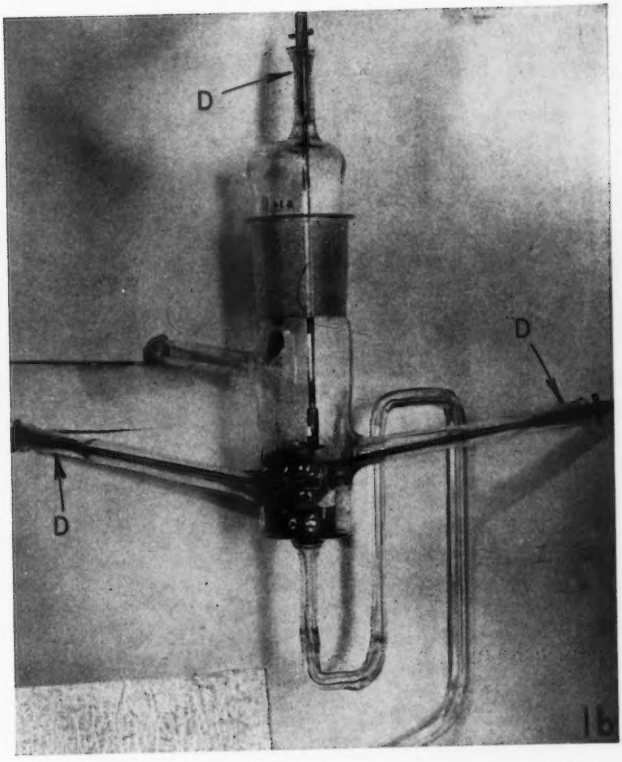

FIG. 1B. *The containing vessel for the spark gap. The spark gap and operating rods are shown in position.*

frozen in flask *S*. After evacuation was complete the system was isolated from the rotary oil pump used and tests were carried out.

The design and method of operation briefly described, coupled with an initial steaming of the apparatus to remove dust particles, reduced the effects of dust, products of breakdown, and the pitting of the electrodes to negligible proportions.

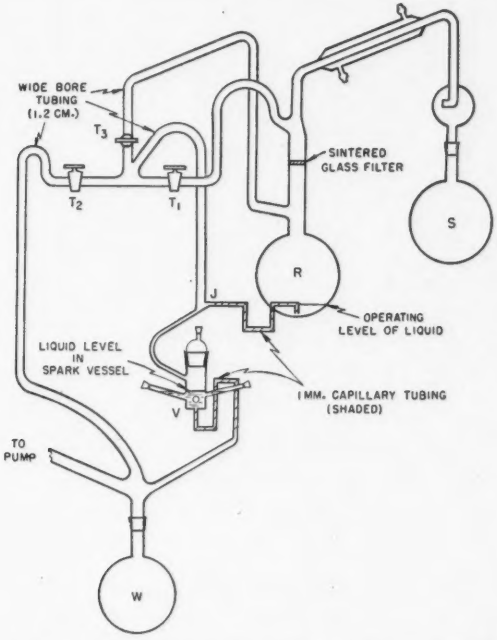

FIG. 2. *A schematic diagram of the distillation system necessary for the production of pure, dust free liquid samples.*

Single, rectangular voltage pulses of given duration were applied to the sphere gap (one sphere being grounded and the other negative with respect to ground). The pulse amplitudes were increased by 0.2 kv. steps until breakdown took place. Pulse durations of 0.1 to 20 μsec. and amplitudes of 1.0 to 10 kv. were used. The durations and amplitudes of these negative pulses, which were produced by vacuum tube circuits (5), were measured with a cathode ray oscilloscope.

The Time Delay in Breakdown

Experimental Evidence of a Time Delay in Breakdown

Experiments were performed on a number of liquids under conditions of normal and reduced pressure. Phosphor bronze electrodes, buffed to a high

polish, were used except as otherwise stated. In Fig. 3 is shown the relation between breakdown strength and pulse length found for benzene at a reduced pressure of the order of one centimeter of mercury. The benzene (B.D.H. purity rating 'Analar') was dried over phosphorus pentoxide prior to distillation. The breakdown strength of 1.08×10^6 v. per cm. obtained for pulses of duration greater than one microsecond is expected to equal the d-c. value, as for these long pulses the breakdown strength appears to be independent of pulse length.

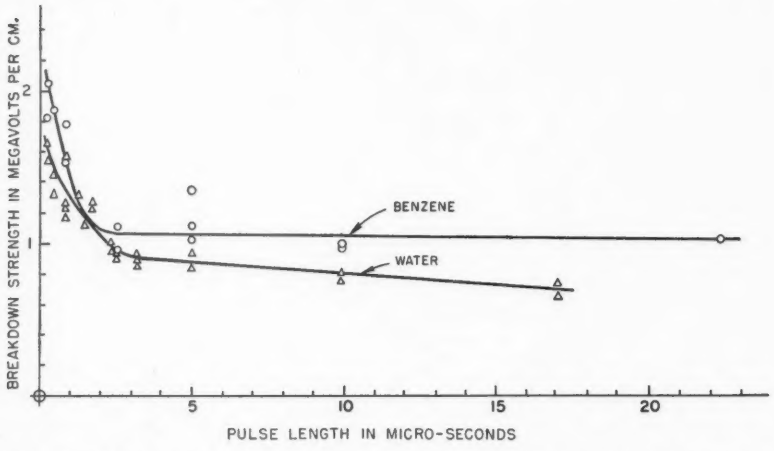

FIG. 3. *The relations found between breakdown strength and applied voltage pulse length for benzene and for triply distilled water.*

In Fig. 4 the results obtained for hexane, heptane, and octane are shown. Whilst the hexane was of 'Analar' purity, the heptane and octane were obtainable in commercial grades only and probably contained appreciable fractions of the adjacent members of the paraffin series. All three liquids were dried by distillation over phosphorus pentoxide and the tests were carried out at a reduced pressure of the order of one centimeter of mercury.

The relation found between breakdown strength and applied pulse length for triply distilled water at a reduced pressure of approximately one centimeter of mercury is shown in Fig. 3. The results of two tests (two polishing operations) are plotted and are of interest as they show a continual decrease of breakdown strength with increase of pulse length even for the longest pulse lengths used. Fig. 5 shows the relation between breakdown strength and applied pulse length obtained for ethyl alcohol (at a reduced pressure of 1 cm. of mercury). Prior to the test the alcohol was refluxed with caustic potash to remove aldehyde and then distilled. Water was removed by further distillation over quick-lime followed by refluxing over metallic calcium. The alcohol was finally distilled at 78°C. and kept in a glass stoppered bottle until

required for the experiment. Carbon tetrachloride of 'Analar' purity and dried over phosphorus pentoxide yielded, for conditions at atmospheric pressure, the results shown in Fig. 5.

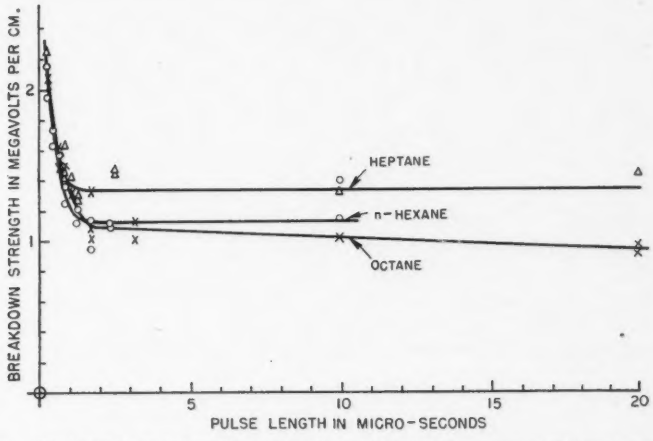

FIG. 4. *The dependence of breakdown strength on applied voltage pulse length for three members of the paraffin series.*

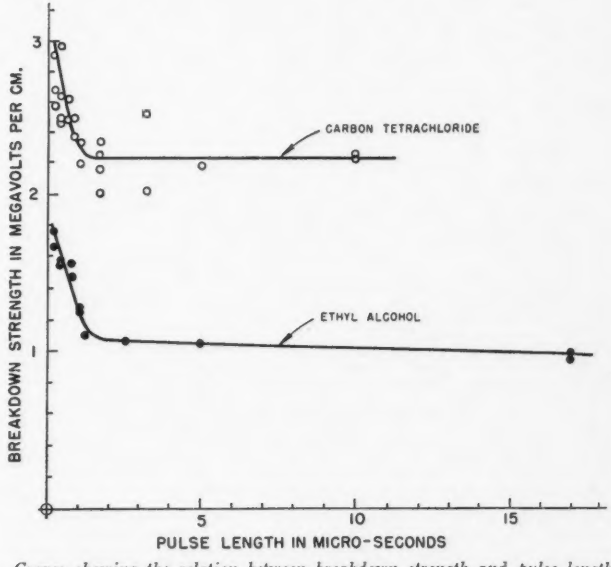

FIG. 5. *Curves showing the relation between breakdown strength and pulse length for ethyl alcohol and for carbon tetrachloride.*

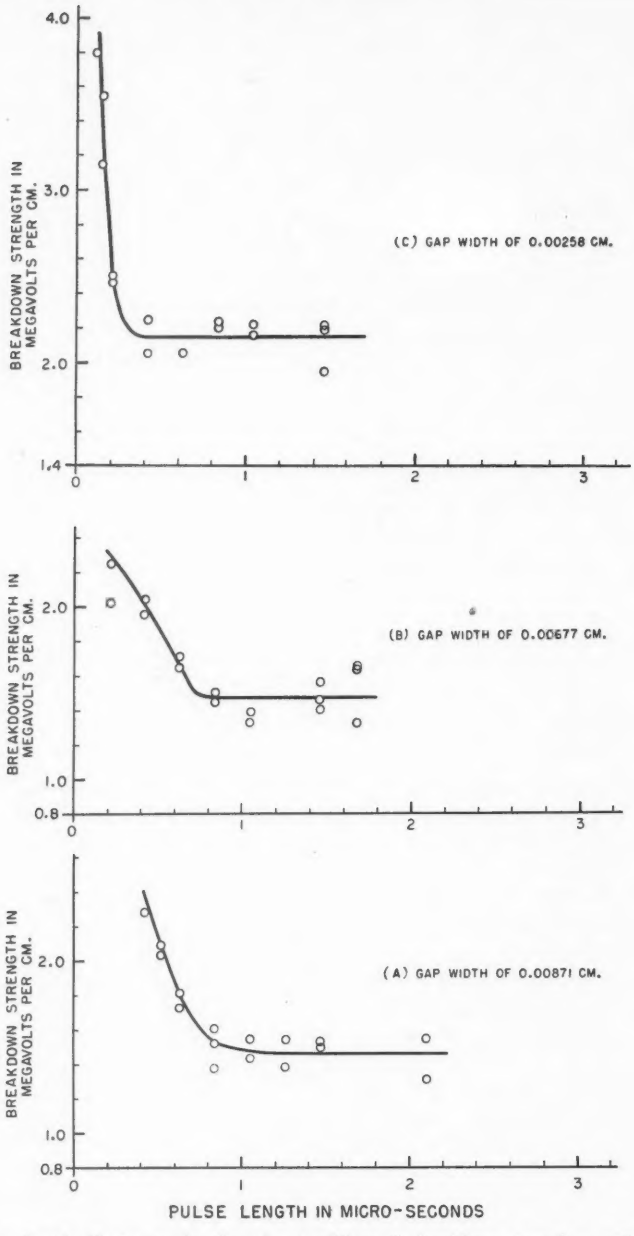

FIG. 6. *Graphs illustrating the effect of gap width on the breakdown strength vs. pulse length relation for benzene.*

For the liquids investigated, both polar and nonpolar, under conditions of normal and of reduced pressure, it is seen from Figs. 3, 4, and 5 that a sharp increase in breakdown strength commences, as the pulse length is reduced, at values of less than one microsecond. It seems reasonable to assume that the effect is due to a time delay in the breakdown process which is determined from the time interval between the instant of application of the field and the

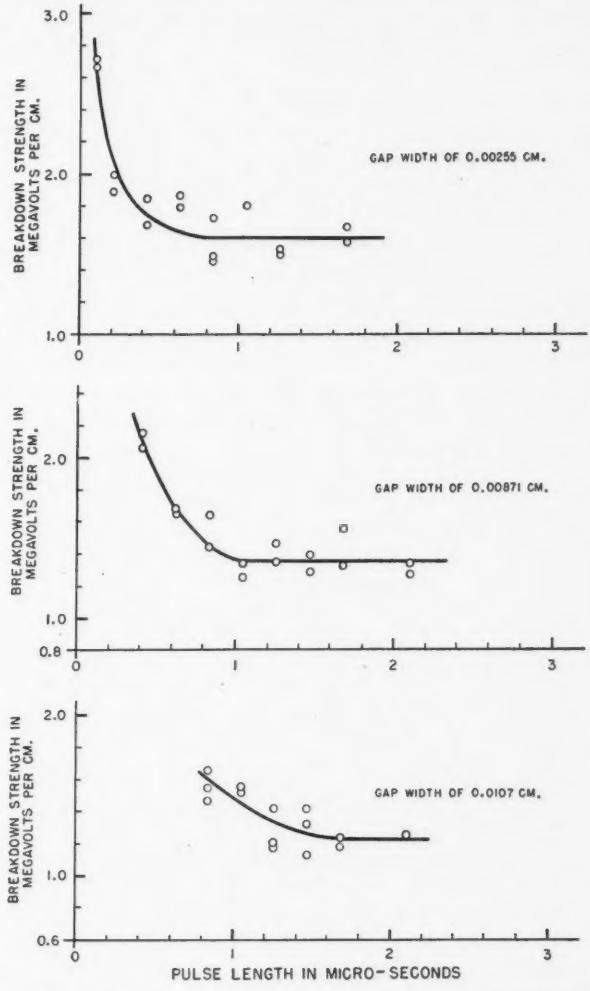
BREAKDOWN STRENGTH IN MEGAVOLTS PER CM.
GAP WIDTH OF 0.00255 CM.
BREAKDOWN STRENGTH IN MEGAVOLTS PER CM.
GAP WIDTH OF 0.00871 CM.
BREAKDOWN STRENGTH IN MEGAVOLTS PER CM.
GAP WIDTH OF 0.0107 CM.
PULSE LENGTH IN MICRO-SECONDS

FIG. 7. *Graphs illustrating the effect of gap width on the breakdown strength vs. pulse length relation for n-hexane.*

breakdown itself. The delay time for the cases considered is of the order of one microsecond. Water is an exception, the rapid increase in breakdown strength taking place for pulse lengths of less than approximately $2\frac{1}{2}$ microseconds. The similarity between the results suggests that the mechanism giving rise to the delay is almost independent of the liquids tested.

With benzene as test dielectric the effect of gap width on delay time was investigated. The results are shown in Fig. 6. Fig. 7 shows a similar set of curves which were obtained with *n*-hexane as test liquid. Clearly, the delay time increases as the gap width increases.

Discussion of the Time Delay in Breakdown

The delay may originate in either or both of two main causes. The delays due to these two factors may be loosely referred to as 'pre-ionization' and 'post-ionization' delays. With the assumption of an electronic mechanism of breakdown these delays may be defined as:

(i) The length of time it takes for the electrons to reach ionization energies from the moment of applying the field (pre-ionization delay).

(ii) The length of time the process goes on, following the commencement of ionization, before a low resistance path between the electrodes is established (post-ionization delay).

For uniform field conditions and for dielectric samples whose dimensions are large compared with the electronic mean free path a delay of the first type is expected to be independent of the shape and exact dimensions of the specimen. The results shown in Figs. 6 and 7 suggest that a post-ionization delay occurs in addition to any pre-ionization delay which may be present. The pre-ionization delay will appear as a constant in the relation between delay time and gap width. The scatter in the results so far obtained prevents the elimination of such a constant but certainly it can be stated that the pre-ionization delay is less than 0.1 microsecond for the cases of benzene and hexane. In the following paragraphs a qualitative explanation of the post-ionization delay is put forward.

The breakdown of liquids has been studied photographically by Komellkov (6). His results show that space-charge streamers play a major role in the final stages of liquid breakdown; in fact, a role analogous to that described for gases by Loeb and Meek (7). It is thought that breakdown in liquids, once initiated, proceeds to the arc stage and consequent degeneration of the dielectric via a streamer mechanism rather similar to that taking place in gases. However, the picture of the development of breakdown in gases has necessarily to be modified in a number of ways in order to apply to liquids. Shorter electronic mean free paths, absence of a statistical time lag in breakdown, and high electron and positive ion densities in which the forces of mutual repulsion may be sufficient to vaporize the liquid, are among the most important factors arising from the large increase in density. Breakdown will not take place until the positive, space-charge streamer reaches the cathode.

There will thus be a time delay in the breakdown process, usually termed the formative time lag, which depends on the rate of formation of the electron avalanche and on the rate of propagation of the positive space-charge streamer. The results of Komellkov indicate that for liquids, the rate of progression of the streamer will be very rapid and, as for gases, the main part of the formative time lag will be due to the time taken by the electron avalanche to cross the gap. For a given gap width, there will be a minimum value of field strength required to give breakdown. It is expected that this critical breakdown field strength will be constant for all durations of the applied voltage which are long enough to enable the breakdown to reach the final stage of a large, discontinuous current flow across the gap. If, however, a field of critical strength is applied for a duration less than the formative time lag, breakdown will not take place. Among other factors the delay will depend on electron mobility and on gap width. Enhanced field strengths, which occur in 'over-volted' gaps, will reduce the delay time. The results shown in Figs. 3, 4, and 5 demonstrate this effect. For applied pulse lengths of greater than approximately one microsecond (the formative time lag) the breakdown strength is independent of pulse length as expected. However, for pulses of duration less than one microsecond it is necessary to considerably increase the applied field strength in order to reduce the formative time lag of the gap used and make breakdown possible for such short pulses.

If, from Fig. 6*C*, the value of the pulse length at which the sharp increase in breakdown strength occurs is taken to be the formative time lag, a space-charge streamer velocity of not less than 10^4 cm. per sec. is obtained. This value is the minimum possible obtained by neglecting the delay due to the electron avalanche and as this delay is probably much greater than the delay due to the progression of the positive streamer, a streamer velocity of the order of 10^5 cm. per sec. or more seems likely. Observation of the drop to zero of the pulse voltage at breakdown showed that breakdown, when once started, was complete in 10^{-9} sec. or less.

To sum up, the formative time lag for a given gap width is a maximum for the critical breakdown field and is reduced as the field strength is increased. For the type of mechanism discussed above, it is expected that a gap width increase will increase the time required by the electron avalanche and later the space-charge streamer to cross the gap. The formative time lag, which depends on the sum of these two factors, will increase as the gap width increases. The breakdown strength vs. pulse length relations of benzene and hexane for a number of gap widths, Figs. 6 and 7, demonstrate this effect but more confirming results are needed.

Other Characteristics of the Breakdown Process

In the following paragraphs experiments are described in which rectangular voltage pulses are used to investigate the effect on breakdown strength of pressure, electrode metal, external irradiation of the gap, and temperature.

The explanation presented above of the relation between pulse length and breakdown strength was concerned with the development of breakdown, and the initial state, during which the instability developed, was not considered. The experiments described here have a bearing upon this initial state since the parameters involved (temperature, work function, etc.) are important in deciding when there will be a net multiplication of electrons leading to the formation of an electron avalanche.

A pulse length of 3.16 μsec. was used in all cases. This value is considerably greater than the formative time lags of the gaps used and hence, if space-charge effects due to the motion of ions are negligible, the results found for critical breakdown strengths should equal the d-c. breakdown strengths. Phosphor bronze electrodes were used in all tests except where otherwise stated.

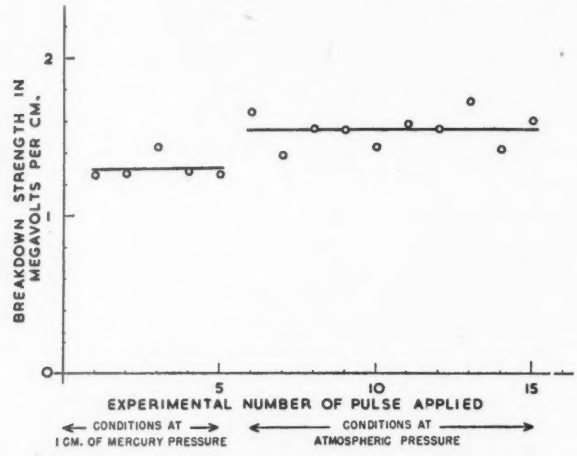

FIG. 8. *A diagram to show the effect of pressure on the breakdown strength of benzene.*

The effect of a reduction in pressure was investigated using benzene as test liquid. In Fig. 8 the results are shown plotted in the order in which they were obtained experimentally. The results numbered 1 to 5 inclusive were taken while the benzene was under a reduced pressure of 1 cm. of mercury. Argon was later released into the system raising the pressure to one atmosphere and Results 6 to 10 inclusive were obtained. The argon was replaced by dust free, undried air at one atmosphere pressure and five further values of breakdown strength, Points 11 to 15, were obtained. It is seen that whilst a small but significant increase in breakdown strength takes place as the conditions at a pressure of 1 cm. of mercury are replaced by conditions at one atmosphere pressure, no change in breakdown strength results from changing the gas present within the system.

A preliminary investigation of the effect of electrode metal on breakdown strength has been made. Table I summarizes the results so far obtained. Each of these results is the mean value of at least eight breakdown strength measurements. Both for carbon tetrachloride and for benzene the breakdown strength found when steel electrodes were used was appreciably greater than the value found for phosphor bronze electrodes. The difference between the results for silver and phosphor bronze electrodes in benzene was much smaller and, assuming a Gaussian distribution of errors, a calculation showed that the

TABLE I

A SUMMARY OF THE LONG PULSE LENGTH VALUES OF BREAKDOWN STRENGTH FOUND

Liquid	Breakdown strength at atmospheric pressure	Breakdown strength under vacuum conditions	Gap width in cm.	Electrode metal	Temperature
Carbon tetrachloride	2.25		0.0047	p. bronze	300° A.
		1.97	0.0042	p. bronze	"
		2.43	0.00255	p. bronze	"
	2.48		0.00321	p. bronze	"
	3.19		0.00321	steel	"
Chloroform	2.07		0.00422	p. bronze	300° A.
Benzene	1.54		0.0047	p. bronze	300° A.
		1.30	0.0047	p. bronze	"
		1.08	0.0047	p. bronze	"
	1.57		0.0047	p. bronze	"
	1.68		0.0047	silver	"
	1.82		0.0047	steel	"
Hexane	1.38		0.0047	p. bronze	300° A.
		1.12	0.0047	p. bronze	"
	2.23		0.0047	p. bronze	210° A.
Heptane		1.32	0.0047	p. bronze	300° A.
Octane		1.08*	0.0047	p. bronze	300° A.
Ethyl alcohol		1.06*		p. bronze	300° A.
	1.27			p. bronze	"
	1.62			p. bronze	170° A.
Water		0.91*	0.0047	p. bronze	300° A.

Note: Breakdown strengths measured in megavolts per cm.
**These three values of breakdown strength are for an applied pulse length of 3.16 μsec.*

two values of breakdown strength were not significantly different. The interesting effect of electrode metal was further investigated with a sphere gap in benzene which had one electrode of steel and the other of phosphor bronze. One half of the results were taken with the steel as anode, the other half with the steel as cathode. The results showed the breakdown strength to be independent of the anode metal but markedly dependent on the cathode metal.

Experiments with benzene and hexane showed that for the short gaps used (between 0.0025 cm. and 0.01 cm.) the breakdown strength increases as the

gap width is reduced, as may be seen in Fig. 9. Voltage limitations prevented the use of wider gaps and the difficulties of gap measurement made the use of gaps smaller than 0.0025 cm. impracticable.

No effect on the breakdown strength of either benzene or of carbon tetrachloride was observed when a 5 mgm. radium source was placed in close proximity to the sphere gap. However, these results were later found to be inconclusive. A calculation showed that approximately 10^4 ions per second were being produced in the immediate vicinity of the gap. If the life-time of the electrons produced is very short it is quite likely that no additional electrons, produced as a result of the gamma rays, existed in a free state at the moment of application of the 3 μsec. pulse.

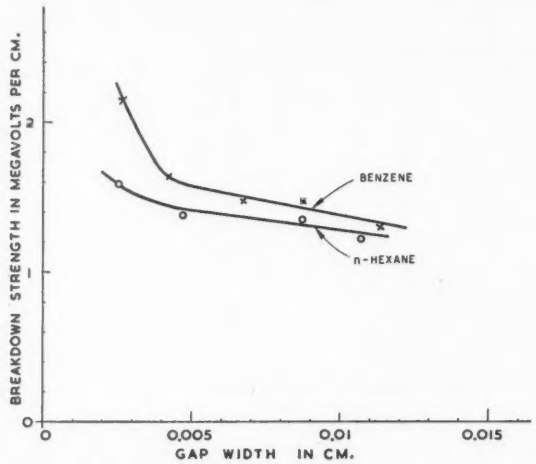

FIG. 9. *The relations found between breakdown strength and gap width for n-hexane and for benzene.*

The breakdown strength vs. temperature relation was investigated for one polar and for one nonpolar liquid. To attain low temperatures the spark vessel was enclosed by a thermally insulating jacket. A stream of air, cooled by passage through a glass spiral immersed in liquid air, was passed between the jacket and the spark vessel, thus cooling the vessel. The temperature, which was measured by means of a thermocouple, was adjusted to the desired value by varying the rate of flow of the air stream. Fig. 10 shows the relations found between breakdown strength and temperature for *n*-hexane and ethyl alcohol. Hexane, which has a breakdown strength independent of temperature between room temperature and its boiling point, shows a marked negative temperature coefficient of breakdown strength below room temperature. The graph for ethyl alcohol shows an approximately constant, negative temperature coefficient of breakdown strength over the temperature range investigated.

A comparison of the breakdown strengths of these two liquids shows that whilst alcohol has a breakdown strength of the same order as that of hexane at room temperature, it has a much lower value at −60°C. A change in the relations between the breakdown strengths of the other liquids studied may well take place and hence it is impracticable to draw definite conclusions from the relative magnitudes of the breakdown strengths found at room temperature only.

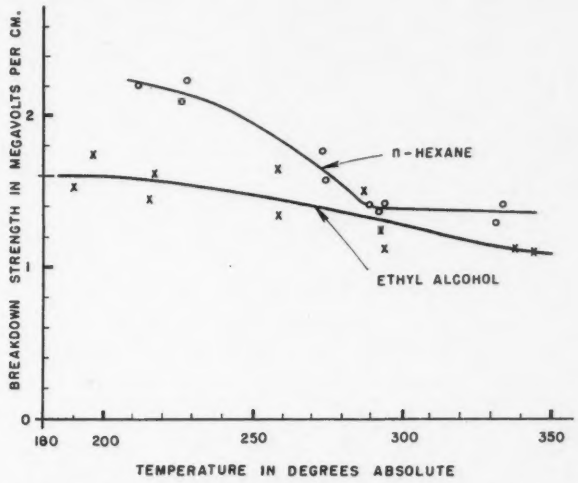

FIG. 10. *Curves to illustrate the dependence on temperature of the breakdown strengths of n-hexane and ethyl alcohol.*

Conclusion

The results presented here are incomplete, in that the ranges of the variables involved (gap width, temperature, etc.) are rather small and the scatter of the results is larger than is desirable. The evidence on most of the characteristics studied is quite definite however. It is felt that this, together with the fact that unforeseen circumstances have delayed continuation of the work, justifies publication at this time.

The photographic evidence of Komellkov (6) in favor of a space-charge streamer process to explain the development of breakdown in liquids is supported by the experimental data reported here. The increase in breakdown strength for short pulses of voltage may be explained in terms of a time delay in the development of breakdown, i.e., the post-ionization delay. The increase in time delay as the gap width is increased, obtained experimentally, is also expected for such a mechanism. The results do not give any information on the time required for the few electrons originally present to gain energies sufficient to ionize the liquid molecules (the pre-ionization delay), except to indicate that it is less than 0.1 μsec., the length of the shortest pulse used.

Acknowledgments

The writer wishes to thank Prof. M. L. E. Oliphant, F.R.S., for the provision of facilities for this work and Mr. K. A. Macfadyen for suggesting the problem, for much helpful advice and many valuable discussions. The author is also indebted to the Dudley Docker and Chidlaw Scholarship Trusts for maintenance grants.

References

1. DORNTE, R. W. J. Applied Phys. 10: 514. 1939.
2. FRANZ, W. Z. Physik, 113: 607. 1939.
3. GEMANT, A. Liquid dielectrics. Chapman and Hall Ltd., London. 1933.
4. HIPPEL, A. VON. J. Applied Phys. 8: 815. 1937.
5. JOHNSON, R. H. J. Inst. Elec. Engrs. (London.) 93: 3A, 1043. 1946.
6. KOMELLKOV, V. S. Compt. rend. acad. sci. U.R.S.S. 47: 265. 1945.
7. LOEB, L. B. and MEEK, J. M. The mechanism of the electric spark. Oxford University Press, 1940.
8. RUSSELL, A. Phil. Mag. 11: 253. 1906.

ANGULAR CORRELATION OF ANNIHILATION RADIATION FROM POSITRONS DECAYING IN SEVERAL SUBSTANCES[1]

By J. B. Warren and G. M. Griffiths

Abstract

Using anthracene scintillation counters in coincidence, the angular correlation between annihilation quanta produced by the decay of positrons in the following materials has been measured: the pure elements Mg, S, Cu, Sn, Pt, and Hg, and the chemical compounds LiCl, KCl, CsCl, KF, and KI.

Calculations were performed to determine the effect of the geometry on the shape of the angular correlation curves, and the effects of scattering were investigated.

The curves for copper, platinum, and possibly mercury could be approximated to by the expression $C(\theta) = Ke^{-\theta/\theta_0}$, where $C(\theta)$ is the coincidence counting rate as a function of θ, the angular departure of the two quanta from collinearity, and K and θ_0 are constants. The curves for the other materials are more complicated and suggest that there is a relation between the shape of the curves and the outer electronic structure of the atoms with which the positrons annihilate. In alkali halides the positrons appear to annihilate only against the outer electrons of the negatively charged halogen ions.

Introduction

If, at the instant a positron electron pair annihilates, the center of gravity is moving with respect to the observer, then momentum is conserved only by a lack of collinearity between the two emitted annihilation quanta. It is easily shown that to a first approximation

$$\theta = \frac{p}{mc},$$

where θ = angle of departure from collinearity of the two quanta,

p = momentum of the electron, with respect to the positron which is assumed to be at rest.

Heitler (6) has shown that most of the positrons sent into a material reach the end of their path of ionization before annihilation. At the end of this path the positrons have energies of the order of 10 ev. Subsequent energy losses are then possible through inelastic collisions with the lattice of the material. Calculations of the mean time for annihilation and of the time required for the positrons to attain thermal equilibrium with the lattice show (4) that the positrons are thermalized in a time short compared to the mean time for annihilation. Therefore the energies of most of the positrons are reduced to about 1/40 ev. before annihilation. Du Mond *et al.* (5) pointed out that these low velocity positrons should annihilate only with the outer electrons of an atom since they are repelled by the nucleus. Consequently a study of the angular correlation of annihilation radiation should yield information about the momenta of the outer electrons of the atoms with which the positrons annihilate.

[1] *Manuscript received January 9, 1951.*
Contribution from the Physics Department, University of British Columbia, Vancouver, B.C.

The angular departure from collinearity is small, being, for example, about ¼ degree for a 10 ev. electron annihilating with a positron at rest. The first accurate attempt to detect this departure by Beringer and Montgomery (3) gave no evidence for any lack of collinearity to within one degree. More precise measurements have become possible with the advent of scintillation counters and stronger sources. De Benedetti *et al.* (4) with Cu^{64} positrons annihilating in gold and Argyle and Warren (2) using Cu^{64} positrons annihilating in copper have found that the two annihilation quanta are not always emitted in exactly opposite directions. The angular distribution curves obtained by coincidence counting in both cases could be well represented by

$$C(\theta) = Ke^{-\theta/\theta_0},$$

where $C(\theta)$ is the coincidence counting rate as a function of θ, the angular departure from collinearity, and K and θ_0 are constants.

A theoretical treatment for the case of positrons annihilating in gold has been given (4) assuming that the positrons annihilate only with the outer 6*s* electrons of the gold atom; this yields a distribution qualitatively similar to the above exponential form. As yet no accurate calculations have been performed, owing to lack of information concerning the outer electronic momentum wave functions.

The present paper describes measurements of the angular correlation between annihilation quanta produced by positrons annihilating in 11 materials:

(*a*) the pure elements Mg, S, Cu, Sn, Pt, and Hg,
(*b*) the two alkali halide series: (1) LiCl, KCl, CsCl.
(2) KF, KCl, KI.

Experimental Details

Two scintillation counters were placed 4.4 m. apart with the source halfway between them as shown in Fig. 1, and the coincidence counting rate was measured as a function of the horizontal position of one of the counters which was mounted on a traveling microscope carriage. The positron source con-

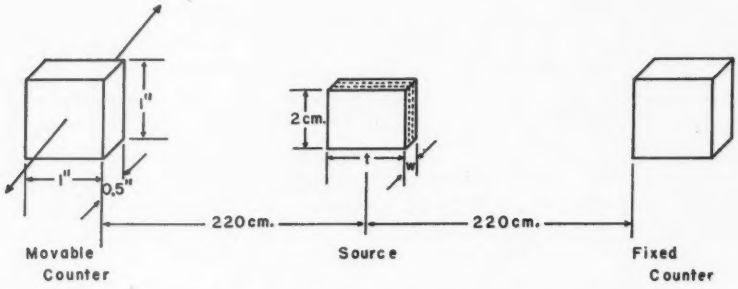

FIG. 1. *Geometrical arrangement of the source and counting crystals.*

sisted of three foils of copper 3 by 2 by 0.0012 cm. with a total activity of 100 mc. at the start of the experiment. The copper foils were of such a thickness (0.0012 cm.) that at least 90% of the positrons escaped into the surrounding stopping material, where they produced annihilation radiation. The material under study was placed in layers in a thin aluminum box with the copper foils between the layers. The thickness of the layers was just sufficient to stop positrons of the maximum range, and the number of layers used depended on the number of copper foils necessary at any time to give a reasonable counting rate. At first, while the copper activity was high, only one foil was used in each source, as this gave narrow sources and minimized geometry corrections. The length of the source, t, was varied from 0.25 cm. to 3 cm., depending on the density, and thence the absorption coefficient, of the material under study.

The counters consisted of 1 by 1 by ½ in. anthracene blocks mounted in thin aluminum boxes on the ends of RCA 5819 photomultiplier tubes. The 1 by 1 in. crystal surface placed against the tube made efficient use of the photocathode area, and good optical coupling was achieved by filling the spaces between the tube, crystal, and front of the mounting box with a clear mineral oil. The photomultipliers were operated at a supply voltage of about 1000 v. obtained from a battery referenced supply. The noise background was 5 to 10 counts per second.

The amplifiers (including head amplifiers) had a gain of 1200 with a band pass from 10 kc. to 8 mc. (½ gain points). Care was taken to avoid overshooting in the main-ring of three amplifiers (7), since they are required to handle the wide range of pulse sizes produced by the photomultipliers. The amplifier output pulses were fed to a coincidence mixer where they were standardized by univibrators and mixed at a Rossi stage with a resolving time of 0.15 μsec.

Coincidence counting rates taken with the cascade gamma rays of a Co^{60} source obtained on different days were repeatable to within the statistical accuracy, thus indicating the high stability of the apparatus. The stability during the experiment was assessed by following the decay of the Cu^{64} activity; also a least squares analysis of a lead absorption curve (1) gave smaller residuals when a 12.88 hr. half life (8) was used than with a 12.80 hr. half life. By coincidence counting on the cascade γ rays of Co^{60} the counter efficiencies were found to be 18%, which is within 1% of the efficiency calculated for 1.2 Mev. γ rays and the particular crystals used. The quite considerable effect of backscatter was investigated and corrected for in these measurements. The annihilation radiation from a 0.2 mc. source of Zn^{65} (approximately 1% positron emission) was readily detected in the presence of the large 1.14 Mev. gamma-ray background by means of an angular correlation experiment, and a comparison of the peak coincidence rate and the single channel counting rate showed that the counter efficiencies for 0.51 Mev. quanta are about the same as those predicted by the Klein–Nishina formula, namely 25%.

For the final geometry used, approximate calculations based on the differential cross section for scattering indicate that scattering in the source produced a coincidence background of the order of 2% of the coincidence rate obtained for the outer portions of the tails of the distribution curves. Experimental tests made during the experiment by placing scatterers in the beam and by putting lead shields around the counters showed that scattering from the walls and tables produced errors as large as 5 to 10% of the counting rate at the outer portion of the tails of the curves. Since the statistical accuracy at these points was of the order of 20%, the errors due to scattering are not serious. Approximate calculations show that the effect of backscatter from one counter to the other is negligible in this experiment.

Geometry

The plane angles subtended at the counters by the source and at the source by the counters were comparable to the angular departure from collinearity of pairs of annihilation quanta, so it was necessary to determine the effect of the geometry on the angular correlation curves.

If two counters and a source of annihilation radiation are arranged as in Fig. 2 and the number of pairs of quanta with an angular departure from collinearity between ϕ and $\phi + d\phi$ is given by $N(\phi)d\phi$, then the coincidence counting rate measured as a function of the angle θ (see Fig. 2) is given by

$$C(\theta) = B \int_S \int_{C_1} \int_{C_2} N(\phi)\, dS\, dC_1\, dC_2,$$

where θ is the angular departure of the movable counter from the position where counters and source are in line;

B is a constant involving the annihilation radiation activity of the source, absorption in the source, the distance D and the counter efficiencies;

and for any given angle θ, the integrations are to be performed over the areas of the source S, and the areas of the counters C_1 and C_2, while ϕ depends on the positions of the elements of area dS, dC_1, and dC_2 as shown in Fig. 2.

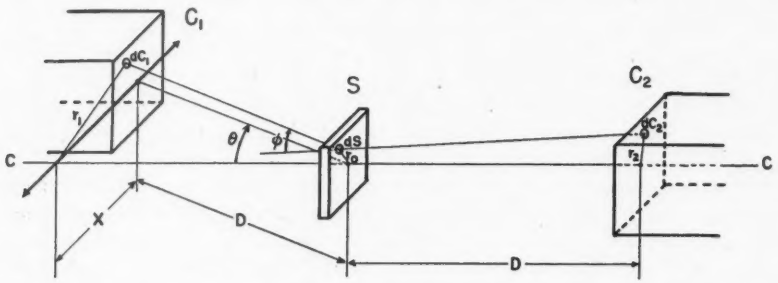

FIG. 2. *Geometrical arrangement for calculating the effect of geometry on the angular correlation curves.*

In the experiment, counter 1 was moved in a direction perpendicular to the line C–C, rather than along the arc of a circle with center at the source, and the angle θ was assumed to be proportional to the displacement, x, of counter 1 from its central position. Since θ was always less than 1.5°, the errors introduced by this assumption are small. Making the same assumption here, ϕ can be evaluated in terms of the vectors $\boldsymbol{r}_1$, $\boldsymbol{r}_2$, and $\boldsymbol{r}_0$ shown in Fig. 2. Thus

$$\phi = \frac{|\boldsymbol{r}_2 + \boldsymbol{r}_1 - 2\boldsymbol{r}_0|}{D}.$$

Here the vector $\boldsymbol{r}_1$ depends on the angle θ and the position of dC_1 on the surface of counter 1. It is measured from the position of the center point of counter 1, when both counters and source are in line. The vectors $\boldsymbol{r}_0$ and $\boldsymbol{r}_2$ are measured from the centers of the source and of counter 2 respectively.

No method was found for solving this problem with a general angular correlation function $N(\phi)$. So, to evaluate the above integral, $N(\phi)$ was assumed to be equal to $Ke^{-\phi/\phi_0}$, as was found experimentally by previous authors, where K and ϕ_0 are constants, in which case the integral becomes

$$C(\theta) = A \int_S \int_{C_1} \int_{C_2} e^{-\frac{|\boldsymbol{r}_2 + \boldsymbol{r}_1 - 2\boldsymbol{r}_0|}{D\phi_0}} .dS.\, dC_1.\, dC_2.$$

An approximate numerical solution was obtained for several cases by dividing the source and counters into sections, evaluating the integrand for each combination of sections, and summing to get $C(\theta)$ for several values of θ. Thus

$$C(\theta) = A \sum_S \sum_{C_1} \sum_{C_2} e^{-\frac{[(x_2 + x_1 - 2x_0)^2 + (y_2 + y_1 - 2y_0)^2]^{\frac{1}{2}}}{\phi_0 D}} .dS.\, dC_1.\, dC_2,$$

where dS, dC_1, and dC_2 are the areas of the sections and $\boldsymbol{r}_1$, $\boldsymbol{r}_2$, and $\boldsymbol{r}_0$ have been expressed in rectangular co-ordinates using the same origins as for the vectors. For the calculations, the counter areas 1 in. by ½ in. were divided into eight square sections. The results of calculations for several source sizes are shown in Fig. 3. Since only the change in *shape* of the curves with changing geometry is of interest, the vertical positions of the curves of Fig. 3 have been adjusted to facilitate comparison and therefore no conclusions concerning relative counting rates may be drawn from them. The ordinates are plotted as logarithm to base 10 of the counting rate.

For an exponential correlation between the quanta, the measured correlation is no longer exponential as a function of angle. However, beyond the overlap region (where a straight line can be drawn passing through both counters and the source), the curves deviate only slightly from strict linearity on the logarithmic plot. Also the average slopes of the calculated curves are different from that of the assumed correlation curve (beyond the overlap region), the difference increasing with source size. This matters in those cases where the experimentally observed curves can be approximated to by an exponential form, since a value for the mean center of mass momentum of annihilating pairs

can be obtained from the slope of this curve. Consequently, a correction based on the above calculations was applied to the experimental results in those cases where an interpretation in terms of mean center of mass momentum is given.

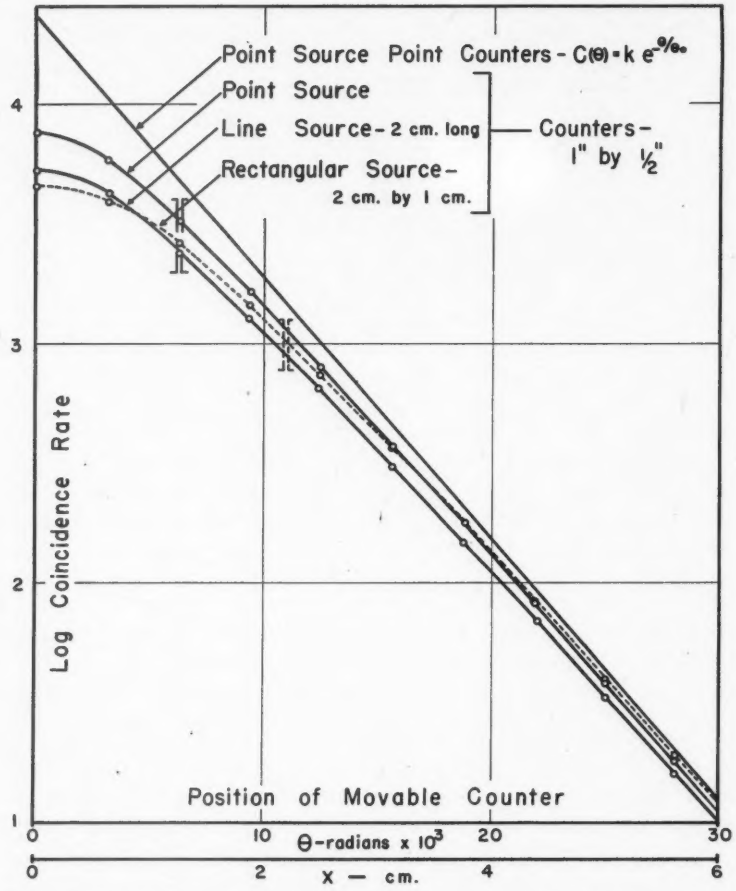

FIG. 3. *Calculated angular correlation curves showing the effect of geometry on an assumed angular correlation of the form* $Ke^{-\theta/\theta_0}$, *with counters 1 in. by ½ in. placed 200 cm. from sources of various sizes.*

Results

The final results of the measurements of the angular correlation of annihilation quanta from the materials examined are shown in the form of curves as follows:

Fig. 4—results for the pure elements Mg, S, Cu, Sn, Pt, and Hg,

Fig. 5—results for the alkali chlorides LiCl, KCl, and CsCl,

Fig. 6—results for the potassium halides KF, KCl, and KI.

The statistical accuracy of each point based on the total number of coincidences and the number of accidental coincidences is shown by the vertical strokes. The end of the geometrical overlap region is shown for each curve by a double vertical line.

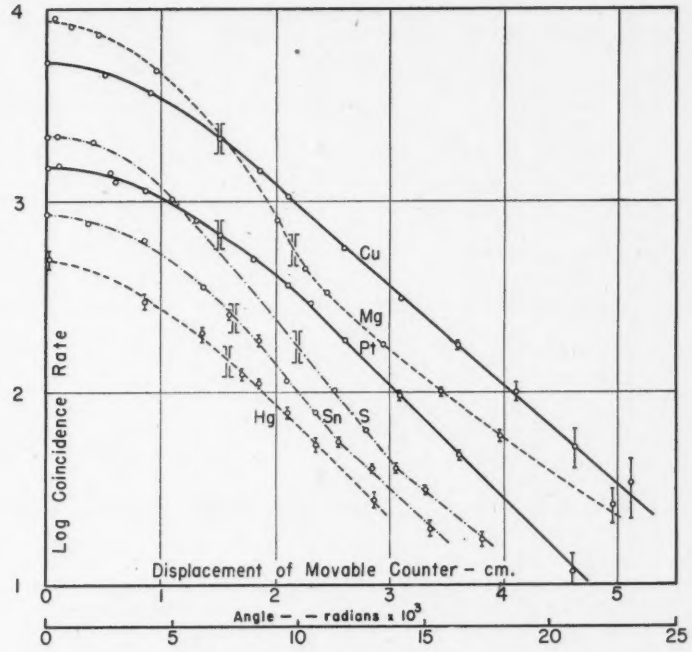

FIG. 4. *Angular correlation curves for annihilation radiation from several pure elements.*

The vertical scales showing the logarithm to the base 10 of the coincidence counting rates are arbitrary as explained for Fig. 3. The coincidence counting rates at the peaks of the curves (zero displacement) varied from 1100 counts per minute for the copper curve measured with a single active foil to 100 counts per minute for KCl measured three days later with two active foils.

(*a*) *Pure Elements*

The tails of the curves for copper, platinum, and mercury (the latter was investigated over a rather small angular range and with less satisfactory statistics) can be closely approximated to by exponentials of the form $C(\theta) = Ke^{-\theta/\theta_0}$. For the other cases, the discrepancies from the exponential form are greater than can be accounted for by scattering, geometry, or other sources of

error. These curves (Fig. 4) suggest that there is a relation between the outer electronic structure of an element and the shape of the corresponding angular correlation curve as shown in Table I.

TABLE I

RELATION BETWEEN THE ANGULAR CORRELATION CURVE SHAPE AND THE OUTER ELECTRONIC STRUCTURE OF AN ELEMENT

Element	Z	Electronic shell structure						Angular correlation curve shape
		K	L	M	N	O	P	
Mg	12	2	2 6	2				Curved
S	16	2	2 6	2 4				Curved—2 sections
Cu	29	2	2 6	2 6 10	1			Straight
Sn	50	2	2 6	2 6 10	2 6 10	2 2		Curved—2 sections
Pt	78	2	2 6	2 6 10	2 6 10 14	2 6 9	1	Straight
Hg	80	2	2 6	2 6 10	2 6 10 14	2 6 10	2	Straight (?)

The elements copper and platinum which have one electron in their outer shells have simple exponential angular correlation curves; mercury is a doubtful case, since the angular range studied was small. The curves for sulphur

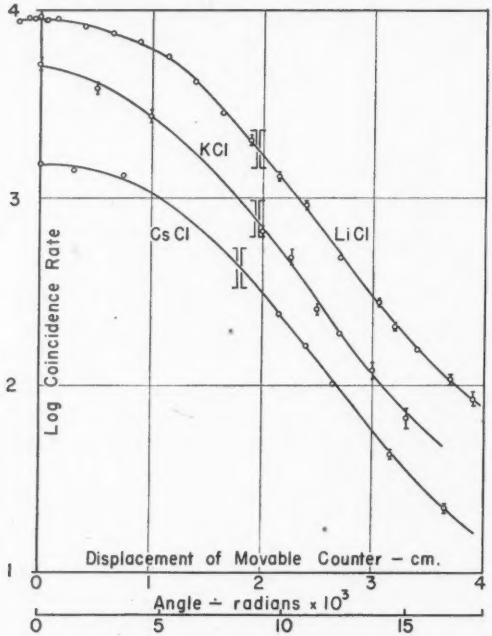

FIG. 5. *Angular correlation curves for annihilation radiation from the alkali chlorides LiCl, KCl, and CsCl.*

and tin consist of two distinct and approximately exponential sections; these elements have two groups of electrons with different angular momenta in their outer shells.

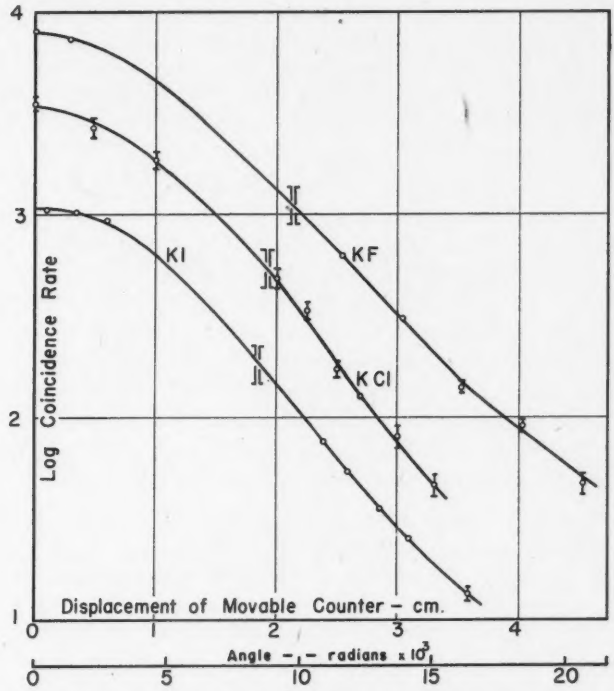

FIG. 6. *Angular correlation curves for annihilation radiation from the potassium halogens KF, KCl, and KI.*

In the cases where there is evidence for a simple exponential type of angular correlation $C(\theta) = Ke^{-\theta/\theta_0}$, the mean center of mass momentum of annihilating pairs can be calculated if it is assumed that the exponential correlation continues into regions of large angle, where measurements were not taken, and of small angles where the measurements are masked by the geometry. A check indicated that the shape of the curves inside the overlap region did agree with the shape to be expected from an exponential relation for the cases of copper and platinum.

Suppose $N(p)dp$ be the number of annihilating pairs with center of mass momentum between p and $p + dp$. Now the vertical angular aperture of the detectors was large enough, compared to the angular departure from collinearity of the annihilation quanta, that the problem can be treated in the horizontal plane only without too large an error. In this case, the experimentally ob-

served quantity $C(\theta)$ is proportional to $Nz(p)$, the distribution of the annihilating pairs according to their horizontal (z) components of center of mass momentum (see reference 4). If $N(p)$ is spherically symmetrical, then $N(p) = -2p\frac{dN_z(p)}{dp}$. Therefore, if $C(\theta) = Ke^{-\theta/\theta_0}$, $N_z(p) = Ae^{-p/mc\theta_0}$, where A is constant and $\theta = p/mc$ and $N(p) = Bpe^{-p/mc\theta_0}$, where B is a constant.

The mean center of mass momentum $\bar{p}$ can then be obtained in terms of the experimental parameter θ_0 by integration; thus

$$\bar{p} = \frac{\int_0^\infty p\,N(p)\,dp}{\int_0^\infty N(p)\,dp} = 2mc\theta_0.$$

If $E << mc^2$ the average center of mass energy is given by

$$\bar{E} = 3m\,(c\theta_0)_2.$$

Thus for copper and platinum the following values were obtained from the experimental results after applying corrections for the geometry:

$\bar{p}_{Cu} = (7.24 \pm 0.1) \times 10^{-3}$ mc. $(2mc\,\theta_0)_{Cu} = (7.24 \pm 0.04) \times 10^{-3}$ mc.

$\bar{E}_{Cu} = (20.1 \pm 0.6)$ ev.

$\bar{p}_{Pt} = (6.41 \pm .4) \times 10^{-3}$ mc.

$\bar{E}_{Pt} = (15.8 \pm 2.2)$ ev.

The error for copper has been increased from about 0.6% (the value given at the left) as obtained from the residuals of a least squares analysis of the tail of the curve, to about 1.5% to allow for the rather uncertain sources of errors due to scattering and geometry. This result is in good agreement with that previously obtained in this laboratory (2). The error for platinum is based on inspection of the curve. No correction has been made for the fact that about 10% of the positrons decay in the copper foils of the source. For the cases where the angular correlation is not of a simple exponential form, the accuracy of the results does not justify a tedious analysis to determine the mean center of mass of annihilating pairs and, in any case, the mean momentum in such cases would not have much physical significance.

(*b*) *Alkali Halides*

De Benedetti *et al.* (4) suggested that in an alkali halide compound the positrons should annihilate only against the outer electrons of the negatively charged halogen ions, since the positive alkali ions would repel the positrons from their neighborhood. If this is true, one would expect that the series (i) LiCl, KCl, and CsCl should all have similar angular correlation curves, whereas the series (ii) KF, KCl, and KI should have differing curves. Figs. 5 and 6 give some confirmation for this view. The curves for the (i) series (Fig. 5) are more alike in general shape and slope of the tail than those of the (ii) series (Fig. 6). Owing to the decay of the source, the accuracy of the KCl curve is not great enough to obtain quantitative comparisons of the curves.

Conclusion

From these experiments it is evident that the angular distribution of annihilation radiation is affected by the chemical constitution of the solid absorber in which the positrons are annihilated. The results, so far as the mean momentum of the annihilating pairs is concerned, are in qualitative agreement with the theoretical view that the positrons, essentially at rest, annihilate with the most loosely bound electrons in the solid concerned. Owing to the inadequacy of our knowledge of momentum wave functions it does not seem possible to provide a quantitative theory and check thereon except possibly by allowing the positrons to annihilate in liquid or solid hydrogen or helium.

It also appears that, if the outermost parts of the tails of the curves for the pure elements are examined, there is some indication of the steepness decreasing with increasing atomic number. It is hoped to improve the accuracy of the experiment in the near future in order to obtain conclusive evidence on this point.

The maximum deviation from antiparallelism of the two quanta which was observed corresponded to an energy of 130 ev. This limit was set, in these experiments, by the source strength or rather specific activity, the counting rate at larger angular deviations being too slow to achieve any statistical accuracy. Consequently no conclusions can be drawn regarding the annihilation of positrons in motion.

Acknowledgments

One of us (G.M.G.) acknowledges with gratitude the award of an Ontario Research Foundation scholarship covering the period in which this work was done. The work was carried out with the facilities of the Nuclear Physics Techniques Laboratory set up in this department with the generous assistance of the Defence Research Board.

References

1. ARGYLE, P. E., GRIFFITHS, G. M., and WARREN, J. B. Can. J. Phys. 29: 83. 1951.
2. ARGYLE, P. E. and WARREN, J. B. Can. J. Phys. 29: 32. 1951.
3. BERINGER, R. and MONTGOMERY, C. G. Phys. Rev. 61: 222. 1942.
4. DE BENEDETTI, S., COWAN, C. E., KONNECKER, W. R., and PRIMAKOFF, H. Phys. Rev. 77: 205. 1950.
5. DU MOND, J. W. M., LIND, D. A., and WATSON, B. B. Phys. Rev. 75: 1226. 1949.
6. HEITLER, W. H. Quantum theory of radiation. Oxford University Press, 1944.
7. MOODY, N. F. and HOWELL, W. D. National Research Council of Canada Report I.M.—8, April, 1950.
8. SILVER, MISS L. M. Can. J. Phys. 29: 59. 1951.

SPECTRUM AND STRUCTURE OF THE BORON MONOSULPHIDE (BS) MOLECULE[1]

By P. B. Zeeman[2]

Abstract

Two band systems of the BS molecule, called the α and γ systems, have been excited in a discharge through B_2S_3 vapor in a quartz discharge tube. Vibrational and rotational analyses of these systems have been carried out, and it is shown that both systems have the same lower state, which is a $^2\Sigma$ state. Both the upper states are $^2\Pi$ states. The α system is analogous to the α system of BO, but the γ system has not been observed for BO. Tables giving the vibrational and rotational constants of the various states are given. A third system of strong bands in the blue-green region is observed simultaneously with the α and γ bands in the discharge. These bands have not yet been interpreted. By means of the observed isotopic bands, it has been proved that BS is the emitter of the α and γ systems.

A. Introduction

The spectrum of the boron monoxide (BO) molecule has been analyzed by Mulliken (6), Jenkins and McKellar (5), and others. It consists of the strong α and β systems and a weak intercombination system. These bands occur in carbon arcs containing B_2O_3. They are also well developed when a volatile boron compound like BCl_3 is introduced into active nitrogen containing a trace of oxygen.

The α system consists of double double-headed bands and originates from an $A^2\Pi \rightarrow X^2\Sigma$ transition. The β bands are single-headed, and are due to a $B^2\Sigma \rightarrow X^2\Sigma$ transition. The combination system is due to transitions between the upper states of the α and β systems.

The spectrum of the BS molecule should bear a close resemblance to that of BO, since oxygen and sulphur have the same number of valence electrons. Recently the writer has observed three band systems in an electric discharge through boron trisulphide and has attributed these bands to the BS molecule, the spectrum of which has not been previously observed. A preliminary report (8) of this work has already been published, and the present paper gives further details of these band systems.

B. Experimental

In preliminary experiments to excite the BS spectrum, the vapors of BCl_3 and sulphur were introduced into flowing active nitrogen, but no new spectrum was observed.

In a subsequent experiment an uncondensed discharge was passed through a mixture of BCl_3 and sulphur vapors. A new spectrum then developed, but

[1] *Manuscript received April 12, 1951.*
Contribution from Merensky Institute for Physics, University of Stellenbosch, South Africa, and Division of Physics, National Research Council, Ottawa, Canada. Issued as N.R.C. No. 2465.
[2] *Holder of a Postdoctorate Fellowship under the National Research Council of Canada.*

disappeared after a few minutes. However, it could be restored by readmitting the BCl_3 and sulphur vapors. Intermittent exposures were made on a medium Hilger spectrograph on Kodak Polychrome and Kodak III F plates. Besides the bands of the BO, BCl, AlCl, SiO, SiCl, SiS, S_2, and BH molecules, a number of new double double-headed bands in the ultraviolet region from $\lambda\lambda 2409.9$ to 3031.9Å and a few bands in the visible region at $\lambda\lambda$ = 5180.4, 5283.2, 5350.3, 5378.5, 5490.5, and 5593.3Å appeared on the plates. It was considered likely that these two band groups belong to the BS molecule.

In order to free the observed bands from other interfering band systems, a third method was devised in which an electric discharge was passed through B_2S_3 vapor in the presence of helium or argon gas. The apparatus consisted of a vacuum system of Pyrex glass, and a quartz discharge tube of the end-on type. At one end of the capillary of the discharge tube a horizontal quartz tube was attached which contained amorphous boron in a silica boat. From the center of this quartz tube a reservoir containing vacuum distilled sulphur protruded vertically downwards. By means of an electrical heater the amorphous boron could be heated to the desired temperature, while the amount of sulphur vapor entering the system could be controlled separately. A mercury diffusion pump circulated helium or argon gas through the system at low pressure, and this circulating gas carried the sulphur vapor over the heated boron. At about 700° C. boron trisulphide (B_2S_3) was formed, and was carried into the capillary of the discharge tube. When this reaction started, the S_2 spectrum, excited in the capillary at the early stages of the heating process, disappeared, and the discharge became very bright resembling a "daylight" fluorescent lamp.

The following three new band systems were observed simultaneously in this discharge: (*a*) An extensive system of open bands degraded to the red, in the visible, red, and infrared regions of the spectrum. This system will be referred to as the α system of BS and includes the visible bands observed in the first discharge mentioned above. (*b*) A system consisting mainly of two band groups, each with several heads in the blue–green region of the spectrum. This system, which has a very close fine structure, is degraded to the violet. It will be called the blue–green system. (*c*) A system of double double-headed bands in the ultraviolet, degraded to the red. This system, which includes the ultraviolet bands mentioned before, also has a close fine structure and will be referred to as the γ system of BS.

The α bands were photographed with the glass system of a large Hilger spectrograph, and in the first and third orders of a 21 ft. concave grating in Paschen mounting. In Fig. 1 spectrograms of both components of the (4,0) band in the third order are given. The γ bands were photographed with the quartz system of the Hilger spectrograph and in the first to sixth orders of the grating mentioned above. In Fig. 2 a spectrogram of the (0,1) band in the sixth order is given.

Overlapping wave lengths of lower orders of the γ system were filtered out

by means of the cylindrical lens method described by Herzberg and Curry (3). However, the writer used an adjustable auxiliary slit in addition. This was mounted near the window of the discharge tube, and enables one to vary the width of the spectral region transmitted through the grating slit.

All plates were measured on an Abbé comparator, using the iron arc lines for comparison. Wave numbers were calculated by the method of Almy and Horsfall (1).

The following experiments were carried out in order to ascertain what the emitter of the new spectrum was.

1. The aluminum electrodes were replaced by molybdenum electrodes, but the same spectrum was obtained.

2. Spectrographic analysis of the amorphous boron showed that the most important impurities were Cu, Al, and Mg. When pure samples of these metals were introduced into the silica boat instead of the boron, no new spectrum was observed.

3. A sample of the boron was partially purified by heating it at 1100° C. for 18 hr. at a pressure of 0.1 mm. of mercury. The residue was then placed in the silica boat, and the new spectrum was observed as before.

4. Evidence of the formation of B_2S_3 during a run of the experiment was given by the violent reaction with water and the evolution of H_2S gas which was always observed when the quartz parts of the apparatus were cleaned afterwards.

In view of all these facts it seemed very likely that BS is the bearer of the new spectrum. This assumption was proved to be correct by the measurement of the isotope effect.

C. The α System

1. Rotational Analysis

By analogy to the α system of BO one would expect the α system of BS to belong to a $^2\Pi(a) \rightarrow {}^2\Sigma$ system with the $^2\Pi$ state inverted.

When the $^2\Pi$ state belongs to Hund's case (a), each band can be divided into two sub-bands, $^2\Pi_{\frac{1}{2}} \rightarrow {}^2\Sigma$ and $^2\Pi_{3/2} \rightarrow {}^2\Sigma$. These sub-bands are separated from each other by the amount of the doublet splitting of the $^2\Pi$ state. Each sub-band contains six branches which in the case of inverted $^2\Pi$ states are designated by R_1, $^QR_{12}$, Q_1, $^PQ_{12}$, P_1, and $^OP_{12}$ for the $^2\Pi_{3/2} \rightarrow {}^2\Sigma$ sub-band, and by $^SR_{21}$, R_2, $^RQ_{21}$, Q_2, $^OP_{21}$, and P_2 for the $^2\Pi_{\frac{1}{2}} \rightarrow {}^2\Sigma$ sub-band. Of these, the Q_1, $^PQ_{12}$, and $^RQ_{21}$, Q_2 branches are the strongest as was shown by Earls (2).

According to Mulliken (7) the following expressions for the rotational terms of an inverted $^2\Pi$ state hold (omitting the subscripts v):—

$$^2\Pi_{\frac{1}{2}}: F_{2,d}(J) = B^{(2)}_{eff.} J(J+1) - D^{(2)}_{eff.} J^2(J+1)^2 + \tfrac{1}{2}a(J+\tfrac{1}{2}) \quad (1)$$

$$F_{2,c}(J) = B^{(2)}_{eff.} J(J+1) - D^{(2)}_{eff.} J^2(J+1)^2 - \tfrac{1}{2}a(J+\tfrac{1}{2}) \quad (2)$$

$$^2\Pi_{3/2}: F_{1,d}(J) = F_{1,c}(J) = B^{(1)}_{eff.} J(J+1) - D^{(1)}_{eff.} J^2(J+1)^2, \quad (3)$$

$$\text{where } B^{(2),(1)}_{eff.} = B\left(1 \pm \frac{B}{A\Lambda}\right). \quad (4)$$

PLATE I

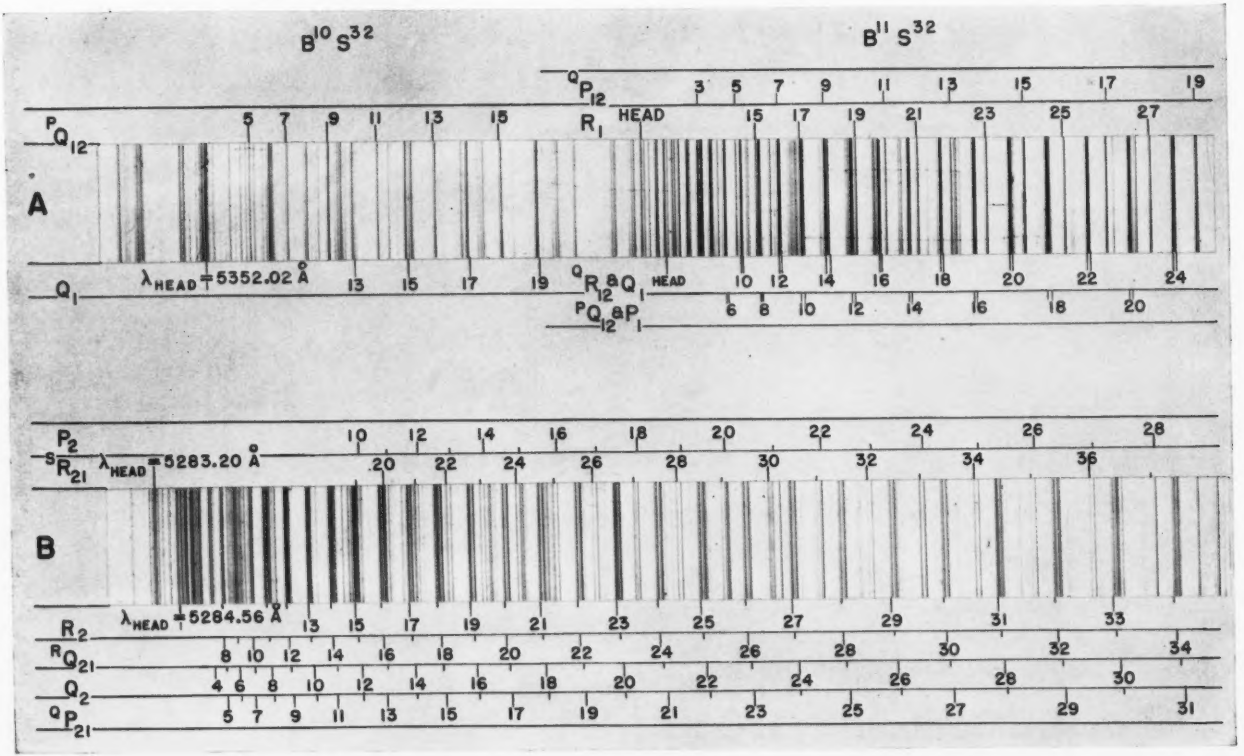

FIG. 1. *Spectrograms of the (4,0) α band.*

(A) Fine structure of the $^2\Pi_{3/2} \rightarrow {}^2\Sigma$ *sub-band photographed in the third order of a 21 ft. concave grating, showing portions of the strong* $B^{11}S^{32}$ *main band, and the weaker* $B^{10}S^{32}$ *band.*

(B) Portion of the fine structure of the $^2\Pi_{\frac{1}{2}} \rightarrow {}^2\Sigma$ *sub-band photographed in the third order of the grating.*

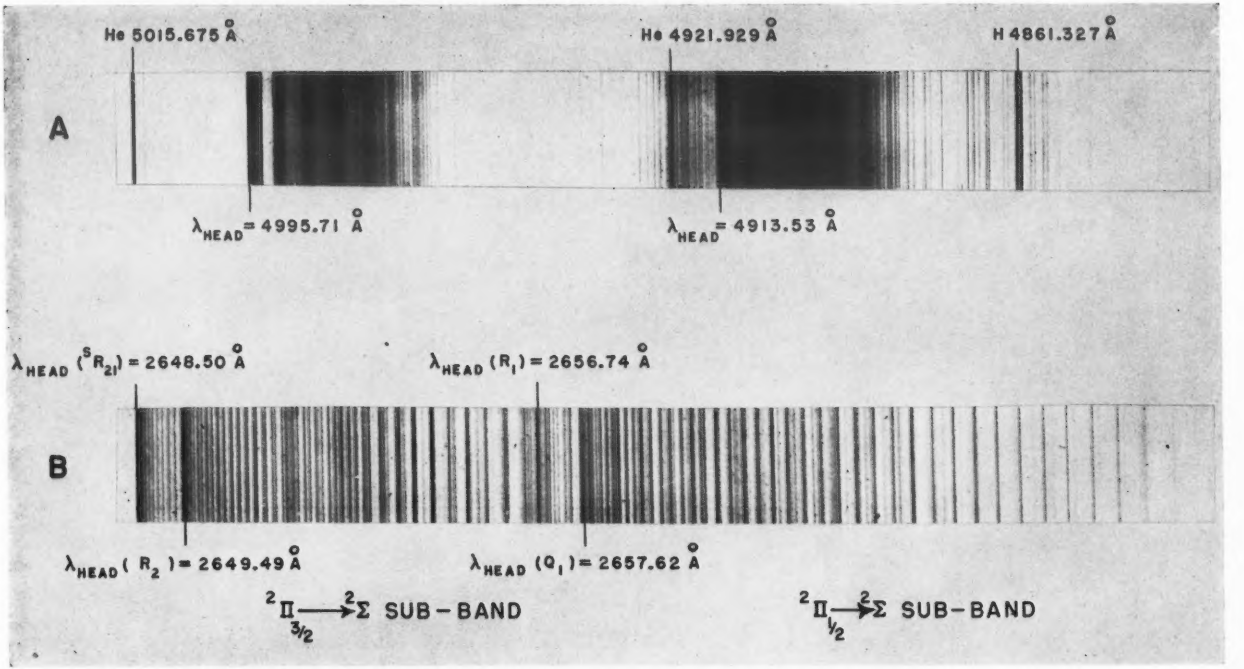

FIG. 2. *Spectrograms of the blue-green and γ bands.*

(A) Strongest band groups of the blue-green system photographed in the first order of the grating.

(B) Fine structure of the (0,1) γ band photographed in the sixth order of the grating.

In equations (1) and (2) the constants a and D are measures of the Λ-doubling, and the influence of the centrifugal force respectively.

For the $^2\Sigma$ state we have the following expressions for the rotational terms:—

$$\left.\begin{aligned} &^2\Sigma: J = K + \tfrac{1}{2}: F_1(K) = BK(K+1) - DK^2(K+1)^2 + \tfrac{1}{2}\gamma K \\ \text{or}\quad &F_1(J) = B(J-\tfrac{1}{2})(J+\tfrac{1}{2}) - D(J-\tfrac{1}{2})^2(J+\tfrac{1}{2})^2 + \tfrac{1}{2}\gamma(J-\tfrac{1}{2}), \end{aligned}\right\} \quad (5)$$

and

$$\left.\begin{aligned} &^2\Sigma: J = K - \tfrac{1}{2}: F_2(K) = BK(K+1) - DK^2(K+1)^2 - \tfrac{1}{2}\gamma(K+1) \\ \text{or}\quad &F_2(J) = B(J+\tfrac{1}{2})(J+3/2) - D(J+\tfrac{1}{2})^2(J+3/2)^2 - \tfrac{1}{2}\gamma(J+3/2), \end{aligned}\right\} \quad (6)$$

where the constant γ is a measure of the spin doubling.

The following relations were used to calculate the second differences $\Delta_2 F_i''(K)$ $(i = 1 \text{ or } 2)$:—

$$\left.\begin{aligned} \Delta_2 F_1''(K) &= R_1(K-1) - P_1(K+1) \\ &= {}^S R_{21}(K-1) - {}^O P_{21}(K+1), \end{aligned}\right\} \quad (7)$$

and

$$\left.\begin{aligned} \Delta_2 F_2''(K) &= R_2(K-1) - P_2(K+1) \\ &= {}^O R_{12}(K-1) - {}^O P_{12}(K+1). \end{aligned}\right\} \quad (8)$$

For $^2\Sigma$ states it can be proved that $\Delta_2 F_1(K) = 4B_v(K+\tfrac{1}{2}) + \gamma$ and $\Delta_2 F_2(K) = 4B_v(K+\tfrac{1}{2}) - \gamma$. Hence if the average of $\Delta_2 F_1(K)$ and $\Delta_2 F_2(K)$ is taken, γ cancels out and the value of B_v can be obtained without a knowledge of γ. This procedure was used to obtain B_0'' as described below.

In Table I the wave numbers of the lines of the various bands are given. The combination differences $\Delta_2 F_i''(K)$ for the (3,0), (4,0) and (5,0) bands are given in Table II. The second last column of Table II gives the average of these numbers, and the last column gives the corresponding average combination differences for the γ system. The close agreement of these two columns proves that both systems have the same lower state. The observation of the required number of branches in each sub-band, and the fact that the combination relations (7) and (8) are fulfilled as shown by Table II confirm the original assumption that the α system is a $^2\Pi(a) \rightarrow {}^2\Sigma$ transition like that of BO.

The rotational constants can also be determined from the $\Delta_1 F$ values instead of $\Delta_2 F$ values had it not been for the so-called "combination defect" that occurs in $^2\Pi \rightarrow {}^2\Sigma$ bands. This is due to the Λ-type doubling of the $^2\Pi$ state. As a result of this, the lines of the P and R branches start from slightly different energy levels than those of the Q branches. Hence the $\Delta_1 F'(J')$ as well as the $\Delta_1 F''(K'')$ values calculated from the P and Q branches do not quite agree with those calculated from the R and Q branches. Therefore, in such cases the $\Delta_1 F$ values do not yield accurate rotational constants. However, an indication of the magnitude of the Λ-type doubling can be obtained from these values. A knowledge of this magnitude enables us to decide whether the spin splitting of the $^2\Pi$ state is normal or inverted. According to theory (4, p. 263) the Λ-type doubling is considerably smaller for the $^2\Pi_{3/2}$ state than

for the $^2\Pi_{\frac{1}{2}}$ state. In the present investigation the magnitude of the Λ-type doubling was found to be much smaller for the longward components of individual bands. This indicates that the lower components of the upper $^2\Pi$ states are the $^2\Pi_{3/2}$ states. Thus the $^2\Pi$ upper state of the α bands of BS is inverted. This is analogous to the $^2\Pi$ upper state of the α bands of BO.

To determine the best possible values for the rotational constants the following steps were carried out. The rotational constant D_0'' was determined from the slope of the graph $\Delta_2F''(K)/(K+\frac{1}{2})$ against $(K+\frac{1}{2})^2$ as is described by Herzberg (4, p. 181). The necessary data for this plot were obtained from the average values of $\Delta_2F''(K)$ for the $v''=0$ vibrational level of the $^2\Sigma$ state given in Table II. The value $D_0''=1.40\times10^{-6}$ cm.$^{-1}$ obtained in this way

TABLE I

WAVE NUMBERS OF THE LINES OF THE (3,0), (4,0), (5,0), AND (2,1) BANDS OF THE α SYSTEM OF BS

$^2\Pi_{3/2}\rightarrow{}^2\Sigma$ sub-band of the (3,0) band; $\lambda(Q_1)=5594.92$ Å head

K''	R_1	$^QR_{12}$	Q_1	$^PQ_{12}$	P_1	$^OP_{12}$
1	17871.45	17867.77	17867.77			
2	72.30	67.97	67.97	17864.46	17864.46	17862.60
3	72.61	67.25	67.25	63.09	63.09	59.78
4	72.95	66.26	66.26	60.97	60.97	56.42
5	72.61	64.74	64.74	58.06	58.06	52.64
6	72.30	63.25	63.25	55.52	55.19	49.13
7	71.45	61.21	61.21	52.29	52.03	44.47
8	70.11	58.76	58.76	48.61	48.32	39.66
9	68.45	55.86	55.86	44.60	44.47	34.38
10	66.43	52.64	52.64	40.20	40.03	28.80
11	64.03	49.20	49.12	35.43	35.22	22.77
12	61.21	45.23	45.05	30.22	30.01	16.40
13	58.06	40.87	40.65	24.65	24.44	09.65
14	54.49	36.10	35.89	18.73	18.49	02.51
15	50.55	30.96	30.75	12.39	12.16	17794.96
16	46.22	25.44	25.21	05.67	05.44	87.09
17	41.50	19.56	19.31	17798.57	17798.35	78.79
18	36.38	13.28	13.02	91.09	90.86	70.13
19	30.96	06.62	06.35	83.23	83.00	61.05
20	25.02	17799.55	17799.29	75.01	74.74	51.62
21	18.73	92.14	91.84	66.37	66.12	41.79
22	12.16	84.27	84.01	57.37	57.06	31.59
23	05.14	76.11	75.80	47.98	47.48	21.00
24	17797.73	67.54	67.21	38.21	37.86	10.01
25	89.93	58.56	58.23	28.04	27.69	17698.66
26	81.74	49.22	48.86	17.47	17.14	86.95
27	73.18	39.46	39.10	06.55	06.19	74.83
28	64.25	29.31	28.97	17695.22	17694.84	62.35
29	54.88	18.83	18.41	83.52	83.14	49.44
30	45.14	07.93	07.51	71.45	71.04	36.20
31	35.03	17696.59	17696.22	58.99	58.59	22.56
32	24.55	84.96	84.53	46.12	45.73	08.52
33	13.65	72.90	72.46	32.92	32.45	17594.11
34	02.35	60.46	60.03	19.29	18.84	79.32
35	17690.71	47.64	47.21	05.30	04.85	64.14
36	78.61	34.45	33.94	17590.94	17590.44	48.58
37	66.20	20.86	20.36	76.16	75.67	32.62
38	53.39	06.90	06.38	61.00	60.48	16.30
39	40.18	17592.61	17591.97	45.45	44.93	17499.63
40	26.58	77.74	77.21	29.53	29.01	82.52
41	12.60	62.63	62.06	13.23	11.67	65.04
42	17598.20	47.05	46.51	17496.55	17495.96	47.18
43	83.42	31.16	30.58	79.46	78.91	28.93
44	68.24	14.85	14.28	62.00	61.43	
45	52.72	17498.17	17497.57	44.14	43.57	
46	36.77	81.10	80.49	26.33	25.57	
47	20.48	63.63	62.98			
48	03.74	45.77	45.11			
49	17486.61	27.47	26.87			
50	69.22					
51	51.33					
52	33.20					

TABLE I (*Cont'd.*)

$^2\Pi_{3/2} \rightarrow {}^2\Sigma$ sub-band of the (4,0) band; $\lambda(Q_1) = 5379.37$ Å head

K''	R_1	$^QR_{12}$	Q_1	$^PQ_{12}$	P_1	$^OP_{12}$
0	18585.92		18584.16			
1	87.32		84.38	18582.59	18582.59	
2	88.30		84.16	81.18	81.18	18579.41
3	88.88	18583.54	83.54	79.41	79.41	76.48
4	89.07	82.59	82.59	77.23	77.23	73.12
5	88.88	81.18	81.18	74.68	74.68	69.36
6	88.30	79.41	79.41	71.72	71.72	65.21
7	87.32	77.23	77.23	68.34	68.34	60.68
8	85.92	74.68	74.68	64.61	64.61	55.72
9	84.16	71.72	71.72	60.41	60.41	50.41
10	81.99	68.34	68.34	55.96	55.96	44.69
11	79.41	64.61	64.61	51.11	50.92	38.55
12	76.48	60.41	60.41	45.80	45.58	32.03
13	73.12	55.96	55.96	40.09	39.86	25.13
14	69.36	51.11	50.92	33.97	33.72	17.82
15	65.21	45.80	45.58	27.44	27.22	10.13
16	60.68	40.09	39.86	20.55	20.33	02.12
17	55.72	33.97	33.72	13.26	13.02	18493.65
18	50.41	27.44	27.22	05.60	05.34	84.79
19	44.69	20.55	20.33	18497.52	18497.25	75.53
20	38.55	13.26	13.02	89.05	88.77	65.87
21	32.03	05.60	05.34	80.19	79.88	55.83
22	25.13	18497.52	18497.25	70.92	70.62	45.38
23	17.82	89.05	88.77	61.25	60.93	34.53
24	10.13	80.19	79.88	51.20	50.85	23.32
25	01.97	70.92	70.62	40.74	40.38	11.67
26	18493.46	61.25	60.93	29.89	29.51	18399.64
27	84.58	51.20	50.85	18.64	18.24	87.23
28	75.30	40.74	40.38	07.00	06.58	74.40
29	65.59	29.89	29.51	18394.95	18394.53	61.22
30	55.59	18.64	18.24	82.51	82.04	47.60
31	44.98	07.00	06.58	69.67	69.20	33.58
32	34.09	18394.95	18394.53	56.45	56.07	19.20
33	22.80	82.51	82.04	42.84	42.43	04.40
34	11.11	69.67	69.20	28.82	28.39	18289.22
35	18398.99	56.45	56.07	14.41	13.94	73.67
36	86.50	42.84	42.43	18299.62	18299.12	57.71
37	73.61	28.66	28.18	84.40	83.92	41.34
38	60.31	14.23	13.74	68.82	68.32	24.57
39	46.61	18299.39	18298.89	52.82	52.30	07.37
40	32.52	84.20	83.62	36.44	35.89	18189.85
41	18.00	68.55	67.99	19.65	19.09	71.87
42	03.14	52.52	51.94	02.47	01.90	
43	18287.82	36.08	35.51	18184.88	18183.98	
44	72.12	19.26	18.68	66.89	66.12	
45	56.03	02.19	01.44	48.53	47.63	
46	39.55	18184.36	18183.79			
47	22.64	66.31	65.74			
48	05.33	47.93	47.32			
49	18187.65					
50	69.51					
51	51.24					
52	32.36					
53	13.06					

$^2\Pi_{\frac{1}{2}} \rightarrow {}^2\Sigma$ sub-band of the (4,0) band; $\lambda(R_2) = 5284.56$ Å head

K''	$^SR_{21}$	R_2	$^RQ_{21}$	Q_2	$^QP_{21}$	P_2
1	18921.01	18917.22	18917.98			
2	21.95	17.75	17.75	18914.74	18914.74	
3	22.48	17.22	17.22	12.96	12.96	18910.01
4	22.66	16.29	16.29	10.79	10.79	06.75
5	22.48	14.93	14.93	08.25	08.25	03.02
6	21.95	13.21	13.21	05.32	05.32	18898.87
7	21.01	11.09	11.09	02.01	02.01	94.44
8	19.67	08.56	08.56	18898.30	18898.30	89.55
9	17.97	05.85	05.70	94.21	94.21	84.23
10	15.87	02.57	02.40	89.74	89.74	78.54
11	13.39	18898.90	18898.74	84.89	84.89	72.56
12	10.47	94.85	94.67	79.62	79.62	66.13
13	07.19	90.40	90.20	73.96	73.76	59.29
14	03.52	85.57	85.36	67.94	67.71	52.10
15	18899.43	80.35	80.13	61.49	61.27	44.50
16	95.02	74.75	74.52	54.67	54.45	36.49
17	90.20	68.73	68.49	47.47	47.23	28.12
18	84.90	62.36	62.10	39.89	39.66	19.37
19	79.38	55.57	55.31	31.89	31.65	10.20
20	73.34	48.39	48.13	23.52	23.24	00.69
21	66.95	40.82	40.55	14.77	14.50	18790.73
22	60.15	32.88	32.58	05.63	05.33	80.43
23	52.96	24.53	24.22	18796.09	18795.78	69.73
24	45.38	15.82	15.48	86.17	85.84	58.64
25	37.41	06.70	06.34	75.87	75.54	47.17
26	29.01	18797.15	18796.80	65.18	64.82	35.27
27	20.31	87.27	86.89	54.09	53.70	23.02
28	11.16	76.96	76.58	42.61	42.21	10.38
29	01.63	66.27	65.88	30.74	30.33	18697.34
30	18791.70	55.18	54.77	18.46	18.08	83.88
31	81.40	43.71	43.29	05.83	05.41	70.08
32	70.68	31.85	31.42	18692.78	18692.35	55.87
33	59.60	19.59	19.14	79.34	78.91	41.27
34	48.08	06.94	06.48	65.52	65.09	26.27
35	36.20	18693.90	18693.42	51.32	50.85	10.82
36	23.91	80.47	79.98	36.71	36.24	18595.08
37	11.22	66.63	66.13	21.70	21.20	
38	18698.18	52.52	51.89	06.30	05.80	
39	84.69	37.78	36.99	18590.49		
40	70.86	22.77	22.21			
41	56.54	07.40	06.78			
42	41.89	18591.54	18590.93			
43	26.83					
44	11.35					
45	18595.50					

TABLE I (*Cont'd.*)

$^2\Pi_{3/2} \rightarrow {}^2\Sigma$ sub-band of the (5,0) band; $\lambda(Q_1)$ = 5182.22 Å head

K''	R_1	QR_{12}	Q_1	PQ_{12}	P_1	OP_{12}
0	19292.48					
1	93.96	19291.44	19291.44	19289.56	19289.56	
2	95.06	91.08	91.08	88.33	88.33	19287.55
3	95.75	90.58	90.58	86.50	86.50	84.38
4	95.97	89.56	89.56	84.27	84.27	80.81
5	95.75	88.07	88.07	81.65	81.65	77.08
6	95.06	86.23	86.23	78.64	78.64	72.90
7	93.96	83.97	83.97	75.19	75.19	68.17
8	92.48	81.32	81.32	71.39	71.39	63.02
9	90.58	78.25	78.25	67.14	67.14	57.14
10	88.28	74.73	74.73	62.51	62.51	51.32
11	85.59	70.86	70.86	57.44	57.44	45.10
12	82.45	66.57	66.57	52.00	51.80	38.48
13	78.91	62.04	61.86	46.17	45.94	31.46
14	74.97	56.92	56.75	39.93	39.71	24.05
15	70.64	51.43	51.27	33.22	33.00	16.21
16	65.92	45.56	45.34	26.16	25.92	07.97
17	60.78	39.26	38.99	18.69	18.42	19198.63
18	55.19	32.53	32.28	10.79	10.54	90.35
19	49.23	25.43	25.14	02.51	02.23	80.85
20	42.85	17.87	17.60	19193.83	19193.53	70.96
21	36.08	09.96	09.65	84.78	84.43	60.66
22	28.88	01.60	01.32	75.25	74.93	49.96
23	21.30	19192.88	19192.56	65.22	65.03	38.85
24	13.29	83.76	83.40	54.89	54.56	27.34
25	04.88	74.24	73.84	44.16	43.82	15.43
26	19196.07	64.32	63.88	33.03	32.68	03.12
27	86.86	53.81	53.44	21.50	21.11	19090.39
28	77.25	42.99	42.61	09.55	09.14	77.28
29	67.24	31.77	31.38	19097.17	19096.77	63.75
30	56.75	20.15	19.75	84.40	83.99	49.95
31	45.83	08.13	07.72	71.22	70.80	35.50
32	34.51	19095.72	19095.28	57.65	57.19	20.77
33	22.79	82.87	82.43	43.68	43.21	05.60
34	10.67	69.60	69.18	29.25	28.80	18990.09
35	19098.15	55.97	55.52	14.48	14.00	74.13
36	85.23	41.95	41.45	18999.23	18998.76	57.76
37	71.89	27.49	26.99	83.62	83.09	40.94
38	58.17	12.61	12.12	67.59	67.12	23.80
39	43.98	18997.34	18996.83	51.19	50.66	
40	29.47	81.69	81.15	34.32	33.79	
41	14.48	65.61	65.06	17.07	16.52	
42	18999.06	49.15	48.58	18899.45	18898.80	
43	83.34	32.32	31.73	81.33	80.75	
44	67.10	15.16	14.52	62.82	52.29	
45	50.48		18897.06	43.95	43.38	
46	33.50		79.13	24.69	24.86	
47	16.07		60.57	04.98	04.36	
48				18784.90	18784.26	
49				64.44	63.80	
50				43.73	42.95	
51				22.38	21.76	
52				00.85	00.15	

$^2\Pi_{\frac{1}{2}} \rightarrow {}^2\Sigma$ sub-band of the (5,0) band; $\lambda(R_2)$ = 5093.53 Å head

K''	SR_{21}	R_2	RQ_{21}	Q_2	QP_{21}	P_2
0	19628.91					
1	29.80	19627.25	19627.25			
2	30.87	26.84	26.84	19623.87	19623.87	
3	31.30	26.29	26.29	22.15	22.15	
4	31.51	25.32	25.32	19.89	19.89	
5	31.30	23.87	23.87	17.30	17.30	
6	30.80	22.15	22.15	14.32	14.32	
7	29.79	19.89	19.89	10.92	10.92	
8	28.38	17.30	17.30	07.09	07.09	
9	26.55	14.32	14.32	03.03	03.03	
10	24.29	10.92	10.92	19598.40	19598.40	19587.31
11	21.64	07.09	07.09	93.42	93.42	81.14
12	18.57	02.81	02.81	88.03	88.03	74.56
13	15.14	19598.20	19598.20	82.26	82.26	67.67
14	11.29	93.16	93.16	76.06	76.06	60.28
15	07.05	88.03	87.77	69.47	69.47	52.51
16	02.44	82.26	81.91	62.48	62.29	44.35
17	19597.38	76.06	75.73	55.08	54.91	35.79
18	91.90	69.47	69.10	47.29	47.07	26.82
19	86.06	62.29	62.10	39.10	38.88	17.45
20	79.82	54.91	54.66	30.50	30.29	07.71
21	73.15	47.07	46.83	21.51	21.26	19497.55
22	66.10	38.88	38.60	12.12	11.87	86.99
23	58.62	30.29	29.98	02.32	02.06	76.00
24	50.76	21.26	20.96	19492.15	19491.84	64.76
25	42.50	11.87	11.51	81.54	81.20	52.90
26	33.83	02.06	01.69	70.54	70.17	40.74
27	24.75	19491.84	19491.45	59.15	58.75	28.17
28	15.27	81.20	80.79	47.33	46.92	
29	05.40	70.17	69.76	35.14	34.70	
30	19495.13		58.30	22.55	22.07	
31	84.41		46.46	09.55	08.95	
32	73.34		34.22	19396.16	19395.49	

TABLE I (*Concl'd.*)

$^2\Pi_{1/2} \rightarrow {}^2\Sigma$ sub-band of the (2,1) band; $\lambda(Q_1)$ = 6258.08 Å head

K''	R_1	$^OR_{12}$	Q_1	$^PQ_{12}$	P_1	$^OP_{12}$
1				15972.81	15972.81	
2	15979.19	15974.94	15974.94	71.84	71.84	
3	79.89	74.40	74.40	70.15	70.15	15967.45
4	80.22	73.59	73.59	68.19	68.19	63.99
5	80.22	72.39	72.39	65.77	65.77	60.68
6	79.89	70.84	70.84	62.99	62.99	56.43
7	79.19	68.90	68.90	59.86	59.86	52.41
8	78.14	66.67	66.67	56.43	56.32	47.76
9	76.71	64.22	63.99	52.62	52.41	42.33
10	74.94	61.14	61.04	48.41	48.28	36.89
11	72.81	57.83	57.66	43.88	43.71	31.15
12	70.29	54.10	53.95	38.97	38.79	25.05
13	67.45	50.10	49.98	33.71	33.54	18.57
14	64.22	45.69	45.44	28.11	27.89	11.68
15	60.68	40.87	40.67	22.12	21.91	04.72
16	56.74	35.77	35.53	15.79	15.53	15897.11
17	52.41	30.28	30.04	09.09	08.85	89.09
18	47.77	24.44	24.16	02.03	01.83	80.81
19	42.76	18.21	17.95	15894.60	15894.33	72.22
20	37.37	11.68	11.36	86.82	86.59	63.20
21	31.63	04.72	04.43	78.69	78.42	53.91
22	25.56	15897.46	15897.11	70.21	69.91	44.18
23	19.07	89.76	89.44	61.35	61.03	34.11
24	12.28	81.74	81.42	52.14	51.81	23.70
25	05.07	73.39	73.06	42.56	42.21	12.94
26	15897.46	64.66	64.31	32.63	32.26	01.80
27	89.76	55.56	55.18	22.31	21.96	15790.31
28	81.42	46.10	45.73	11.70	11.31	78.42
29	72.72	36.26	35.89	00.63	00.26	66.24
30	63.69	26.10	25.78	15789.28	15788.86	53.68
31	54.33	15.53	15.15	77.52	77.11	40.71
32	44.59	04.64	04.22	65.43	65.02	27.44
33	34.52	15793.37	15792.94	52.98	52.52	13.79
34	24.03	81.73	81.29	40.14	39.69	15699.77
35	13.25	69.77	69.29	26.97	26.48	85.41
36	02.07	57.41	56.93	13.44	12.95	70.67
37	15790.52	44.68	44.19	15699.50	15699.04	55.61
38	78.59	31.61	31.12	85.26	84.77	40.10
39	66.49	18.14	17.65	70.67	70.10	24.06
40	53.68	04.35	03.81	55.61	55.13	07.99
41	40.71	15690.16	15689.62	40.29	39.76	
42	27.30	75.64	75.08	24.58	24.06	
43	13.58	60.72	60.17	08.54	07.99	
44	15699.50	45.48	44.89			
45	84.98	29.89	29.28			
46	70.10					

is in satisfactory agreement with the value $D_0'' = 1.44 \times 10^{-6}$ calculated from the approximate relation $D_0 = 4B_0^3/\omega_0^2$ using preliminary values for B_0 and ω_0. Using the experimental value of D_0'' in the equation

$$\Delta_2 F''(K) = 4B_0''(K + \tfrac{1}{2}) - 8D_0''(K + \tfrac{1}{2})^3, \qquad (9)$$

and proceeding as described by Herzberg (4, p. 181) the value $B_0'' = 0.7918_7$ was determined.

To evaluate B_4' and B_5' the values $(B_4' - B_0'')$ and $(B_5' - B_0'')$ were determined by making use of the following relations:—

$$\begin{aligned} Q_1(K) + Q_2(K+1) &= \nu_0^{(1)} + F'_{1,c}(J') - F_1''(J'') + \nu_0^{(2)} + F'_{2,c}(J') - F_2''(J'') \\ &= \nu_0^{(1)} + \nu_0^{(2)} + \gamma - \tfrac{1}{2}B'' + 2(B' - B'')J'(J'+1) + 2(D'' - D') \\ &\qquad J^2(J+1)^2 - \tfrac{1}{2}a(J' + \tfrac{1}{2}) \qquad (10) \end{aligned}$$

and

$$\begin{aligned} {}^PQ_{12}(K+1) + {}^RQ_{21}(K) &= \nu_0^{(1)} + \nu_0^{(2)} + \gamma - \tfrac{1}{2}B'' + 2(B' - B'')J'(J'+1) \\ &\quad + 2(D'' - D')J^2(J+1)^2 + \tfrac{1}{2}a(J' + \tfrac{1}{2}). \qquad (11) \end{aligned}$$

TABLE II

COMBINATION DIFFERENCES $\Delta_2F''(K)$ FOR THE $v''=0$ LEVEL OF THE $^2\Sigma$ STATE OF THE α AND γ SYSTEMS OF BS

K''	(3,0) band		(4,0) band		(4,0) band		(5,0) band		(5,0) band		Mean values from α bands	Mean values from γ bands
	$R_1(K-1)-P_1(K+1)$	$QR_{12}(K-1)-OP_{12}(K+1)$	$R_1(K-1)-P_1(K+1)$	$QR_{12}(K-1)-OP_{12}(K+1)$	$SR_{21}(K-1)-QP_{21}(K+1)$	$R_2(K-1)-P_2(K+1)$	$R_1(K-1)-P_1(K+1)$	$QR_{12}(K-1)-OP_{12}(K+1)$	$SR_{21}(K-1)-QP_{21}(K+1)$	$R_2(K-1)-P_2(K+1)$		
1			4.74	4.75					5.04		4.84	
2	8.36	7.99	7.91	7.90					7.65		7.96	
3	11.33	11.55	11.07	11.04	11.16	11.00	10.79	10.17	10.98		11.01	11.25
4	14.55	14.61	14.20	14.18	14.23	14.20	14.10	13.50	14.00		14.17	14.08
5	17.76	17.13	17.35	17.38	17.34	17.42	17.33	16.66	17.19		17.28	17.37
6	20.58	20.27	20.54	20.50	20.47	20.47	20.56	19.90	20.38		20.41	20.69
7	23.98	23.59	23.69	23.69	23.65	23.66	23.67	23.21	23.71		23.65	23.76
8	26.98	26.83	26.91	26.82	26.80	26.86	26.82	26.83	26.76		26.85	26.70
9	30.08	29.96	29.96	29.99	29.93	30.02	29.97	30.00	29.98	29.99	29.99	29.82
10	33.23	33.09	33.24	33.17	33.09	33.29	33.14	33.15	33.13	33.18	33.17	33.24
11	36.57	36.24	36.41	36.31	36.25	36.44	36.48	36.25	36.26	36.36	36.36	36.54
12	39.59	39.55	39.55	39.48	39.63	39.61	39.65	39.40	39.38	39.42	39.53	39.47
13	42.72	42.72	42.76	42.59	42.76	42.75	42.74	42.52	42.51	42.53	42.66	42.63
14	45.90	45.91	45.90	45.83	45.92	45.90	45.91	45.83	45.67	45.69	45.85	45.71
15	49.05	49.01	49.03	48.99	49.07	49.08	49.05	48.99	49.00	48.81	49.01	48.98
16	52.20	52.17	52.19	52.15	52.20	52.23	52.22	52.80	52.14	52.24	52.25	52.24
17	55.36	55.31	55.34	55.30	55.36	55.38	55.38	55.16	55.37	55.44	55.34	55.27
18	58.50	58.51	58.47	58.44	58.55	58.53	58.55	58.41	58.50	58.61	58.51	58.39
19	61.64	61.66	61.64	61.57	61.66	61.67	61.66	61.57	61.61	61.76	61.64	61.72
20	64.84	64.83	64.81	61.72	64.88	64.84	64.80	64.77	64.80	64.74	64.50	64.95
21	67.96	67.96	67.93	67.88	68.01	67.96	67.92	67.91	67.95	67.92	67.94	67.98
22	71.25	71.14	71.10	71.07	71.17	71.09	71.05	71.11	71.09	71.07	71.11	71.14
23	74.30	74.26	74.28	74.20	74.31	74.24	74.32	74.24	74.26	74.12	74.25	74.29
24	77.45	77.45	77.44	77.38	77.42	77.36	77.48	77.45	77.42	77.39	77.42	77.52
25	80.59	80.59	80.62	80.55	80.56	80.55	80.61	80.64	80.59	80.52	80.58	80.50
26	83.74	83.73	83.73	83.69	83.71	83.68	83.77	83.85	83.75	83.70	83.74	83.71
27	86.90	86.87	86.88	86.85	86.80	86.77	86.93	87.04	86.91		86.88	86.83
28	90.04	90.02	90.05	89.98	89.98	89.93	90.09	90.06	90.05		90.02	90.01
29	93.21	93.11	93.26	93.14	93.08	93.08	93.26	93.04	93.20		93.15	93.36
30	96.29	96.27	96.39	96.31	96.22	96.19	96.44	96.27	96.45		96.31	96.26
31	99.41	99.41	99.52	99.44	99.35	99.31	99.56	99.38	99.64		99.45	99.25
32	102.58	102.48	102.55	102.60	102.49	102.44	102.62	102.73			102.56	102.90
33	105.71	105.64	105.70	105.73	105.59	105.58	105.71	105.63			105.66	105.57
34	108.80	108.76	108.86	108.84	108.75	108.77	108.79	108.74			108.79	109.14
35	111.91	111.88	111.99	111.96	111.74	111.86	111.91	111.84			111.89	112.07
36	115.04	115.02	115.07	115.11	115.00		115.06	115.03			115.05	115.01
37	118.13	118.15	118.18	118.27	118.11		118.11	118.15			118.16	117.92
38	121.27	121.23	121.31	121.29	121.21		121.23				121.26	121.46
39	124.38	124.48	124.42	124.38			124.38				124.41	
40	127.51	127.57	127.52	127.52			127.46				127.52	
41	130.62	130.56	130.62				130.67				130.62	
42	133.69	133.70	134.02				133.73				133.79	
43	136.77		137.02								136.90	
44	139.85		140.19								140 02	

It is clear from the above that if the average of equations (10) and (11) is taken, the effect of the Λ-doubling in the $^2\Pi_{\frac{1}{2}}$ state cancels out. If, further, the term in D is subtracted from the average of the left hand sides of Equations

TABLE III

ROTATIONAL CONSTANTS OF THE α SYSTEM OF BS

State	v	$B_{eff.}^{(1)}$ (obs.) cm.$^{-1}$	$B_{eff.}^{(1)}$ (calc.) cm.$^{-1}$	$B_{eff.}^{(2)}$ (obs.) cm.$^{-1}$	$B_{eff.}^{(2)}$ (calc.) cm.$^{-1}$	B_v(obs.) cm.$^{-1}$	B_v(calc.) cm.$^{-1}$
$^2\Pi$	0		0.6184_2		0.6214_6		0.6199_5
	1		0.6125_3		0.6155_2		0.6140_5
	2	0.6066_6	0.6066_4		0.6095_8		0.6081_1
	3	0.6007_4	0.6007_5		0.6036_4		0.6021_9
	4	0.5948_4	0.5948_6	0.5976_8	0.5977_0	0.5962_6	0.5962_7
	5	0.5889_9	0.5889_7	0.5917_8	0.5917_6	0.5903_8	0.5903_5
$^2\Sigma$	0					0.7918_7	0.7918_6
	1					0.7858_2	0.7858_1

(10) and (11), and if the resulting values are plotted against $J'(J'+1)$, a straight line is obtained. The slope of this straight line gives $(B' - B'')$, and the intercept gives $(\nu_0^{(1)} + \nu_0^{(2)} - \frac{1}{2}B'')$ if the small constant γ is neglected. For the subtraction of the term in D a value for D', calculated from $D_e = \dfrac{4B_e^3}{\omega_e^2}$ was used. In this way the values of the constants B_4' and B_5' listed in Table III were obtained. The graph for determining $(B_4' - B_0'')$ in this way is given in Fig. 3.

In order to obtain separately $B_{4,\,eff.}^{\prime(1)}$, $B_{4,\,eff.}^{\prime(2)}$ and $B_{5,\,eff.}^{\prime(1)}$, $B_{5,\,eff.}^{\prime(2)}$, use was made of the following relations:—

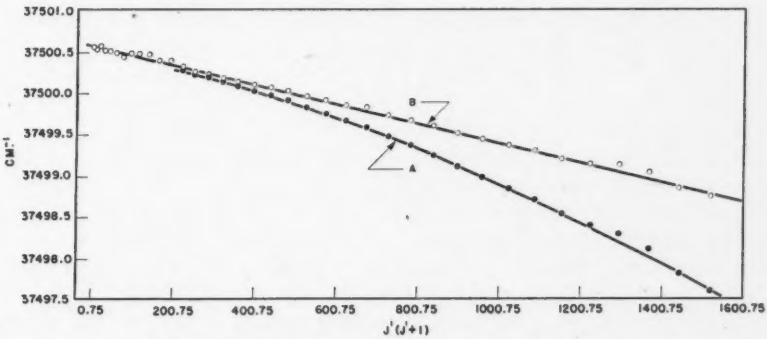

FIG. 3. *Graphical determination of* $(B'_4 - B''_0)$ *and* $(\nu_0^{(1)} + \nu_0^{(2)} - \frac{1}{2}B''_0)$ *for the* (4,0) α *band of BS.*

Curve A: $\frac{1}{2}\left[\{Q_1(K) + Q_2(K+1)\} + \{{}^PQ_{12}(K+1) + {}^RQ_{21}(K)\}\right] + \overline{(B' - B'')}J'(J'+1)$ *versus* $J'(J'+1)$.

Curve B: $\frac{1}{2}\left[\{Q_1(K) + Q_2(K+1)\} + \{{}^PQ_{12}(K+1) + {}^RQ_{21}(K)\}\right] + \overline{(B' - B'')}J'(J'+1) + 2(D'' - D')J'^2(J'+1)^2$ *versus* $J'(J'+1)$.

$$
\begin{aligned}
{}^{S}R_{21}(K) - R_1(K) &= Q_2(K+2) - {}^{P}Q_{12}(K+2) \\
&= {}^{Q}P_{21}(K+2) - P_1(K+2) \qquad (12) \\
&= \nu_0^{(2)} - \nu_0^{(1)} + (B'^{(2)}_{eff.} - B'^{(1)}_{eff.})\, J'(J'+1) - \tfrac{1}{2}a(J'+\tfrac{1}{2})
\end{aligned}
$$

and

$$
\begin{aligned}
R_2(K+1) - {}^{Q}R_{12}(K+1) &= {}^{R}Q_{21}(K+1) - Q_1(K+1) \\
&= P_2(K+3) - {}^{O}P_{12}(K+3) \qquad (13) \\
&= \nu_0^{(2)} - \nu_0^{(1)} + (B'^{(2)}_{eff.} - B'^{(1)}_{eff.})\, J'(J'+1) \\
&\qquad + \tfrac{1}{2}a(J'+\tfrac{1}{2})\,.
\end{aligned}
$$

By averaging equations (12) and (13) the influence of the Λ-doubling can again be eliminated. By plotting this average value against $J'(J'+1)$, the values of $(\nu_0^{(2)} - \nu_0^{(1)})$ and $(B'^{(2)}_{eff.} - B'^{(1)}_{eff.})$ can be determined. In this way the following constants were obtained:— $(B'^{(2)}_{4,\,eff.} - B'^{(1)}_{4,\,eff.}) = 0.0028_4$ and $(B'^{(2)}_{5,\,eff.} - B'^{(1)}_{5,\,eff.}) = 0.0027_9$. By combining the values of $(B'^{(2)}_{eff.} - B'^{(1)}_{eff.})$ with those of $B' = \frac{1}{2}(B'^{(2)}_{eff.} + B'^{(1)}_{eff.})$ the individual constants for the $^2\Pi$ state listed in Table III were obtained. At the same time it was found that for the (4,0) band $\nu_0^{(1)} = 18583.69$, $\nu_0^{(2)} = 18917.30$ cm.$^{-1}$, and for the (5,0) band $\nu_0^{(1)} = 19290.83$, $\nu_0^{(2)} = 19626.52$ cm.$^{-1}$

In the case of the (3,0) band only the $^2\Pi_{3/2} \rightarrow {}^2\Sigma$ sub-band was analyzed. To obtain the rotational constant $B'^{(1)}_{3,\,eff.}$ the quantity $(B'^{(1)}_{3,\,eff.} - B''_0)$ was determined from a plot of the average of quantities like $\underset{(4,\,0)}{Q_1(K)} - \underset{(3,\,0)}{Q_1(K)}$ against $J'(J'+1)$. The value of $B'^{(1)}_{3,\,eff.} = 0.6007_4$ cm.$^{-1}$ was obtained.

For the (2,1) band the constants $B'^{(1)}_{2,\,eff.}$ and B''_1 were determined from $\Delta_2F(K)$ values as described above for the determination of B''_0 and the values listed in Table III were obtained.

In Table III a summary of the various rotational constants is given.

From the $B^{(1)}_{eff.}$ values in Table III, the average value $\alpha_e^{(1)} = 0.0058_9$ cm.$^{-1}$ is obtained. From the individual $B_{eff.}$ values for the (4,0) and (5,0) bands we obtain $\alpha_e'^{(2)} - \alpha_e'^{(1)} = 0.00005_3$. This difference can also be obtained by using the formula $\alpha_e'^{(2)} - \alpha_e'^{(1)} = 2(B_4^2/A - B_5^2/A)$ which is derived from Equation (4). This gives a value of $\alpha_e'^{(2)} - \alpha_e'^{(1)} = 0.00005_6$. Because of this satisfactory agreement the value $\alpha_e' - \alpha_e'^{(1)} = 0.00002_7$ cm.$^{-1}$ was used to calculate α_e' from $\alpha_e'^{(1)}$. In this way the value $\alpha_e' = 0.0059_2$ cm.$^{-1}$ was obtained. The values $B_e'^{(1)} = 0.6213_7$ cm.$^{-1}$, $B_e'^{(2)} = 0.6244_3$, and $B_e' = 0.6229_1$ cm.$^{-1}$ were obtained by using the formula $B_v = B_e' - \alpha_e(v+\frac{1}{2})$. The $B'^{(1),\,(2)}_{v,\,eff.}$ and B_v' values calculated with these values of $B_e'^{(1),\,(2)}$, B_e', $\alpha_e'^{(1),\,(2)}$, and α_e' are given in the fourth, sixth, and eighth columns respectively of Table III. For the $^2\Sigma$ state the values $\alpha_e'' = 0.0060_5$ and $B_e'' = 0.7948_9$ cm.$^{-1}$ were obtained from the values of B_0'' and B_1'' given previously.

2. Isotope Effect and Vibrational Analysis

When the band heads were arranged in a Deslandres table, a head at 18679.35 cm.$^{-1}$ could not be fitted into the scheme. This band appeared very

similar to the adjacent $^2\Pi_{3/2} \rightarrow {}^2\Sigma$ component of the (4,0) band as can be seen in Fig. 1, and it was thought likely that it represented the corresponding component of the (4,0) band of the $B^{10}S^{32}$ molecule. This assumption was tested by a more detailed study of the isotope shift.

The vibrational isotopic displacement of a given band is given by

$$\Delta\nu_v = (\rho - 1)\left[\omega_e'(v' + \tfrac{1}{2}) - \omega_e''(v'' + \tfrac{1}{2})\right] - (\rho^2 - 1)\left[\omega_e' x_e'(v' + \tfrac{1}{2})^2 - \omega_e'' x_e''(v'' + \tfrac{1}{2})^2\right]. \quad (14)$$

The following vibrational quanta of the upper state were determined simultaneously with the rotational constants listed above:—
$\Delta G'^{(1)}_{3\frac{1}{2}} = 716.38_0$ cm.$^{-1}$, $\Delta G'^{(1)}_{4\frac{1}{2}} = 707.13_7$ cm.$^{-1}$ Hence we have $\omega_e'^{(1)} = 753.35_2$ cm.$^{-1}$ and $\omega_e' x_e' = 4.62_2$ cm.$^{-1}$ From the Deslandres table of the α bands given in Table V we obtain the values $\omega_e'' = 1180.17$ cm.$^{-1}$ and $\omega_e'' x_e'' = 6.31$ cm.$^{-1}$ Substituting these values in equation (14) and using $\rho = 1.03635$ for the $B^{10}S^{32}$ and $B^{11}S^{32}$ molecules, we obtain $\Delta\nu_v = 94.97$ cm.$^{-1}$ for the (4,0) band. Therefore the origin and head of the longward component of the (4,0) band of $B^{10}S^{32}$ are expected to be $\nu_0^{i(1)} = 18583.69 + 94.97 = 18678.66$ cm.$^{-1}$ and $\nu_{head}^i = 18584.38 + 94.97 = 18679.35$ cm.$^{-1}$ The latter value agrees satisfactorily with the measured position of the (4,0) isotopic head at 18679.36 cm.$^{-1}$

Fig. 1 shows that there are only two branches clearly visible in the isotopic band and these were interpreted as the Q_1 and $^PQ_{12}$ branches, which are the strongest in the main bands. We have

$$\left.\begin{aligned} Q_1(J) &= \nu_0^{(1)} + B'^{(1)}_{v',\,eff.} J(J+1) - B''_{v''}(J - \tfrac{1}{2})(J + \tfrac{1}{2}), \\ {}^PQ_{12}(J) &= \nu_0^{(1)} + B'^{(1)}_{v',\,eff.} J(J+1) - B''_{v''}(J + \tfrac{1}{2})(J + 3/2). \end{aligned}\right\} \quad (15)$$

Remembering that $B_e^i = \rho^2 B_e$ and $\alpha_e^i = \rho^3 \alpha_e$, and substituting the rotational constants of $B^{11}S^{32}$ listed above and $\rho = 1.03635$, we obtain for the rotational isotope shifts of the Q_1 and $^PQ_{12}$ branches

$$\left.\begin{aligned} \Delta\nu_r(Q_1) &= 0.02 + 0.0429_9 J - 0.0154_9 J^2 \\ \text{and} \quad \Delta\nu_r({}^PQ_{12}) &= -0.04 - 0.0483_1 J - 0.0154_9 J^2. \end{aligned}\right\} \quad (16)$$

The numbering of the isotopic band was easily determined since the isotopic displacement is small. In Table IV the observed and calculated wave numbers of the Q_1 branch are given. It will be noticed that there is a small nearly constant difference between the observed and calculated values. A difference of approximately the same magnitude exists between the observed and calculated values of the $^PQ_{12}$ isotopic branch. Since this difference does not vary with J, it can be taken into account by a suitable adjustment of $\Delta\nu_v$. This drift may be due to slight inaccuracies in the values of ω_e'' and $\omega_e'' x_e''$. The satisfactory agreement of the observed and calculated values in Table IV confirms the assumption that the band at 18679.36 cm.$^{-1}$ is the head of the isotopic (4,0) band, and at the same time confirms that BS is the emitter of the new band system.

TABLE IV

COMPARISON OF THE OBSERVED AND CALCULATED WAVE NUMBERS OF THE Q_1 BRANCH OF THE $^2\Pi_{3/2} \rightarrow {}^2\Sigma$ COMPONENT OF THE (4,0) BAND OF THE $B^{10}S^{32}$ MOLECULE

J''	Q_1(obs.) cm.$^{-1}$	Q_1(calc.) cm.$^{-1}$	o–c cm.$^{-1}$
$2\frac{1}{2}$	18679.36	18679.16	+0.20
$3\frac{1}{2}$	78.75	78.45	+0.30
$4\frac{1}{2}$	77.67	77.42	+0.25
$5\frac{1}{2}$	76.18	75.90	+0.28
$6\frac{1}{2}$	74.27	73.98	+0.29
$7\frac{1}{2}$	71.94	71.63	+0.31
$8\frac{1}{2}$	69.12	68.86	+0.26
$9\frac{1}{2}$	65.90	65.68	+0.22
$10\frac{1}{2}$	62.28	62.03	+0.25
$11\frac{1}{2}$	58.25	58.00	+0.25
$12\frac{1}{2}$	53.78	53.48	+0.30
$13\frac{1}{2}$	48.84	48.67	+0.17
$14\frac{1}{2}$	43.55	43.23	+0.32
$15\frac{1}{2}$	37.78	37.47	+0.31
$16\frac{1}{2}$	31.62	31.30	+0.32
$17\frac{1}{2}$	25.01	24.68	+0.33
$18\frac{1}{2}$	17.98	17.66	+0.32
$19\frac{1}{2}$	10.51	10.22	+0.29
$20\frac{1}{2}$	02.63	02.34	+0.29
$21\frac{1}{2}$	594.31	594.05	+0.26
$22\frac{1}{2}$	85.58	85.32	+0.26
$23\frac{1}{2}$	76.48	76.17	+0.31
$24\frac{1}{2}$	66.92	66.58	+0.34
$25\frac{1}{2}$	56.85	56.59	+0.26

In Table V the Deslandres table of all the measured band heads of the α system is given. All values refer to the more abundant isotopic molecule $B^{11}S^{32}$. Except for a few heads at the short wave length side, all heads were measured on first and third order grating plates. Four heads are given for each band wherever possible. These heads are formed by the Q_1 and R_1 branches for the longward component and by the R_2 and $^SR_{21}$ branches for the shortward component of each band. No sequences were obvious in this system, and the bands could only be arranged in a Deslandres table after the rotational analyses of several bands indicated which ones have the same upper or lower vibrational levels. The values of the vibrational constants ω_e and $\omega_e x_e$ of the lower state were obtained directly from the average vibrational quanta given in the Deslandres table. A summary of the vibrational constants will be given, together with those of the γ system, in Table IX. The following equations give the heads of the α bands of the more abundant isotope.

$$^2\Pi_{3/2} \rightarrow {}^2\Sigma : \nu_{head} = \left.\begin{matrix}15663.1\\15668.5\end{matrix}\right\} + [748.94v' - 4.67v'^2] - [1173.87v'' - 6.31v''^2], \quad (17)$$

$$^2\Pi_{\frac{1}{2}} \rightarrow {}^2\Sigma : \nu_{head} = \left.\begin{matrix}15996.8\\16002.2\end{matrix}\right\} + [748.94v' - 4.67v'^2] - [1173.87v'' - 6.31v''^2]. \quad (18)$$

TABLE V

DESLANDRES TABLE OF THE α BANDS OF BS

v' \ v''	0		1		2		3		4	Average $\Delta G'_{v+\frac{1}{2}}$
0			14495.4	1154.7	13340.7	1140.7	12198.3	1129.8	11068.5	
			—		—		12204.3	1129.5	11074.8	
			—		13672.9	1142.5	12530.4	1129.7	11400.7	
			—		—		12537.6		—	
			744.6				744.9			
							743.3			744.27
1			15240.0		—		12943.2			
			15245.5	1154.6	14090.9	1143.3	12947.6			
			15572.6		—		—			
			—		—		—			
			735.1							
			734.8							735.20
			735.7							
	17142.4	1167.3	15975.1	1154.5	14820.6					
2	17147.6	1167.3	15980.3		—					
	—		16308.3		—					
	—		16313.4		—					
	726.0		725.6							
	725.4		727.0							725.77
			725.9							
			724.7							
	17868.4	1167.7	16700.7							
3	17873.0	1166.5	16706.5							
	18202.0	1167.8	17034.2							
	18207.1	1169.0	17038.1							
	716.0		716.4							
	716.1									716.02
	715.8									
	715.8									
	18584.4	1167.3	17417.1							
4	18589.1		—							
	18917.8		—							
	18922.7		—							
	707.0									
	706.9									706.95
5	19291.4									
	19296.0									
Average $\Delta G''_{v+\frac{1}{2}}$		1167.56		1154.45		1142.07		1129.73		

D. The γ System

1. Rotational Analysis

As was stated before, the lines of these bands are much closer together than those of the α bands, and the ${}^{R}Q_{21}$ and ${}^{Q}P_{21}$ branches in the ${}^{2}\Pi_{3/2} \rightarrow {}^{2}\Sigma$ sub-bands as well as the ${}^{Q}R_{12}$ and ${}^{P}Q_{12}$ branches in the ${}^{2}\Pi_{\frac{1}{2}} \rightarrow {}^{2}\Sigma$ sub-bands were not resolved from the R_2, Q_2 and Q_1, P_1 branches respectively. In Table VI

TABLE VI

WAVE NUMBERS OF THE LINES OF THE (0,0) AND (0,1) BANDS OF THE γ SYSTEM OF BS

$^2\Pi_{3/2} \rightarrow {}^2\Sigma$ sub-band of the (0,0) band; $\lambda(R_2)$ = 2570.01 Å head

K''	SR_{21}	R_2	Q_2	P_2
0	38900.20			
1	02.19	38897.10		
2	03.98	97.83	38894.11	
3	05.53	98.27	93.14	38889.91
4	06.91	98.66	92.02	86.54
5	08.16	98.66	90.69	84.18
6	09.18	98.27	89.03	81.07
7	09.89	97.83	87.16	78.03
8	10.54	97.10	85.17	74.52
9	11.05	96.25	82.94	71.29
10	11.55	95.26	80.58	67.30
11	11.55	94.01	78.03	63.04
12	11.55	92.72	75.25	58.77
13	11.55	91.06	72.28	54.51
14	11.05	89.41	69.15	50.17
15	10.54	87.76	65.83	45.40
16	09.89	85.60	62.31	40.45
17	09.18	83.27	58.77	35.48
18	08.16	80.84	54.83	30.41
19	06.91	78.43	50.82	24.91
20	05.53	75.54	46.69	19.29
21	03.98	72.55	42.39	13.57
22	02.19	69.49	37.84	07.60
23	00.20	66.21	33.11	01.48
24	38898.27	63.04	28.15	38795.17
25	95.67	58.77	23.05	88.81
26	93.14	54.83	17.71	82.70
27	90.69	50.82	12.19	
28		46.35	06.43	
29		41.58	00.49	
30		36.64		
31		30.97		

$^2\Pi_{\frac{1}{2}} \rightarrow {}^2\Sigma$ sub-band of the (0,0) band; $\lambda(Q_1)$ = 2577.66 Å head

K''	R_1	Q_1	P_1	OP_{12}
2	38788.20			
3	89.40			
4	90.87	38783.23	38776.99	38772.01
5	92.21	83.23	75.33	69.30
6	93.07	82.70	73.72	66.01
7	93.87	82.06	71.47	62.71
8	94.27	81.39	69.30	59.39
9	95.13	80.41	67.01	55.69
10	95.13	79.18	64.43	51.50
11	95.13	77.87	61.86	47.49
12	95.13	76.47	58.54	42.97
13	94.72	74.71	55.69	38.46
14	94.27	72.79	52.42	33.74
15	93.64	70.79	48.97	28.96
16	92.66	68.51	45.27	24.00
17	91.63	66.01	41.44	18.60
18	90.85	63.44	37.31	13.37
19	89.38	60.69	33.21	07.67
20	87.63	57.58	28.96	01.71
21	85.82	54.41	24.34	38695.74
22	83.77	51.03	19.62	89.87
23	81.39	47.49	14.62	83.57
24	79.18	43.72	09.52	77.12
25	76.47	39.82	03.95	70.39
26	73.72	35.73	38698.53	63.49
27	70.79	31.38	92.76	56.38
28	67.78	26.97	86.89	49.19
29	64.43	22.26	80.78	41.85
30	60.69	17.47	74.42	34.16
31	57.58	12.39	68.17	26.08
32	53.26	07.16	61.44	18.32
33	49.73	01.71	54.68	09.92
34	45.27	38696.16	47.69	01.78
35	40.66	90.31	40.59	38593.34
36	35.73	84.39	33.20	84.66
37	31.38	78.15	25.65	75.91
38		71.77	17.81	66.65
39		65.15	09.92	
40		58.42	01.78	
41		51.44	38593.34	
42		44.25	84.66	
43		36.64	75.91	
44		28.75	66.65	
45		21.69		

TABLE VI (*Concl'd.*)

$^2\Pi_{3/2} \rightarrow {}^2\Sigma$ sub-band of the (0,1) band; $\lambda(R_2)$ = 2649.52 Å head

K''	$^SR_{21}$	R_2	Q_2	P_2
0	37732.43			
1	34.15	37730.75		
2	36.06	31.20	37727.58	
3	37.77	31.51	26.23	37722.60
4	39.21	31.51	25.25	20.17
5	40.61	31.51	23.41	17.00
6	41.58	31.20	22.09	14.26
7	42.81	30.75	20.17	11.34
8	43.58	30.21	18.20	07.64
9	44.31	29.46	16.07	04.08
10	44.78	28.56	13.76	00.35
11	45.09	27.58	11.34	37696.54
12	45.28	26.23	08.68	92.51
13	45.28	24.79	05.91	88.29
14	45.09	23.20	02.96	83.68
15	44.78	21.36	37699.76	79.42
16	44.31	19.80	96.54	74.80
17	43.58	17.58	93.27	69.90
18	42.81	15.39	89.51	65.02
19	41.58	13.16	85.76	59.68
20	40.61	10.71	81.71	54.42
21	39.21	08.00	77.75	48.83
22	37.77	05.03	73.40	43.11
23	36.06	02.07	69.98	37.31
24	34.15	37698.78	64.32	31.36
25	32.43	95.35	59.43	24.94
26		91.60	54.42	
27		87.77	49.25	
28		83.68	43.81	
29		79.42	38.19	
30		74.80	32.27	
31		69.90	26.02	
32		65.02	19.16	
33		59.68	12.55	

$^2\Pi_{\frac{1}{2}} \rightarrow {}^2\Sigma$ sub-band of the (0,1) band; $\lambda(Q_1)$ = 2657.65 Å head

K''	R_1	Q_1	P_1	$^OP_{12}$
0	37616.58			
1	18.67	37615.13		
2	20.83	15.57		
3	22.47	16.04	37611.09	37607.80
4	23.90	16.04	09.94	05.00
5	24.94	16.04	08.30	02.10
6	26.02	15.57	06.59	37598.92
7	26.89	15.13	04.63	95.65
8	27.56	14.42	02.67	92.19
9	28.11	13.48	00.21	88.47
10	28.44	12.55	37597.88	84.69
11	28.57	11.31	95.13	80.64
12	28.57	09.94	92.19	76.39
13	28.44	08.30	89.42	72.23
14	28.11	06.58	86.43	67.79
15	27.56	04.63	83.00	63.09
16	26.89	02.68	79.53	58.11
17	26.02	00.45	75.98	53.20
18	25.30	37598.22	71.94	48.00
19	23.90	95.49	68.07	42.59
20	22.47	92.64	63.77	37.04
21	20.83	89.62	59.46	31.28
22	19.16	86.66	54.92	25.31
23	17.20	83.39	50.16	19.42
24	15.13	79.96	45.43	13.09
25	12.91	76.39	40.32	06.96
26	10.44	72.46	35.10	00.32
27	07.79	68.44	29.82	37493.93
28	04.99	64.23	24.15	86.56
29	02.10	59.96	18.56	79.59
30	37598.92	55.44	12.63	72.28
31	95.65	50.72	06.57	64.92
32	92.19	45.86	00.32	57.23
33	88.47	40.86	37493.93	
34	84.69	35.66	87.35	
35	80.64	30.30	80.45	
36	76.39	24.74		
37	71.94	18.86		
38	67.49	13.09		
39	63.77	06.96		
40	59.46	00.71		
41	54.92	37494.19		
42	50.16	87.35		
43	45.43	80.45		
44	40.32	73.97		
45	35.10	66.97		
46	29.82	59.76		

the wave numbers of the lines of the (0,0) and (0,1) γ bands are given. The average combination differences $\Delta_2F_1''(K)$ and $\Delta_2F_2''(K)$ are given in the last column of Table II.

The magnitude of the combination defect ϵ indicates that the higher energy doublet component is $^2\Pi_{3/2}$, and the lower energy doublet component is $^2\Pi_{\frac{1}{2}}$. Hence the $^2\Pi$ state is normal in this case.

Since the measurements of the α system are more accurate than those of the γ system, the values of B_0'' and $\Delta G_{\frac{1}{2}}''$ for the α system were taken over. However, as a check the quantities

$$\begin{matrix}(0,0) & (0,1)\\ Q_1(K) - Q_1(K) = \Delta G_{\frac{1}{2}}'' + (B_1'' - B_0'')\,K\,(K+1)\end{matrix} \qquad (19)$$

were plotted, and the values $\Delta G_{\frac{1}{2}}'' = 1167.54$ cm.$^{-1}$ and $\alpha_e'' = 0.0060_3$ cm.$^{-1}$ were obtained which agree well with $\Delta G_{\frac{1}{2}}'' = 1167.56$ cm.$^{-1}$ and $\alpha_e'' = 0.0060_5$ cm.$^{-1}$ determined for the α system.

The value of B_0' for the γ system was determined by making use of the fact that the two systems have the same lower state. For corresponding lines of the Q_2 branches in a γ and an α band we have

$$\begin{aligned}Q_{2,\,\gamma}(K) - Q_{2,\,\alpha}(K) = {} & \nu_{0,\gamma}^{(2)} - \nu_{0,\alpha}^{(2)} + (B_\gamma'^{(2)} - B_\alpha'^{(2)})\,J'(J'+1)\\ & - (D_\gamma'^{(2)} - D_\alpha'^{(2)})J'^2(J'+1)^2 + \tfrac{1}{2}a(J'+\tfrac{1}{2}).\end{aligned} \qquad (20)$$

A similar expression holds for $R_2,\,\gamma(K-1) - R_2,\,\alpha(K-1)$ except that the term $+\frac{1}{2}a(J'+\frac{1}{2})$ in (20) changes to $-\frac{1}{2}a(J'+\frac{1}{2})$. Hence, by averaging the left hand sides of those equations which contain the term $+\frac{1}{2}a(J'+\frac{1}{2})$ and those that contain the term $-\frac{1}{2}a(J'+\frac{1}{2})$, the effect of the Λ-doubling in the $^2\Pi_{\frac{1}{2}}$ state involved cancels out. Subtracting the term in D from these average values, and plotting against $J'(J'+1)$, one obtains the quantities $\nu_{0,\gamma}^{(2)}$ and $B_\gamma'^{(2)}$. A similar procedure can be applied to $\nu_{0,\gamma}^{(1)}$ and $B_\gamma'^{(1)}$. By combining the (4,0) and (5,0) α bands with the (0,0) γ band, the following rotational constants were obtained: $B_{0,\gamma}'^{(1)} = 0.6998_4$, $B_{0,\gamma}'^{(2)} = 0.7052_4$ cm.$^{-1}$ This gives the average value $B_{0,\gamma}' = 0.7025_4$ cm.$^{-1}$ At the same time the quantities $\nu_0{}^{(1)}(0,0)$ and $\nu_0{}^{(2)}(0,0)$ for the γ bands, given in Table IX, were obtained.

The equilibrium values of the rotational constants of the three observed states of the BS molecule are collected in Table VII.

TABLE VII

EQUILIBRIUM ROTATIONAL CONSTANTS OF THE OBSERVED ELECTRONIC STATES OF BS

State	B_e cm.$^{-1}$	α_e cm.$^{-1}$	$r_e \times 10^{-8}$ cm.
$C^2\Pi$	$(B_0 = 0.7025_4)$	....	$(r_0 = 1.7116)$
$A^2\Pi$	0.6229_1	0.0059_2	1.8177
$X^2\Sigma$	0.7948_9	0.0060_5	1.6091

2. *Vibrational Analysis*

The $v''-$ progression with $v' = 0$ of the γ bands could easily be recognized as such. In Table VIII the Deslandres table of the $B^{11}S^{32}$ heads is given.

TABLE VIII

DESLANDRES TABLE OF THE γ BANDS OF BS

v' \ v''	0		1		2		3		4	Average $\Delta G'_{v+\frac{1}{2}}$
	38785	1168	37617	1155	36462	1143	35319	1128	34191	
0	38796	1167	37629	1154	36475	1141	35334	1128	34206	
	38899	1167	37732	1155	36577	1143	35434	1128	34306	
	38912	1166	37746	1155	36591	1140	35451	1129	34322	
	881						877		878	
	882						882		878	879.2
	878								875	
	878						883			
	39666						36196	1127	35069	
1	39678						36216	1132	35084	
	39777						—		35181	
	39790						36334		—	
	863									
	865									
	868									866.0
	868									
	40529	1167	39362	1153	38209					
2	40543	1169	39372	1148	38224					
	40645	1170	39475	1151	38324					
	40658	1166	39492	1155	38337					
	851		854							
	849		856							
	852		855		851					851.5
	849		848		850					
	41380	1164	40216		—		37916	1130	36786	
3	41392	1164	40228		—		37928	1130	36798	
	41497	1167	40330	1155	39175	1143	38032	1127	36905	
	41507	1167	40340	1153	39187	1143	38044	1126	36918	
			837							
			839		837					838.5
			841							
			—		39896					
4			41065	1154	39911					
			41169	1157	40012					
			41181		—					
					828					
					823					
					825					825.3
					40724					
5					40734					
					40837					
					—					
Average $G''_{v+\frac{1}{2}}$		1166.9		1154.6		1142.2		1128.5		

The four heads listed opposite each upper state vibrational quantum number are the Q_1 and R_1 heads of the ${}^2\Pi_{\frac{1}{2}} \rightarrow {}^2\Sigma$ sub-bands, and the R_2 and ${}^SR_{21}$ heads of the ${}^2\Pi_{3/2} \rightarrow {}^2\Sigma$ sub-bands. The following equations for the γ band heads were derived from the Deslandres table:

$$ {}^2\Pi_{\frac{1}{2}} \rightarrow {}^2\Sigma : \nu_{head} = \left.\begin{matrix} 38785 \\ 38796 \end{matrix}\right\} + [885.9v' - 6.74v'^2] - [1173.3v'' - 6.40v''^2], \tag{21} $$

$$ {}^2\Pi_{3/2} \rightarrow {}^2\Sigma : \nu_{head} = \left.\begin{matrix} 38899 \\ 38912 \end{matrix}\right\} + [885.9v' - 6.74v'^2] - [1173.3v'' - 6.40v''^2]. \tag{22} $$

The constants ω_0 and $\omega_0 x_0$ were obtained from the average vibrational quanta given in the Deslandres table. A comparison of Tables V and VIII shows unambiguously that the α and γ systems have the same lower state. This fact is also proved by the equality of the combination differences $\Delta_2 F''(K)$ of the two systems as shown in Table II. Since the data for the α system are considered to be more accurate than those of the γ system, the constants obtained from the α system were used in the summary of vibrational constants given in Table IX.

TABLE IX

VIBRATIONAL CONSTANTS AND FORCE CONSTANTS OF THE OBSERVED ELECTRONIC STATES* OF BS

Constant	$X^2\Sigma$	$A^2\Pi$	$C^2\Pi$
ν_e	0	15875.07 cm.$^{-1}$ 16208.68	38925.80 cm.$^{-1}$ 39041.15
ν_{00}	0	15662.73 15996.34	38781.93 38897.28
ω_e	1180.17 cm.$^{-1}$	753.35	892.6$_4$
ω_0	1173.86	748.73	885.9$_0$
$\omega_e x_e$	6.31	4.62	6.74
k_e	6.718$_5$ × 10 ^{5}dynes/cm.	2.737$_6$ × 10^5 dynes/cm.	3.843$_6$ × 10^5 dynes/cm.

* *The $A^2\Pi$ state is analogous to the $A^2\Pi$ state of BO. The $C^2\Pi$ state has not been observed for BO. All conversion factors were obtained from (4).*

3. Isotope Effect

The bands on the high frequency side of the origin of the γ system have a rather complex appearance. Hence the isotopic heads do not stand out well. However, on the low frequency side, the isotopic heads can be seen superimposed on the fine structure of the (0,1), (0,2), and (0,3) bands. No great accuracy can be claimed for the measurement of these bands, but they lie approximately at the positions calculated from the formula giving the vibrational isotopic shift as is shown in Table X. No rotational analysis of any of the isotopic bands was attempted.

TABLE X

COMPARISON OF THE OBSERVED AND CALCULATED WAVE NUMBERS OF THE HEADS OF THE γ BANDS OF $B^{10}S^{32}$

Band	ν (calculated)	ν (observed)
(0,1)	37570	37568
	37582	37582
	37685	37687
	37699	37700
(0,2)	36375	36376
	36389	36391
	36490	36488
	36504	36506
(0,3)	35192	35194
	35207	35211
	35307	35309
	35322	35319

E. The Blue–Green System

In the same discharge in which the α and γ systems are excited a strong system of violet degraded bands always appears in the region between 4900 Å

TABLE XI

WAVE NUMBERS AND WAVE LENGTHS OF THE BLUE-GREEN SYSTEM OF BANDS

Intensity (max. = 10)	Wave number $cm.^{-1}$	Wave length Å
2	20408.31	4898.60
4	20407.48	4898.80
3	20388.08	4903.45
4	20385.52	4904.08
8	20366.20	4908.73
8	20364.97	4909.03
10	20348.57	4912.98
10	20346.32	4913.53
7	20051.79	4985.70
8	20050.70	4985.97
6	20032.10	4990.60
8	20030.55	4990.99
8	20014.48	4994.99
4	20014.15	4995.08
8	20012.00	4995.61
3	20011.62	4995.71
2	19725.77	5068.10
3	19724.81	5068.35
4	19693.97	5076.29
4	19693.37	5076,44
2	19662.79	5084.33
3	19662.18	5084.49
4	19359.35	5164.03
3	19358.68	5164.21
2	19327.27	5172.60
4	19326.42	5172.83
1	19299.47	5180.05
2	19298.43	5180.33

and 5200 Å. This system consists mainly of the two strong band groups shown in Fig. 2 with two similar weaker groups lying to the red. Each group consists of several heads. The lines in these bands are much closer together than those of the other systems. In Table XI the wave lengths and wave numbers of the blue–green bands are given. The separations of some of the heads agree with the spin doublet splitting of the $A^2\Pi$ state. A satisfactory interpretation of these bands has not yet been found.

Acknowledgments

The writer wishes to thank Dr. G. Herzberg, who suggested the problem, for valuable advice and criticism during the whole course of this work and for his guidance in the course of the writing of the manuscript. The writer also wishes to thank Dr. A. E. Douglas for many helpful suggestions.

The writer acknowledges a grant from the South African Council for Scientific and Industrial Research in aid of the work done.

References

1. ALMY, G. and HORSFALL, R. Phys. Rev. 51: 492. 1937.
2. EARLS, L. T. Phys. Rev. 48: 423. 1935.
3. HERZBERG, G. and CURRY, J. Ann. Physik, 19: 800. 1934.
4. HERZBERG, G. Molecular spectra and molecular structure. Vol. 1. Diatomic molecules. 2nd ed. Dover Publications, New York. 1950.
5. JENKINS, F. A. and MCKELLAR, A. Phys. Rev. 42: 464. 1932.
6. MULLIKEN, R. S. Phys. Rev. 25: 259. 1925.
7. MULLIKEN, R. S. Revs. Modern Phys. 3: 129. 1931.
8. ZEEMAN, P. B. Phys. Rev. 80: 902. 1950.

CANADIAN JOURNAL OF PHYSICS

Notice to Contributors

GENERAL: Manuscripts should be typewritten, double spaced, and the **original and one extra copy** submitted. Style, arrangement, spelling, and abbreviations should conform to the usage of this Journal. Names of all simple compounds, rather than their formulas, should be used in the text. Greek letters or unusual signs should be written plainly or explained by marginal notes. Superscripts and subscripts must be legible and carefully placed. Manuscripts should be carefully checked before being submitted, to reduce the need for changes after the type has been set. If authors require changes to be made after the type is set, they will be charged for changes that are considered to be excessive. **All pages, whether text, figures, or tables, should be numbered.**

ABSTRACT: **An abstract of not more than about 200 words, indicating the scope of the work and the principal findings, is required.**

ILLUSTRATIONS:

(i) *Line Drawings:* All lines should be of sufficient thickness to reproduce well. Drawings should be carefully made with India ink on white drawing paper, blue tracing linen, or co-ordinate paper **ruled in blue only;** any co-ordinate lines that are to appear in the reproduction should be ruled in black ink. Paper ruled in **green, yellow, or red should not be used** unless it is desired to have all the co-ordinate lines show. Lettering and numerals should be neatly done in India ink preferably with a stencil (**do not use typewriting**) and be of such size that they will be legible and not less than one millimeter in height when reproduced in a cut three inches wide. All experimental points should be carefully drawn with instruments. Illustrations need not be more than two or three times the size of the desired reproduction, but the ratio of height to width should conform with that of the type page. **The original drawings and one set of small but clear photographic copies are to be submitted.**

(ii) *Photographs:* Prints should be made on glossy paper, with strong contrasts; they should be trimmed to remove all extraneous material so that essential features only are shown. Photographs should be submitted **in duplicate;** if they are to be reproduced in groups, one set should be so arranged and mounted on cardboard with rubber cement; the duplicate set should be unmounted.

(iii) *General:* **The author's name, title of paper, and figure number should be written in the lower left hand corner (outside the illustration proper) of the sheets on which the illustrations appear.** Captions should not be written on the illustrations, but typed on a separate page of the manuscript. All figures (including each figure of the plates) should be numbered consecutively from 1 up (arabic numerals). **Each figure should be referred to in the text.** If authors desire to alter a cut, they will be charged for the new cut.

TABLES: Each table should be typed on a separate sheet. Titles should be given for all tables, which should be numbered in Roman numerals. Column heads should be brief and textual matter in tables confined to a minimum. **Each table should be referred to in the text.**

REFERENCES: **These should be listed alphabetically by authors' names, numbered in that order, and placed at the end of the paper.** The form of literature citation should be that used in this Journal. **Titles of papers should not be given.** The first page only of the references cited should be given. **All citations should be checked with the original articles.** Each citation should be referred to in the text by means of the key number.

REPRINTS: A total of 50 reprints of each paper, without covers, are supplied free to the authors. Additional reprints will be supplied according to a prescribed schedule of charges. On request, covers can be supplied at cost.

Approximate charges for reprints may be calculated from the number of printed pages, obtained by multiplying by 0.6 the number of manuscript pages (double-spaced typewritten sheets, 8½ in. by 11 in.) and making allowance for space occupied by line drawings and half-tones (not inserts). The cost per page is tabulated at the back of the reprint request form sent with the galley.

Manuscripts should be addressed: *Canadian Journal of Physics,*
National Research Council,
Ottawa, Canada.

Contents

Page

The Emission of Radioactive Nuclei in Cosmic Ray Stars—*E. Pickup and L. Voyvodic* - - - - - - - - - - - - - - - - - - 263

On the Theory of the Hall Effect—*H. Koppe and J. M. Bryan* - - 274

Scale Model Experiments in Electromagnetic Methods of Geophysical Exploration—*A. R. Clark and A. G. Mungal* - - - - - - 285

Predissociation and Dissociation of the N_2 Molecule—*A. E. Douglas and G. Herzberg* - - - - - - - - - - - - - - - - - - 294

Absorption Corrections for Radium Standardization—*G. M. Keyser* 301

Some Results on the Electrical Breakdown of Liquids Using Pulse Techniques—*W. D. Edwards* - - - - - - - - - - - - - - 310

Angular Correlation of Annihilation Radiation from Positrons Decaying in Several Substances—*J. B. Warren and G. M. Griffiths* 325

Spectrum and Structure of the Boron Monosulphide (BS) Molecule —*P. B. Zeeman* - 336

Printed in Canada *by* University of Toronto Press

VIRUS